Aus dem Universitätsklinikum Münster

Klinik und Poliklinik für Augenheilkunde

- Direktorin: Univ.-Prof. Dr. med. Nicole Eter -

Forschungslabor der Augenklinik

- Leiter: Prof. Dr. rer. nat. Peter Heiduschka -

Effects of Subretinal Injection of Human Lipofuscin on Murine Retina as a Novel Animal Model of Age-related Macular Degeneration

Effekte der subretinalen Injektion von humanem Lipofuszin auf die Retina der Maus als ein neues Tiermodell der altersbedingten Makuladegeneration

Inaugural-Dissertation

zur Erlangung des doctor medicinae

der Medizinischen Fakultät

der Westfälischen Wilhelms-Universität Münster

vorgelegt von

Nan Su

aus Zheng Zhou (VR China)

2022

Gedruckt mit Genehmigung der Medizinischen Fakultät der Westfälischen Wilhelms-Universität Münster

Dekan: Univ.-Prof. Dr. med. Frank Ulrich Müller

1. Berichterstatter: Prof. Dr. rer. nat. Peter Heiduschka
2. Berichterstatterin: Univ.-Prof. Dr. med. Markus Missler

Tag der mündlichen Prüfung: 07.Februar 2022

Aus dem Universitätsklinikum Münster
Klinik und Poliklinik für Augenheikunde
-Direktorin: Univ.-Prof. Dr. Nicole Eter

Koreferent: Univ.-Prof. Dr. med. Markus Missler

Zusammenfassung

Effekte der subretinalen Injektion von humanem Lipofuszin auf die Retina der Maus als ein neues Tiermodell der altersbedingten Makuladegeneration

Nan Su

Lipofuszin ist ein altersbedingtes Pigment in postmitotischen Zellen. Es ist in einem weiten Wellenlängenbereich autofluoreszierend und gilt als wichtiger Risikofaktor für die geographische Atrophie.
Die Mikrogliazellen sind die Immunzellen in der Netzhaut. Sie helfen, die Homöostase aufrechtzuerhalten, indem sie den Zustand der Netzhaut überwachen. In pathologischen Situationen gehen sie in einen aktivierten Zustand über und können Entzündungen fördern und verletzte Neuronen phagozytieren. Daher kann eine Hemmung der Mikroglia die Entzündung verringern und dementsprechend zum Überleben geschädigter Neuronen beitragen.
Das Ziel dieser Studie ist es, die Rolle des Lipofuscins in der Retina zu überprüfen. Zu diesem Zweck etablierten wir ein Mausmodell mit subretinaler Injektion von Lipofuszin, das aus menschlichem retinalem Pigmentepithel (RPE) isoliert wurde. Als Negativ-kontrollen verwendeten wir altersentsprechende Mäuse ohne jegliche Behandlung oder Eingriff, scheinbehandelte Mäuse oder Mäuse mit einer subretinalen Injektion von PBS.
Wir untersuchten die Mäuse mittels OCT und ERG. Wir führten Immunfärbungen von histologischen Schnitten durch, überprüften die Expression von Zytokinen mittels qPCR und machten einige Aufnahmen mittels Elektronenmikroskopie.
Nach der Injektion von Lipofuszin sind im Vergleich zur Kontrolle bereits die frühen Merkmale der AMD sichtbar. Die RPE-Schicht verlor ihre normale Struktur und die RPE-Zellen wurden dünner; einige drusenähnliche Granula lagerten sich im subretinalen Raum ab.
Die Behandlung mit Mikroglia-Inhibitoren (TKP und Minozyklin) führte zu weniger Mikrogliazellen in der Netzhaut und im subretinalen Raum nach der Injektion von Lipofuszin. Die Inhibitoren, insbesondere TKP, konnten die Expression von pro-inflammatorischen Zytokinen in den meisten Fällen reduzieren.
Die Injektion von menschlichem Lipofuszin in den subretinalen Raum der Mäuse, imitiert maximal die pathologischen Prozesse der frühen AMD, und unser experimenteller Ansatz kann ein hilfreiches Modell für die Vorgänge bei diesem Stadium der Erkrankung sein.
Die Ergebnisse unserer Studie deuten darauf hin, dass die Phagozytose von Lipofuszin durch subretinale Mikroglia möglicherweise an der Pathogenese der AMD beteiligt ist, eine Hemmung der inflammatorischen Reaktionen der Mikroglia könnte ein mögliches therapeutisches Ziel sein.

Tag der mündlichen Prüfung: **07. Februar 2022**

Aus dem Universitätsklinikum Münster
Klinik und Poliklinik für Augenheikunde
-Direktorin: Univ.-Prof. Dr. Nicole Eter
Koreferent: Univ.-Prof. Dr. med. Markus Missler

SUMMARY

Effects of Sub-retinal Injection of Human Lipofuscin on Murine Retina as a Novel Animal Model of Age-related Macular Degeneration

Nan Su

Lipofuscin is an age-related pigment in post-mitotic cells. It is auto-fluorescent in a wide wavelength range and is considered an important risk factor for geographic atrophy.

The microglial cells are the immune cells in the retina. They help to keep the homeostasis by monitoring the state of the retina. In pathological situations, they turn to an activated state and can promote inflammation and phagocytose injured neurons. Thus, inhibition of microglia may decrease inflammation and accordingly contribute damaged neurons to survive.

The purpose of this study is to check the role of the lipofuscin in the retina. For this aim, we established a mouse model of subretinal injection of lipofuscin. As negative controls, we used age-matched mice without any treatment and intervention, sham treated mice or mice with a subretinal injection of PBS.

We checked the mice by OCT and ERG. We did immunostaining of histological sections, checked expression of cytokines by qPCR and took some images using electron microscopy.

After lipofuscin injection, early features of AMD are already visible compared to the control. RPE layer lost its normal structure and RPE cells became thinner; some drusen-like granular deposited in the subretinal space.

Treatment with microglial inhibitors (TKP and minocycline) resulted in fewer microglial cells in retina and in subretinal space after lipofuscin injected. The inhibitors, especially TKP, can reduce the expression of pro-inflammatory cytokines in most cases.

Injecting human lipofuscin into the subretinal space of the mice maximally imitates the pathological processes of early AMD, and our experimental approach may be a useful model for the processes that happen at that stage of this disease. The results of our study indicate that the phagocytosis of lipofuscin by subretinal microglia maybe involved in the pathogenesis of AMD, inhibition of the inflammatory reaction of the microglia could potentially be a therapeutic target.

Date of the defence: 07. February 2022

ERKLÄRUNG

Ich gebe hiermit die Erklärung ab, dass ich die Dissertation mit dem Titel:

„Effekte der subretinalen Injektion von humanem Lipofuszin auf die Retina der Maus als ein neues Tiermodell der altersbedingten Makuladegeneration“
“Effects of Sub-retinal Injection of Human Lipofuscin on Murine Retina as a Novel Animal Model of Age-related Macular Degeneration”

in der Klinik und Poliklinik für Augenheilkunde des Universitätsklinikums Münster unter der Anleitung von Prof. Dr. Peter Heiduschka

1. selbständig angefertigt,

2. nur unter der Nutzung der im Literaturverzeichnis angegebenen Arbeiten angefertigt und sonst kein anderes gedrucktes oder ungedrucktes Material verwendet,

3. keine unerlaubte fremde Hilfe in Anspruch genommen,

4. sie weder in der gegenwärtigen noch in einer anderen Fassung einer in- oder ausländischen Fakultät als Dissertation, Semesterarbeit, Prüfungsarbeit oder zur Erlangung eines akademischen Grades vorgelegt habe.

Münster, den 10. Februar 2022

Ort, Datum Unterschrift

Table of Contents

List of Figures

List of Tables

List of Abbreviations

A	
A2E	bis-retinoid *N*-retinylidene-*N*-retinylethanolamine (A2E)
ADP	adenosine diphosphate
AF	autofluorescence
AMD	age-related macular degeneration
ATP	adenosine triphosphate
B	
BSA	bovine serum albumin
BM	Bruch's membrane
BRB	blood-retinal barrier
C	
CC	choriocapillaris
CCL2	CC-cytokine ligand 2
CD	cluster of differentiation molecule
CF	complement factor
CNS	central nervous system
CNTF	ciliary neurotrophic factor
CNV	choroidal neovascularisation
CNVMs	CNV membranes
C3-CR3	complement component 3 and complement receptor 3
CX3CL1	CX3C chemokine ligand 1
CX3CR1	CX3C chemokine receptor 1
CXCL	C-X-C motif chemokine ligand
D	
DAPI	4′6′-diamidino-2-phenylondole dihydrochloride
DMOG	dimethyloxaloylglycine
DVD	deep vessel density
E	
E	embryonic day
e.g.	exempli gratia, for example
ELM	external limiting membrane

ER	endoplasmic reticulum
ERG	electroretinography
Ex	excitation wavelength
EZ	ellipsoid zone
F	
FA	fluorescein angiography
FGF	fibroblast growth factor
Fig.	figure
FKN	fractalkine
G	
GA	geographic atrophy
GCL	ganglion cell layer
GFAP	glial fibrillary acidic protein
GFP	green fluorescent protein
GPCR	G protein-coupled receptor
GS	glutamine synthetase
H	
Hbegf-α	Heparin-binding EGF-like growth factor
HIF	Hypoxia-inducible factor
I	
Iba1	ionized calcium-binding adapter molecule 1
iBRB	inner blood-retinal barrier
i.e.	id est, that is to say
IL	interleukin
IL-6R	IL-6 receptor
ILM	inner limiting membrane
INL	inner nuclear layer
IPL	inner plexiform layer
IR	Immunoreactivity
IZ	interdigitation zone

L

LF	lipofuscin
LPS	lipopolysaccharide

M

MBP	myelin basic protein
MCP	monocyte chemotactic protein
MHC	major histocompatibility complex
Mino	minocycline
MIP	macrophage inflammatory proteins
MG	microglia cell
MOG	myelin oligodendrocyte glycoprotein
MRI	magnetic resonance imaging
MS	multiple sclerosis

N

nAMD	neovascular AMD
NFL	nerve fiber layer
NLRP3	NOD-, LRR- and pyrin domain-containing protein 3
NeuN	neuronal nuclei

O

oBRB	outer blood-retinal barrier
OCT	optical coherence tomography
OCTA	optical coherence tomography angiography
OIR	oxygen-induced retinopathy
ONL	outer nuclear layer
OPL	outer plexiform layer

P

PBS	phosphate buffered saline
PBMC	peripheral blood mononuclear cells
PC	pyruvate carboxylase
PEDF	pigment epithelium-derived factor
PGs	proteoglycans
POS	photoreceptor out segment

PR	purinergic receptor
PR IS	inner segment of the photoreceptors
PR OS	out segment of the photoreceptors
PRRs	pattern-recognition receptors
P2rx4 (P2X4)	P2X purinergic receptor 4
Q	
qPCR	quantitative polymerase chain reaction
R	
RAP	retinal angiomatous proliferation
RCS	Royal College of Surgeons
RGC	ganglion cell layer
ROI	reactive oxygen intermediates
ROS	reactive oxygen species
RP	retinitis pigmentosa
RPE	retinal pigment epithelium
S	
SLO	scanning laser ophthalmoscopy
SVD	superficial vessel density
sIL-6R	soluble IL-6 receptor
T	
TGF	transforming growth factor
TKP	Thr-Lys-Pro or threonine-lysine-proline
TMEM	transmembrane protein
TNF-α	tumour necrosis factor alpha
V	
VCAM	vascular cell adhesion molecule
VEGF	vascular endothelial growth factor
VEGFR	vascular endothelial growth factor receptor
VEP	visual evoked potential

1. Introduction

1.1 Synopsis

AMD (age-related macular degeneration) is the leading cause of irreversible legal blindness on three continents (Smith, Assink *et al*. 2001). With the aging of the population and the changes in the diet of modern people, the incidence of AMD will gradually increase. As one of the main causes of blindness, AMD has received much attention.

AMD is characterised by the deposition of lipofuscin（LF) in the retinal pigment epithelium (RPE). This contributes to geographic atrophy (GA) in advanced AMD, as well as the loss of RPE and photoreceptors. The retina, RPE, and the choroid deteriorate progressively, leading to severe vision loss.

The progressive degeneration of the retina, RPE and underlying choroid results in severe vision loss (Ambati, Anand *et al*. 2003). However, for this leading cause of blindness, the lack of animals' models restricts its research and treatment. Here we report about subretinal injection of human LF in mice as a potential dry AMD animal model.

The LF in the RPE arises from the fact that the discs of photoreceptor outer segments phagocytosed by the RPE cannot be completely degraded over the years. The reason is the oxidative and phototoxic stress to which the backside of the eye is exposed and which leads to the oxidation and cross-linking of proteins and lipid molecules. Despite some approaches, there is still no effective therapy to control the GA, nor is there a good animal model for early AMD from which the GA can develop. It is well known that LF has toxic effects on RPE cells. In addition, massive presence of LF indicated by fundus autofluorescence is a risk factor for AMD development. Therefore, LF is involved in neurodegenerative and degenerative ocular disorders, as well as it has been related to AMD pathogenesis.

It is of great importance to reliable detect microglial cells in the tissue in research on diseases of the central nervous system including ocular diseases affecting the retina. The microglia cell (MG) is the intrinsic immune cell of the central nervous system. In the healthy mammalian

retina, microglial cells are located in the ganglion cell layer, the inner plexiform layer, and the outer plexiform layer where they permanently survey the status of the nervous tissue. In case of an injury or a disease, microglial cells switch into an activated state, can release a big variety of cytokines and other compounds, and phagocytose debris and damaged cells (Madeira, Boia *et al*. 2015).

LF accumulates in the RPE in the aged retina and can be released to both basal and apical sides. With increasing age, as microglial cells may migrate into the sub-retinal space, the reaction of microglial cells towards LF may have key implications for AMD development and progression.

1.2 Introduction of LF

One of the most relevant features of aging is associated with increasing dysfunction in the renewal of cellular components, a mechanism that prevents the removal of damaged bio-molecules and organelles and their replacement by new functional structures. This in efficient persistent recycling mechanism causes the accumulation of unfit molecules that further interfere with cellular functions. (Lopez-Otin, Blasco *et al*. 2013).

Among the main components of this biological "garbage," they could find indigestible protein aggregates, defective mitochondria and LF (Terman 2001).

LF is a post-mitotic pigment usually associated with aging ("age pigment") (Seiberlich, Borchert *et al*. 2013). LF is a brownish-yellowish pigment, is autofluorescent in a wide wave-length range and is considered an important risk factor for geographic atrophy, a late stage of age-related macular degeneration (AMD).

1.2.1 The Composition and Distribution of Lipofuscin

LF is composed of highly oxidised and cross-linked macromolecules proteins, lipids, sugars and metal ions: Fe^{3+}, Fe^{2+}, Mn^{2+}, Ca^{2+}, Cu^{2+}, Zn^{2+}, Al^{3+} (Rodolfo, Campello *et al*. 2018). In LF, the proportion of proteins is 30–70%, the percentage of lipids is 20–50%, the ratio of metals cations is 2%, and the rest is sugar (Double, Dedov *et al*. 2008).

LF autofluorescence exhibits considerable heterogeneity in emission spectra, reflecting differences in its chemical composition as a result of its maturation in particular metabolic

pathways (Schwartsburd 1995). Generally, LF has a maximum excitation wavelength at 364 nm and a fluorescence emission ranges from 400 nm to 700 nm, with a maximum emission wavelength at about 578 nm (Warburton, Davis *et al*. 2007). Because of its high level of autofluorescence in some tissue samples, LF interferes with different analysis techniques that employ fluorescence, such as immunofluorescence imaging. Therefore, people use different experimental protocols to block its autofluorescence in the samples of tissue, for instance by application of copper sulphate, picric acid or Sudan black (Moreno-Garcia, Kun *et al*. 2018).

Due to its property of high cross-linking and aggregation, LF is neither cleared by exocytosis nor degraded. Therefore, LF accumulates in cell cytoplasm of long-lived post-mitotic, senile animal cells and the lysosomes. Conversely, proliferating cells effectively dilute LF particles during cell division, indicating no or low accumulation of pigment (Terman and Brunk 2005).

1.2.2 Mechanisms of LF Accumulation

With increasing age, the effectiveness of cell protein homeostasis decreases, hindering the degradation of misfolded proteins, exposing their hydrophobic domains, and easily forming high-order complexes with other perinuclear/centrosome-proximal proteins, and they tend to form aggregates.(Rodolfo, Campello *et al*. 2018).

Following uptake of these aggregates by macroautophagic lysosomes, highly cross-linked substances, such as LF, then accumulate in the lysosomes. Thus, although most intracellular LF is located in lysosomes, LF can also accumulate in the cytoplasm following inhibition of the macrophage autophagic pathway (Hohn and Grune 2013).

1.2.3 Lipid Metabolism

Since lipids are one of the main components of LF, lipid metabolism dysfunction is believed to be the cause of LF synthesis and accumulation. Therefore, Hebbar and collaborators proposed that the accumulation of LF deposits is a direct result of the imbalance between cerebral ceramide and sphingosine in the early stages.(Hebbar, Khandelwal *et al*. 2017). Zhao and collaborators also demonstrated that defective ceramide biosynthesis causes neurodegeneration, suggesting a novel mechanism for LF formation (Zhao, Spassieva *et al*. 2011). In line with this,

Pan and collaborators demonstrated in a knockout mouse model *in vivo* that neuraminidase 3 and 4 play a role in the function of the central nervous system (CNS) by breaking down gangliosides and preventing them from turning into LF aggregates.(Pan, De Aragao *et al*. 2017).

LF is not only an inert waste product of cellular metabolism; it shows several effects (Figure 1.1A). As an example, LF inhibits the 20S and 26S proteasome, resulting in decreased degradation and further accumulation of oxidised and misfolded proteins, which leads to the formation of protein aggregates further lipofuscin. (Figure 1.1B) Accumulation of LF in lysosomes may impair autophagy and lysosomal degradation of various proteins, protein aggregates, and organelles. Thus, non-functional, impaired mitochondria may also not be degraded and accumulate, which leads to increased amounts of reactive oxygen species (ROS) and further protein oxidation, protein aggregation, and LF formation. (Figure 1.1C) LF can incorporate metal ions that generate highly reactive ROS via the Fenton reaction. (Figure 1.1D) A general consequence of LF formation and accumulation is apoptotic cell death (Figure 1.1E). Lysosomal membranes are very susceptible to oxidative damage, which may lead to lysosome rupture and release of LF into the cytosol, resulting in the consequences described under (Figure.1.1A, D and E).

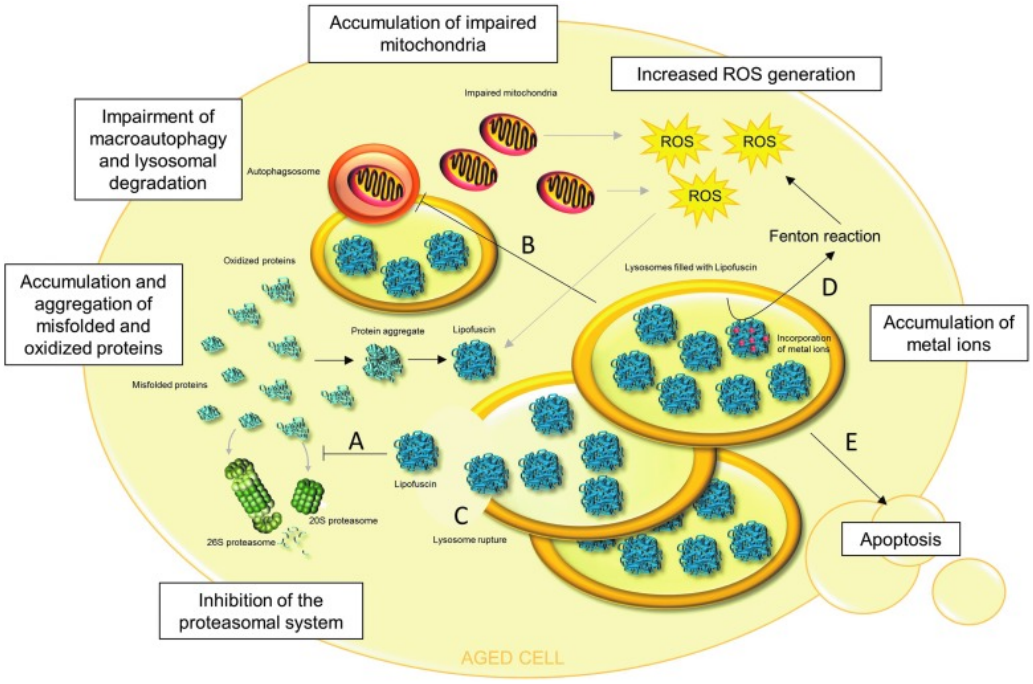

Fig.1.1: Pathophysiological Roles of LF in Aged Cells.
For explanation, see the text. Adapted from (Reeg and Grune 2015).

1.2.4 Relationship between Mitochondria and Lipofuscinogenesis

Oxidative stress and mitochondrial DNA mutations accumulated during the lifetime lead to impaired mitochondrial metabolism, which in turn generates reactive oxygen species (ROS) through oxidative phosphorylation to generate further oxidative stress. Cell quality control mechanisms activate mitosis and eliminate non-functional mitochondria via the lysosomal system (Rodolfo, Campello *et al*. 2018). Non-degradable molecules accumulate, such as mitochondrial small hydrophobic ATP synthase subunit-c, which seems to be the main component of LF in the neuronal cerebellar panniculitis disease. During the aging process, the mitochondrial repair system is further damaged, macroautophagy is generally reduced, and specific mitochondrial proteases are down-regulated, which is responsible for oxidative degradation. (Konig, Ott *et al*. 2017).

These findings emphasise the important tandem between mitochondria and lysosomes during aging, directly involving LF and other macromolecular aggregates (Terman, Kurz *et al*. 2010). The accumulation of LF in the lysosome will reduce autophagy and decrease the turnover rate of mitochondria. In turn, functionally defective mitochondria produce increased ROS levels, which further strengthen the production of LF in the feedback loop of dysfunctional mitochondria and lysosomes, leading to increased oxidative stress, dysfunction of the catabolic pathways reduced energy production (Terman, Kurz *et al*. 2010).

1.2.5 AMD and Lysosome

RPE, a highly specialised single layer of epithelium forming the outermost layer of the retina, is the most active phagocytic system in the body (Young 1971). The outer tips of the photoreceptor outer segments are engulfed every day. They are up-taken by the RPE and digested by phago-lysosomes within RPE (Strauss 2005). Autophagy also facilitates RPE digestion of many materials. An overload of lysosomes results in the synthesis of biological "waste" that reduces RPE efficiency and promotes extracellular protein-lipid sedimentation along Bruch's membrane (Wang, Lukas *et al*. 2009).

Lysosome overload and dysfunction of RPE are suspected to be an important early cause of

AMD (de Jong 2006). It is well known that LF as a polymer composed of proteins and lipids is an elementary component of drusen. Lysosomal isolates in RPE are AMD biomarkers (Kaarniranta, Salminen *et al*. 2009). N-retinoic acid ethanolamine (A2E) is an autofluorescent pigment of LF. At a critical concentration, it inhibits the lysosomal ATPase proton pump, inhibits key enzymes, and causes lysosomal compartments to leak into RPE cytoplasm (de Jong 2006).

Cystatin is a widely expressed lysosomal protease inhibitor that inhibits the secretion of proteolytic regulators, inhibits signalling, leads to inappropriate retention of cellular proteins, and is linked with AMD, as variant B mutations in Cystatin C have been discovered (Sant'Anna, Navarro *et al*. 2016). In addition, lipid peroxidation-modified proteins, similar to those in LF, have been shown to reduce the proteolytic activity of lysosomes in RPE cells (Kaemmerer, Schutt *et al*. 2007). There is also a link between retinal degeneration and the known lysosomal storage disease Niemann-Pick Type C. It was found that mouse transcriptional proteins with Npc1 and Npc2 mutations mediate lipoprotein withdrawal from lysosomes, showing significant retinal degeneration, upregulation of autophagy and significant accumulation of LF in RPE (Claudepierre, Paques *et al*. 2010). These above studies indicate that structural integrity and enzymatic activity of lysosomes in RPE cells may react on the pathogenesis of AMD.

1.2.6 Relationship between AMD and Lipofuscinogenesis

AMD is a degenerative disease of central RPE and the most important cause of vision loss in the elderly population. It has a multifactorial cause characterised by the presence of lysosomal-derived sediments, for example LF and melanolipofuscin. Because of its nature as a fluorochrome, spherical particles of LF are exposed to blue light in RPE, producing phototoxicity and proinflammatory effects, mediated by reactive oxygen intermediates that cause atrophy in AMD patients (Pollreisz, Messinger *et al*. 2018). A2E is a major LF fluorophore and accumulates in the AMD formation process. In this process, it seems to be directly involved in photo induced oxidative stress and the destruction of RPE membrane integrity (Lamb and Simon 2004).

In addition, Stargardt's disease, the most common form of hereditary pubertal macular degeneration, is associated with progressive vision loss due to photoreceptor cell death in the retinal macula and exhibits marked LF accumulation in the lysosomal compartment of the eye's RPE. (Adler, Boyer *et al*. 2015).

Examples of LF accumulation in the RPE with increasing age in two different experimental animals are shown in figures 1.2 and 1.3.

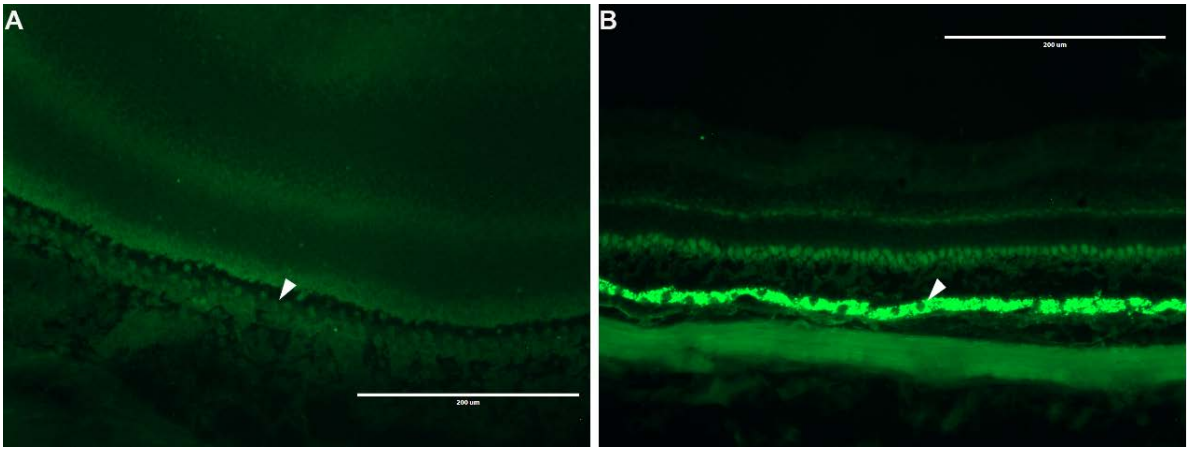

Fig. 1.2: Images Demonstrating Autofluorescence of LF in the RPE of Callithrix.
In the pictures, cryosections are shown of the retina of Callithrix monkey at an age of 3 days **(A)** and 7.5 years **(B)**. Excitation wavelength 488 nm. Arrow heads point to LF accumulated in the RPE. Scale bar: 200 µm. The eyes of the Callithrix monkey were provided by Prof. S. Schlatt from the Institute of Reproductive Medicine, Münster.

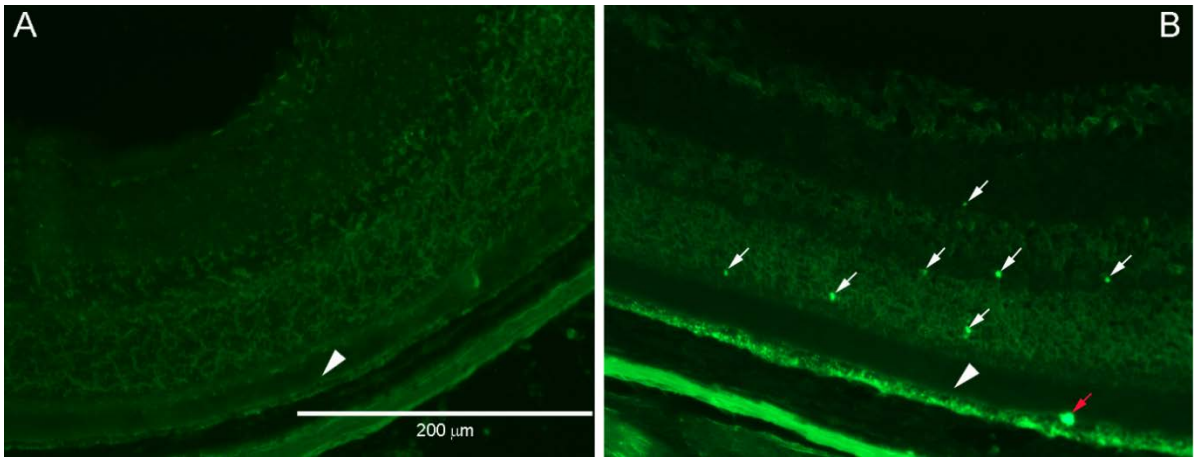

Fig. 1.3: LF Accumulates in the RPE of Wide-type Mice C57BL/6J.
Fluorescence images of retinal cryosections excitation at 488 nm of **(A)** a wild-type mouse 4-month-old and **(B)** a wide-type mouse 21-month-old. Please note white arrows show LF particles in retina different position. Red arrow shows larger granule of LF in RPE of the old mouse. Scale bar: 200 µm.

1.2.7 Closing Words on Lipofuscin

All in all, firstly LF is a fluorescent pigment, it is a mixture of partially digested proteins and lipids. LF accumulates with increasing age in the lysosome chambers of many post-mitotic cells (Adler, Boyer *et al*. 2015). In the retina, a large amount of LF is concentrated in the RPE (Wing, Blanchard *et al*. 1978), and its characteristics and distribution in the living body can be described non-invasively by its strong autofluorescence (Delori, Goger *et al*. 2001), as it emits a unique golden orange fluorescence under blue light stimulation.

Secondly, as LF has a clear cytotoxicity, it is thought to play an important role in retinal degenerative diseases, including AMD and Stargardt's disease, the latter being a macular degeneration that can affect already children (Adler, Boyer *et al*. 2015).

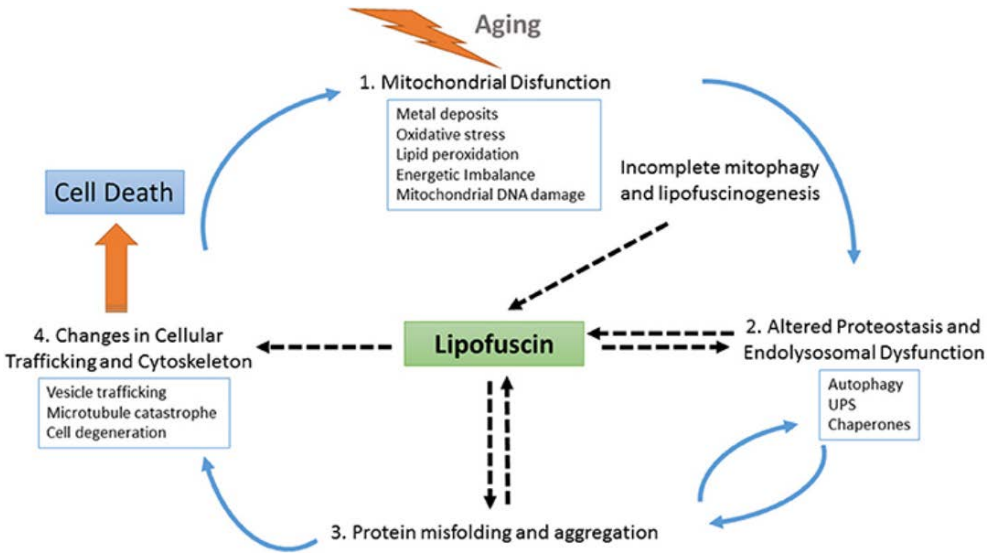

Fig. 1.4: Schematic Representation of LF's Role at Different Points of Cellular Physiology.
For explanation, see the text. Adapted from (Moreno-Garcia, Kun et al. 2018).

Last but not least, diffusion of distributed LF throughout the tissue may provide a basis for the formation of new LF aggregates (Moreno-Garcia, Kun *et al*. 2018). Some findings suggest that LF is not just an inert by-product of cells, however, it actively alters cell metabolism at different levels by inhibiting the proteasome. With aging, several interconnected cellular pathways cause accumulation of LF that harms the proteostasis pathway, further promotes oxidative stress,

energetic imbalance and increased lipofuscinogenesis. Altered proteostasis together with endolysosomal dysfunction also obstructs clearance of misfolded proteins. Finally, as RPE cells are unable to deal with the cascade of damaging events, they degenerate. Pathways of impaired lysosomal degradation and autophagy that lead to reactive oxygen species (ROS) production and apoptotic cell death (Reeg and Grune 2015) are also sketched in figure 1.4.

1.3 Glia Cells in the Mammalian Retina

There are three main types of glial cells in the mammalian retina: astrocytes, Müller cells and microglial cells. See figure 1.5. The fourth type of glial cells of the CNS are oligodendrocytes, which, however, are found only occasionally in the retina and are related to the myelinated ganglion cell axons, in some species such as rabbits (Vecino, Rodriguez *et al*. 2016).

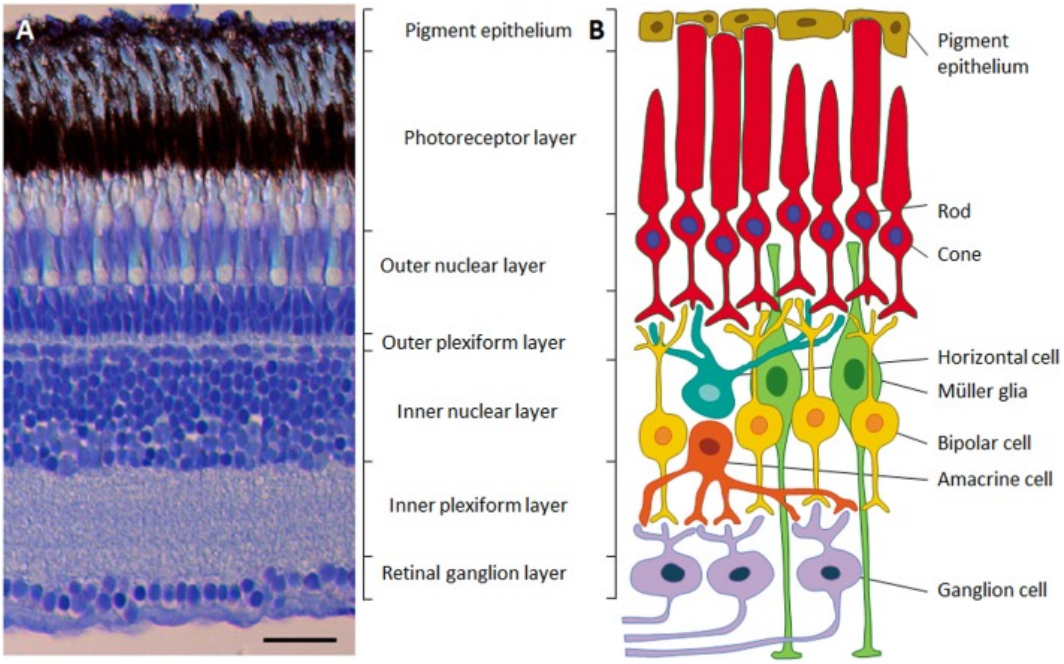

Fig. 1.5: Retinal Layers and Cell Types in an Adult Zebrafish.
A: Microphotograph of a cross-section through the retina of an adult zebrafish, showing the different cellular and synaptic retinal layers. B: Diagram of the neural circuit of the retina, showing the six neuronal cell types and the two supporting cell types (Müller glia and retinal pigmented epithelium). In A, the scale bar: 25 µm. Adapted from (Gramage, Li et al. 2014).

1.3.1 Retinal Müller Cells

Müller cells are the major glial component of the retina, accounting for 90% of retinal glial cells. They are radial cells, passing from their inner (the side of vitreous) boundary, consisting of the inner limiting membrane, through the retina to the outer limiting membrane located at the outer rim of the outer nuclear layer. Müller cells provide structural support, and they are involved in metabolism. Localization and shape of Müller cells can nicely be seen in figure 1.6, where they have been stained against glutamine synthetase (GS).

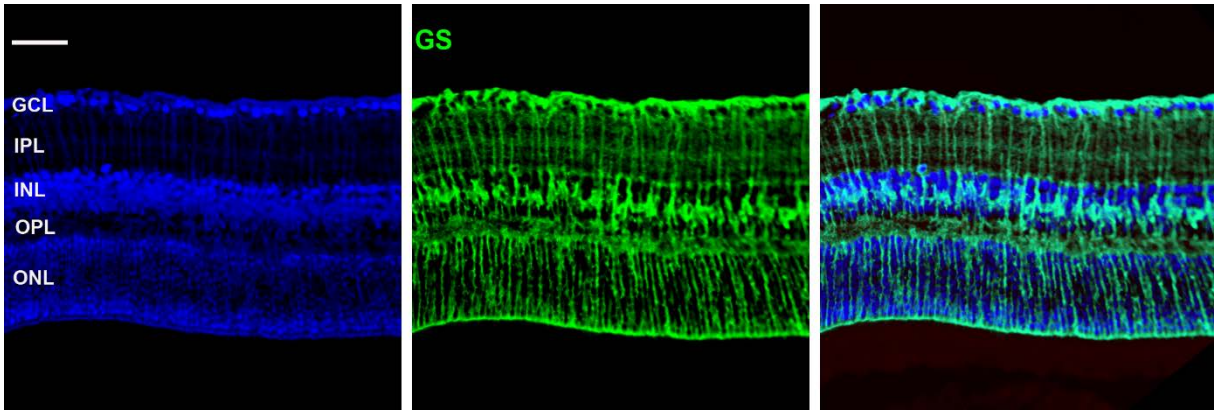

Fig. 1.6: Normal Mouse (1.5 years) Retina.
Demonstration of a GS labelling of Müller cells. Nuclei are stained with DAPI. Image by Nan Su (unpublished). Scale bar: 40 µm.

1.3.2 The Microglial Cells

In the past, the general idea about microglia was that the only function of microglia was to act as a cellular regulator of inflammation in central nervous system diseases. This view seems to be strengthened by certain scientific discoveries that microglia in areas that are adjacent to each other and do not overlap with each other. Therefore, the microglial cells can rapidly response to local damage, even within a few minutes. (Nimmerjahn, Kirchhoff *et al*. 2005). Also, microglia may develop a stimulus-dependent phenotype in response to a broader infection, injury, or disease. Microglial response includes cytoskeletal and morphological changes, as well as proliferation. Therefore, microglia remain alert to the current state of the central nervous

system, in response to specific threats in a highly programmed manner, then acting when needed (Salter and Beggs 2014).

However, in most cases, the CNS is not in danger. So, what is the role of microglia in the normal healthy central nervous system? With the continuous improvement of tools, we can not only understand the function of microglia under attack and threat but also understand their health status. The other function is that microglia may be involved in the concept of CNS in health, there is high activity in the processes of microglia, and constantly monitoring the environment, (Nimmerjahn, Kirchhoff *et al*. 2005). A common point of the physiological role of microglia is that these cells play a beneficial role, unlike microglia being considered reactive only when CNS are infection, disease and during or after injury. Therefore, when some wrong things happen, microglia is not only limited to react, but also plays an active role to re-establish healthy activity of the central nervous system (Salter M.W *et al*. 2014).

1.3.2.1 The Way of Maintenance and Origin of Microglia in the Retina

Several recent kinds of researches verified the hypothesis that microglia originate in the yolk sac and are genetically different from hematopoietic stem cell progeny (Schulz, Gomez Perdiguero *et al*. 2012). These studies are based on a new perspective proposed in 1999 according to research findings on hematopoietic cells in the yolk sac. The authors found that some small colloidal progenitors were detected in the early nerve folds on embryonic day 8 （E8), and the number of cells rapidly increased to a plateau during the second trimester. Thus, they drew the conclusion that microglia progenitors originate from the yolk sac, colonise the brain in early developmental stages, and reach the final number through active proliferation in the brain (Alliot, Lecain *et al*. 1991).

In the next few years, in order to further analyse the offering up of circulating bone marrow-derived progenitor cells to microglial turnover in the central nervous system, another study used a parabiosis experiment (Ransohoff 2007). Parabiosis, a surgical connection between two organisms, allows blood circulation between wild-type and GFP transgenic mice without affecting their blood-brain and blood-retinal barriers (Ransohoff 2007) (Kamran, Sereti *et al*.

2013). The results show that under steady-state conditions, CNS microglia is a closed system with self-renewal ability and is not supplemented by bone marrow derived cells. In fact, it was later confirmed that microglia originated from primitive myeloid progenitors originating from the yolk sac, and postnatal hematopoietic progenitor cells have no significant contribution to the homeostasis of microglia (Ransohoff 2007).

The following studies indicate that refilled retinal microglial exhibits a double additional retinal origin. One origin is microglia remaining from the optic nerve and the other one is from ciliary body/iris macrophages. The remnant optic nerve microglia replenish the retina along the central to peripheral axis, while macrophages from the iris or ciliary body replenish the retina along the periphery, estimated percentage is 15% of the refilled microglia. It is worth noting that these findings not only reveal for the first time the radial migration pathways of retinal microglia but also show the presence of peripheral macrophage-derived microglia, which are notably less ramified than central microglia (Huang, Xu *et al*. 2018). In other research, it supports that microglia in the retina are regulated by neuronal-microglia crosstalk in the form of fractalkine (FKN, CX3CL1) and CX3CL1-CX3CR1 (CX3C chemokine receptor 1) signalling, thereby promoting microglia proliferation and morphological maturation. The important thing is that repopulated cells completely restored microglial function in the retina, including synaptic maintenance and immune surveillance (Zhang, Zhao *et al*. 2018).

1.3.2.2 The Function of Microglia in Healthy Retina

The state of microglia can be divided into two types: resting-state and active state. The MG in resting state does not have phagocytosis, and there are constantly protruding cell processes (Li, Du *et al*. 2012). In the healthy retina, MG is generally in this state.

During retinal development, microglia are mainly localised in the ganglion cell layer, the inner plexiform layer and outer plexiform layer where they devour the cell bodies of superfluous retinal ganglion cells (RGCs) (Bodeutsch and Thanos 2000). The location of microglial cells (see figure 1.7). In addition, microglia participate in the pruning of weak presynaptic terminals of RGCs in the early postnatal period when there is a strong synaptic remodelling. This process

occurs in the complement C3-CR3 (complement component 3 and complement receptor 3) dependent machinery, and activated C3 (iC3b/C3b) selectively labels RGCs that trigger microglia C3 receptor-dependent phagocytic pathways (Karlstetter, Scholz *et al*. 2015). Above all, microglia-dependent apoptosis of superfluous RGCs and removal of high-cost neural connections that are thought to be unsuitable for normal function play a crucial role in normal postnatal formation of cortical visual regions and development in the retinal (Schafer, Lehrman *et al*. 2012).

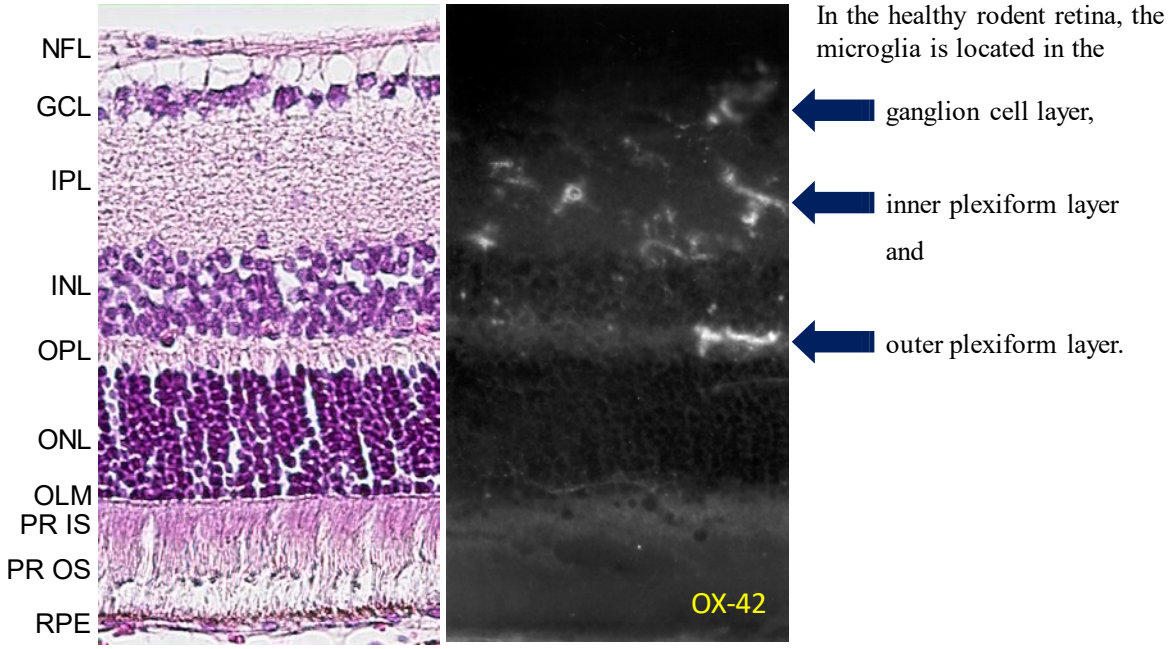

Fig. 1.7: The Location of Microglia in Normal Retina.
The blue arrows point to the location of the microglial cells in the normal rat retina labelled by the OX-42 antibody. NFL-nerve fibre layer; GCL-ganglion cell layer; IPL-inner plexiform layer; INL-inner nuclear layer; OPL-outer plexiform layer; ONL-outer nuclear layer; OLM-outer limiting membrane; PR IS-inner segment of the photoreceptors; PR OS-out segment of the photoreceptors; RPE- retinal pigment epithelium. Image kindly provided by Peter Heiduschka according to (Heiduschka and Thanos 2006).

1.3.2.3 The Behaviour of Microglia in the Diseased Retina

When the CNS is infected or injured by microbes, the microglia becomes activated (Graeber and Streit 2010). The number of processes of activated microglia decreases, and the cells show an amoebic pattern (see figure 1.8). A big variety of cytokines can be released, such as IL-6

(interleukin-6), TNF-α (tumour necrosis factor alpha), FGF-2 (fibroblast growth factor) *etc*. and other compounds, and phagocytose debris and damaged cells (Schafer, Lehrman *et al*. 2012).

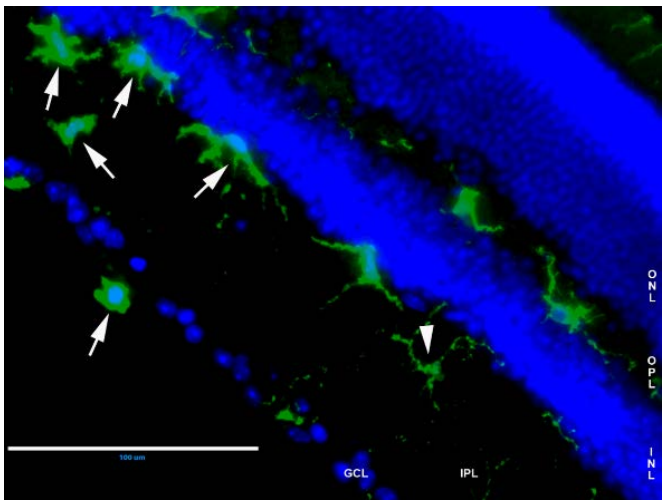

Fig. 1.8: Retinal Section 14 Days after Sub-retinal Injection of Lipofuscin.
Example of retinal microglial cells that were labelled with an antibody against Iba1 (green)**.** The white arrows point to activated micro-glial cells with larger soma as well as reduced length of the processes and number of their ramifications. The white arrowhead points to a resting microglial cell located in the inner plexiform layer with a small soma and thinner, longer ramified process. Scale bar: 100 μm. Image by Nan Su (unpublished).

Activated microglia have two states: M1 and M2. Microglia in different states play different roles. Microglia in the M2 state can release anti-inflammatory factors (such as IL-4, IL-13, *etc*.), phagocytose damaged nerve cell fragments, and promote neuron regeneration and tissue repair (Deierborg, Roybon *et al*. 2010). If microglial cells are activated by overstimulation, which is called secondary stimulus activation, also known as priming of microglia (Perry & Holmes,2014), it will turn to the M1 state and release a large number of neuro-inflammatory factors such as IL-1β, IL-6, TNF-α, ROS, *etc*. These inflammatory factors will have toxic effects on nerve cells. In severe cases, it can cause nerve cell apoptosis. Therefore, maintaining the normal M2 state of microglia and reducing the release of neuro-inflammatory factors has profound significance for protecting the CNS, and it has important theoretical value for finding effective drugs and methods for the treatment of related neurodegenerative diseases.

Activated microglia are considered to be a common feature of various degenerative and inflammatory diseases of the retina. However, there are two sides to this role. In the case of CNS damage, their activation produces a beneficial effect. For example, the actions removing the degenerating cells, rubbish, and secreting neuronal survival factors to control further harm (Rivest 2009). However, on the other side, microglia can become harmful if their actions trigger

a vicious cycle of continuous activation and recruitment of more inflammatory cells (Rivest 2009).

1.3.2.3.1 Microglial Cells and AMD

AMD is a disease of the outer retina in aged people. There are two types of AMD that have been widely described, namely "dry" (atrophic) and "wet" (neovascular) AMD. Depending on the severity of AMD, the current clinical classification of AMD defines three stages. The evaluation criteria are based on fundus lesions, *i.e.*, pigmentary abnormalities, and the size and number of drusen, within two-disc diameters of the macular fovea in people over 55 years old (Garcia-Layana, Cabrera-Lopez *et al*. 2017). When the retina becomes aged or diseased in RPE, some inflammatory factors are released, such as IL-1β, TNF-α, and the microglia enters the subretinal space. Microglia are affected by these pro-inflammatory factors and are stimulated. The M1 and M2 phenotype of microglial cells are imbalanced. Wang *et al*. found that the number of M1 microglia is higher than M2 in Alzheimer's disease (Wang, Tan *et al*. 2015). In the retina degeneration mice model, the number of M1 microglia also was increased (Zhou, Huang *et al*. 2017). their cell bodies are enlarged, and processes are shortened (Harry and Kraft 2008). Microglia-derived factors or reactive microglial cells in the outer retinal layers can induce inflammasome NLRP3 (NOD-, LRR- and pyrin domain-containing protein 3) activation in RPE cell, accompanied by secretion of the pro-inflammatory cytokine IL-1β. Activation of NLRP3 inflammasome leads to RPE cells degeneration. In addition, the accumulation of subretinal microglia can directly lead to the death of nearby photoreceptors in this pro-inflammatory environment. Both of them can cause AMD pathological alterations (Rashid, Akhtar-Schaefer *et al*. 2019).

1.3.2.3.2 Microglial Cells and RPE

RPE phagocytosis of the shed photoreceptor outer segment discs is critical for photoreceptor survival. Abnormal RPE phagocytosis leads to retinal degenerative diseases (Mustafi, Kevany *et al*. 2011). Now it is clear that abnormalities in any stage of phagocytosis may cause diseases, such as AMD (Nandrot 2014).

When the retina ages, drusen are formed between the basal side of the RPE and Bruch's membrane, and the ability of RPE cells for phagocytosis or degradation will decline. When the accumulation of the metabolites (mainly LF) in RPE cells reaches a certain amount, the RPE cells become apoptotic and disintegrate (Ferrington, Sinha *et al*. 2016).

In vitro studies have shown that the effects of activated microglial cells on RPE are mainly reflected in a changed RPE structure as well as a changed ability of its proliferation and phagocytosis. The expression of chemokines and the transcription level of vascular cell adhesion molecule-1(VCAM) mRNA increased. RPE secretion of pro-inflammatory and angiogenic factors also increased. *In vivo* models showed that after retinal microglia were injected into the sub-retina, it can promote choroidal neovascularisation, RPE disintegration, and sub-retinal microglia aggregation (Ma, Zhao *et al*. 2009).

1.3.2.3.3 Accumulation of LF (A2E) in Retinal Microglial Cells

In an aging retina, microglia gather in the outer layers of the retina and form autofluorescent particles in their cytoplasm. *In vitro* experiments show that increased accumulation of A2E by the microglia can activate the microglial cells, consequently weakening its neuroprotective effect on photoreceptors and decreasing the expression of microglial chemokine receptors, thus inhibiting their chemotactic responsiveness. An increased A2E accumulation in the microglial cells leads to a further increase in the accumulation of retinal microglial cells in the subretinal space. By increasing the complement factor (CF) B and decreasing CFH, the complement system can be adjusted to promote the complement system activation and extraretinal deposition of lipofuscin. All these potential factors turn the microglia in the outer retina to a pro-inflammatory state, driving RPE cells and photoreceptors to damage and apoptosis (Ma, Coon *et al*. 2013).

1.3.2.3.4 Microglial Cells and Ageing

Para inflammation is a tissue-adaptive response to harmful stress or dysfunction, with characteristics between basal and inflammatory states. In a normally aging retina, an increase in oxidative stress usually results in the formation of oxidised lipids, DNA, and proteins. Under

physiological conditions, para inflammation also exists in the aging retina and may promote the development of age-related retinopathies. In the quasi-inflammatory response, immune cells including microglia and macrophages, respond to continuous stress stimuli and produce low-level inflammatory responses. The purpose is to restore homeostasis that has been lost with the new changed pathological conditions (Medzhitov 2008).

In the pathogenesis process of AMD, the accumulation of sub-retinal microglia and excessive inflammatory activation of retinal microglia can lead to the destruction of the eye's immune privilege. In other pathological conditions, activated microglia can produce different kinds of products, including complement components, reactive oxygen species, pro-inflammatory cytokines, growth factors and so on. All of these cause chronic local inflammation, and result in further damage (Buschini, Piras *et al*. 2011). As a result, microglia activated by cell death migrate to damaged areas and engulf cell debris. In addition, they also secrete molecules that can kill photoreceptors near the primary degenerate area (Gupta, Brown *et al*. 2003).

1.3.2.3.5 Microglial Cells and Diabetic Retinopathy

Reactive microglia increase in all stages of diabetic retinopathy and promote the progression of the disease into the proliferative stage (Zeng, Green *et al*. 2008).

Activated microglia show up as highly reflective spots on SD-OCT. The thinning of nerve fibre and ganglion cell layers is inversely related to the increase of number of activated microglia. Activated microglia stimulate inflammation, recruit white blood cells, destroy blood vessels, and trigger neuronal death (van Dijk, Verbraak *et al*. 2010).

1.3.2.4 Frequently Used Markers of Microglial Cells

Ionised calcium-binding adapter molecule 1 (Iba1) is a calcium-binding protein specific for microglia and macrophages and is involved in the formation and phagocytosis of activated microglia's cell membranes. Iba1 is the most widely and credible marker to detect microglia in the rat, human, and mouse retina (Ohsawa, Imai *et al*. 2000) (Naskar, Wissing *et al*. 2002).

CX3CR1 (CX3C chemokine receptor 1) is a chemokine receptor that exists on the surface of microglia and macrophages in the CNS and can be activated by CX3CL1 (CX3C chemokine

ligand 1) secreted by neurons.

F4/80 (ADGRE1, EMR1) is a glycoprotein located on the surface of macrophages and microglia. F4/80 is a member of the GPCR (G protein-coupled receptor) family (Yona and Stacey 2010) (Langenhan, Aust *et al*. 2013). F4/80 which is higher in activated microglial cells (Li, Eter *et al*. 2015).

TMEM119 (transmembrane protein) is a cell surface protein and transmembrane molecule. Bennet *et al*. stated that peripheral macrophages were not positive for TMEM119 and introduced a specific marker for microglial cells (Bennett, Bennett *et al*. 2016). Indeed, according to our study, TMEM119 may be a reliable marker of microglial cells in the brain, especially because TMEM119 is not expressed in invading peripheral monocytes. However, in the retina, the situation is more complicated, and it must be checked carefully whether the microglial cells keep TMEM119 expression in pathological situations, such as in a laser spot. Therefore, in our view, Iba1 and CD11b (ITGAM, CR3A) are more useful markers for the retinal microglia than TMEM119 (Su, Marz *et al*. 2019). The comparison of immunoreactivities for CD11b and CD45 can be used to distinguish microglia from macrophages. The immunoreactivity of resting microglia for CD45 is low, while it is higher in macrophages (Krause, Alex *et al*. 2014). For a summary of some microglial markers, see table 1.

	Activated (amoeboid) microglia	**Resting (ramified) microglia**
Markers	TMEM 119 (may be lower)	TMEM 119
	Iba1	Iba1
	CD45 higher	CD45 lower
	CD11b higher	CD11b
	CX3CR1	CX3CR1
	F4/80 higher	F4/80 lower

Table 1 Some Markers of Microglial Cells

1.4 RPE, Bruch's Membrane and Choriocapillaris

The choriocapillaris is made up of a wide and flat network of capillaries that are connected to each other. Due to the large number of small holes (which called fenestrae) in the wall of the endothelial cells, these capillaries are permeable to macromolecules. The fenestrae are located near the Bruch's membrane, which is a thicker acellular structure located between the retinal pigment epithelium (RPE) and the choriocapillaris (Fields, Del Priore *et al*. 2019).

1.4.1 The RPE in AMD

The RPE is embedded between Bruch's membrane and the photoreceptors. It is a monolayer of cubic polygonal cells. RPE cells are rich in organelles and other components, including mitochondria and melanosomes as well as LF and melanolipofuscin. The localisation of the RPE cells, intracellular particle distribution，and their morphology may affect reflectance and autofluorescence, accordingly changing clinical fundus reflectance in the autofluorescence mode (Curcio, Zanzottera *et al*. 2017).

In the area affected by AMD, some RPE cells lose their normal shape, become larger, and fuse. The local density of RPE cells decreases. Changes of the cytoskeleton in RPE cells in AMD include the differential thinning and thickening of F-actin fibres, their division and rupture, and the development of stress fibres. Due to the importance of the polarised pathways for RPE function, these alterations to the cytoskeleton will affect the normal function of RPE in aging and AMD, causing impact on photoreceptor cells and choroidal capillaries (Tarau, Berlin *et al*. 2019).

1.4.2 Bruch's Membrane

There are five layers in Bruch's membrane: from outside to inside the basement membrane of the choriocapillaris, the outer collagenous zone, a central band of elastic fibres layer, the inner collagenous zone, and the basement membrane of the RPE (Lee, Vroom *et al*. 2006).

In the normal mouse, the two basement membranes of RPE and choroid are initially formed, then the collagen layers, and eventually the central elastin layer (Hirabayashi, Fujimori *et al*. 2003). In the whole life of humans, the thickness of normal Bruch's Membrane (BM) has almost

doubled (van der Schaft, Mooy *et al*. 1992). Ramrattan *et al*. studied 120 human donor eyes, and they found a positive linear relationship between age and the total thickness of BM. The thickness of BM increased from 2 μm in young adults to 4.7 μm in 80 years old human. (Ramrattan, van der Schaft *et al*. 1994). Generally, the thickening of BM is due to an increased crosslinking of collagen fibres and increased biomolecules′ deposition, most of which are oxidised waste products metabolised by the RPE. Apparently, BM thickening will finally cause several variations of function, for instance the variations in permeability and elasticity (Booij, Baas *et al*. 2010).

A lot of normal aging processes impact BM, for example, elastic fibres calcification, thickening of its layers caused by LF deposition, drusen formation, and oxidative stress. Obviously, these subclinical or normal events of aging may make RPE and BM susceptible to disease, particularly in the area of the macula. BM is a critical tissue contributing to the development of AMD. The extracellular matrix of BM seems to be a regulatory site of involving systemic and local interactions of cytokines, complement activators, proteoglycans (PGs), chemokines, growth factors as well as the products of waste and toxic reactions.

The regional homeostasis for each person may be limited by the factors of environment, and depend on the local anatomy of BM, RPE, and the neuro-retina, as well as the constitution of the genes. In healthy situations, some molecular interactions (such as chemokines, cytokines, proteoglycans, and complement activators) may be following a settled pattern, thereby maintaining the homeostasis. However, the interactions of the molecules on the BM′s surface have changed as a result of changes caused by normal aging, for instance, immune activation and the long time under oxidative stress. These variations might be adapted until the local steady-state can no longer be maintained, eventually causing AMD (Booij, Baas *et al*. 2010).

1.4.3 The Choriocapillaris (CC)

The choriocapillaris forms an extensively anastomosing and continuous network of capillaries that extends from the ora serrata to the optic nerve margins. It is internally attached to the BM. The fenestrations are one of the obvious characteristics of the vessels of choriocapillaris. They

line up on the inner side of the endothelial cells and allow the exchange of oxygen and metabolites between the choroid and the retina (J， Hogan and J 1971).

The changes in choroidal vasculature depend on the different position in the eye. At the macula, the number of veins and arterioles that inserted into the choroidal capillaries is maximum. The enhanced depth optical coherence tomography (OCT) shows that the choroid was the thickest at the macular fovea (Margolis and Spaide 2009). The choroid thickness varies by up to 70 μm daily (Usui, Ikuno *et al*. 2012).

1.4.4 The Relationship between the RPE, BM and CC

The RPE, BM, and CC are inseparable not only in structure but also in function. Together, they form the retinal blood-retinal barrier.

There are two subassemblies in the blood-retinal barrier (BRB), that is an outer barrier (oBRB) and an inner barrier (iBRB). oBRB is mainly composed of RPE and its tight junctions. RPE is in the outermost layer of the retina and is connected to the choroid. iBRB is composed of tight junctions between adjacent retinal capillary endothelial cells, pericyte cells, and the basement membrane between them. Astrocytes and the processes of Müller cell surround it and participate in the formation of iBRB (Runkle and Antonetti 2011). Many retinal diseases are connected with the destruction of one or both BRB. AMD is associated with the outer blood-retinal barrier, while macular oedema and diabetic retinopathy (DR) normally have to do with the inner blood-retinal barrier. However, there is growing recognition of the role of outer blood-retinal barrier's function in central serous chorioretinopathy (Daruich, Matet *et al*. 2015). and diabetes-related macular oedema (Xu and Le 2011).

The CC and the RPE communicate with each other on Bruch's membrane by diffusible secretion factors, forming a complete unit. As an example, RPE transports metabolic waste from the photoreceptors across Bruch's membrane to the choroid (Fields, Del Priore *et al*. 2019).

In summary, the steadiness of CC relies on the viability and health of BM and the RPE that covered on the BM. Korte *et al*. proved that the RPE can maintain the function and structure of

CC (Korte, Gerszberg *et al*. 1986). Figure 1.9 shows an example of the changes in CC and BM in an old AMD patient.

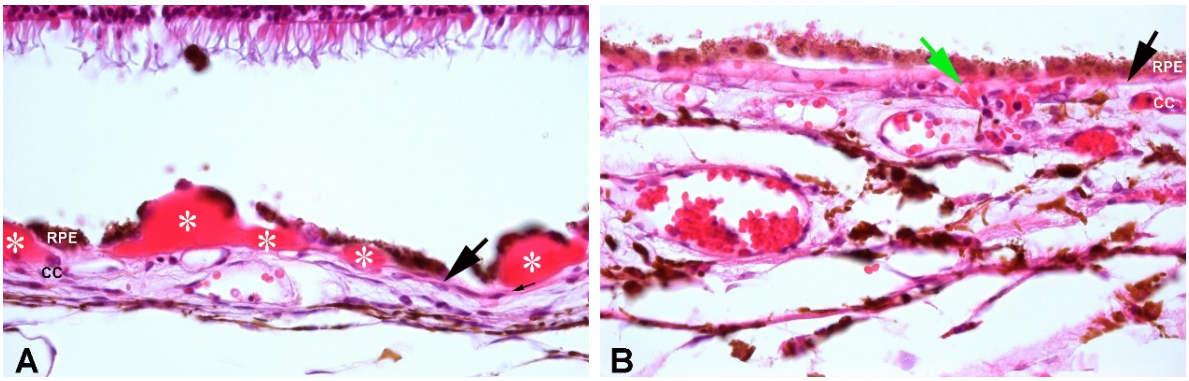

Fig. 1.9: From the Donor Eye of an Old AMD Patient, HE Staining.
The white asterisks in picture **A** show drusen, the black arrows point to Bruch's membrane, the green arrow in picture **B** points to a broken blood vessel releasing blood cells into the space between Bruch's membrane and choroidal capillaries. Images are by Nan Su (unpublished), taken in Tübingen in 2016. Samples (donor eye from USA) were provided by Dr. Antje Biesemeier, Section of Experimental Vitreoretinal Surgery, University Eye Hospital of Tübingen.

1.5 Purpose of this Study

In the aging retina, LF accumulates in the RPE and can be released to the basal and apical side. With increasing age, microglial cells may migrate into the subretinal compartment. Thus, the microglial response to LF may be important for the development and progression of AMD.

In recent *in vitro* experiments, we found that microglia show a strong inflammatory response to lipofuscin. To investigate the effects of LF in the living eye, particularly with respect to the reaction of the microglia towards lipofuscin, we injected LF subretinally in mice as the next step of our studies.

2 Methods and Materials

2.1 Devices

Equipment	Type	Supplier
Centrifuge	Sprout ® Mini Centrifuge	Heathrow Scientific, Vernon Hills, USA
Confocal Microscope	Zeiss ELYRA/LSM 780	Carl Zeiss Microscopy, Jena, Germany
ERG device	RetiPort and Ganzfeld Q450	Roland Consult, Brandenburg, Germany
Fluorescent microscope	AMG EVOS fl	Thermo Fisher Scientific, USA
Heating pad	ThermoLux®	Witte + Sutor GmbH, Murrhardt, Germany
Stereo microscope	Leica M165 C	Leica Biosystems, Germany
Cryostat	Microm HM 550	Thermo Fisher Scientific, Waltham, USA
RT-PCR machine	StepOnePlus	AB Applied Biosystems
Stereo microscope	Leica M165 C	Leica Microsystems GmbH, Wetzlar, Germany
OCT device	HRA+OCT Spectralis	Heidelberg Engineering, Germany
Shaking table	Skyline Shaker DRS 12	Elmi, Calabasas, USA
Thermocycler	PeqStar 2X gradient	PEQLAB Biotechnologie GmbH, Erlangen, Germany

2.2 Chemicals

Chemical	Supplier
Bovine serum albumin (BSA)	Sigma-Aldrich Chemie GmbH, Munich, Germany
β-mercaptoethanol cat. no. M3148	Sigma-Aldrich Chemie GmbH, Munich, Germany
1 M HCl, cat. no. K025.1	Carl Roth GmbH, Karlsruhe, Germany
0.9% NaCl, cat. no. 2350720	B. Braun Melsungen AG, Melsungen, Germany
NaOH, cat. no. S8045	Sigma-Aldrich Chemie GmbH, Munich, Germany
Phenylephrine hydrochloride (Neosynephrin 5%)	Ursapharm Arzneimittel GmbH, Saarbrücken, Germany
Tropicamide	Pharma Stulln GmbH, Stulln, Germany
Proxymetacaine hydrochloride (Proparakain-POS 0,5%)	Ursapharm Arzneimittel GmbH, Saarbrücken, Germany
Paraformaldehyde (PFA)	Carl Roth GmbH, Karlsruhe, Germany
Triton X100 detergent	AppliChem GmbH, Darmstadt, Germany

2.3 Buffers and solutions

Solution Name	Contents
Phosphate-buffered saline (PBS)	80 g NaCl 2 g KCl 14.4 g Na_2HPO_4 2.4 g KH_2PO_4, dissolved in one-liter distilled water
4% paraformaldehyde (PFA)	5 g paraformaldehyde (PFA) 125 ml PBS 50 µl 5 M NaOH 18.75 µl 37% HCl
Power Block™, cat. no. HK085-5KE	BioGenex, Fremont, USA

2.4 Laboratory equipment and consumptive materials

Material	Name
Curved dissecting scissors	Bernhard Hermle GmbH, Tuttlingen, Germany
Curved jeweler forceps	Bernhard Hermle GmbH, Tuttlingen, Germany
Dumont #5 forceps	Fine Science Tools GmbH, Heidelberg, Germany
Pre-Developed TaqMan® Assay Reagents Mouse GAPD	Life Technologies, Warrington, UK
TaqMan™ Gene Expression Master Mix, cat. no. 4369016	Thermo Fisher Scientific, USA
MicroAmp® Fast 96-Well Reaction Plate (0.1 mL) cat. no. 4346907	Life technologies, China.
Gross dissecting scissors	Bernhard Hermle GmbH, Tuttlingen, Germany
Vannas scissors	Bernhard Hermle GmbH, Tuttlingen, Germany
Microliter syringe (5 µL)	Hamilton Bonaduz, Switzerland
Microliter syringe (50 µL)	Hamilton Bonaduz, Switzerland
Plastic Pasteur pipette	Alpha Laboratories Limited, Eastleigh, United Kingdom
76×26 mm² Starfrost Advanced Adhesive microscope slides	Engelbrecht, Edermünde, Germany; or Waldemar Knittel Glasbearbeitungs GmbH, Braunschweig, Germany
Shandon Immu-Mount™	Thermo Scientific, Waltham, USA
24×50 mm² coverslip AutomatStar	Waldemar Knittel Glasbearbeitungs GmbH, Braunschweig, Germany
Richard-Allan Scientific Neg-50 Frozen Section Medium	Thermo Scientific, Waltham, USA
Tissue-Tek O.C.T. Compound	Weckert, Kitzingen, Germany

2.5 Isolation of Lipofuscin

LF used for the experiments was obtained from the RPE isolated from human donor eyes. The donor's eyes were anonymised before they reached us, and the tissue was pooled from at least 15-20 eyes before starting LF isolation. The procedure was based on an established procedure developed by Boulton and Marshall and optimised by our cooperation partner at the German Institute for Nutrition Research, Potsdam-Rehbrücke. (DIfE). All LF used in this work was kindly prepared by Mrs. Jeannette König, Ph.D., from the DIfE. She also provided description of the methods of preparation and characterisation of LF given in the following chapters 2.1.1 and 2.1.2.

2.5.1 Extraction of Lipofuscin

The human donor eyes were provided by the cornea bank of the Department of Ophthalmology, University of Münster Medical Centre. The donor eyes were obtained from elderly donors and did not show signs of specific pathological changes apart from those associated with aging. Written consent about the use of donor material for scientific purposes had been given by all donors. After the removal of the cornea, the eyecups were wrapped in gauze soaked with saline and stored at 4°C until further processing. On a sterile workbench, the sclera was cut open and the lens, iris, vitreous humour, and retina were removed. Afterwards, the RPE/choroid complex was detached using sharp forceps and collected.

For isolation of LF, first, the RPE/choroid complex tissue taken from the human donor eyes was comminuted in 0.25 M sucrose solution with the Ultra-Turrax device at 30,000 rpm. Further homogenisation was then carried out by hand with a Teflon pistol and finally in an ultrasonic bath. After centrifugation at 6,000 g, both the auto-fluorescence intensity (Ex: 360/40 nm, Em: 590/35 nm) for identification of LF and the protein concentration according to Bradford were determined in the supernatants. The supernatant from the above centrifugation was then subjected to ultracentrifugation for 60 minutes at 103,000 g and 4°C. A discontinuous gradient of eight different sucrose solutions was used. The gradient was then decreased in 1 ml increments, and the autofluorescence was measured in each millilitre.

2.5.2 Characterization of Isolated Fractions

The product obtained was characterised not only by its autofluorescence but also by the content of nitrotyrosine, protein carbonyls and methylglyoxal. Intensity and protein concentration were re-measured. See figure 2.1.

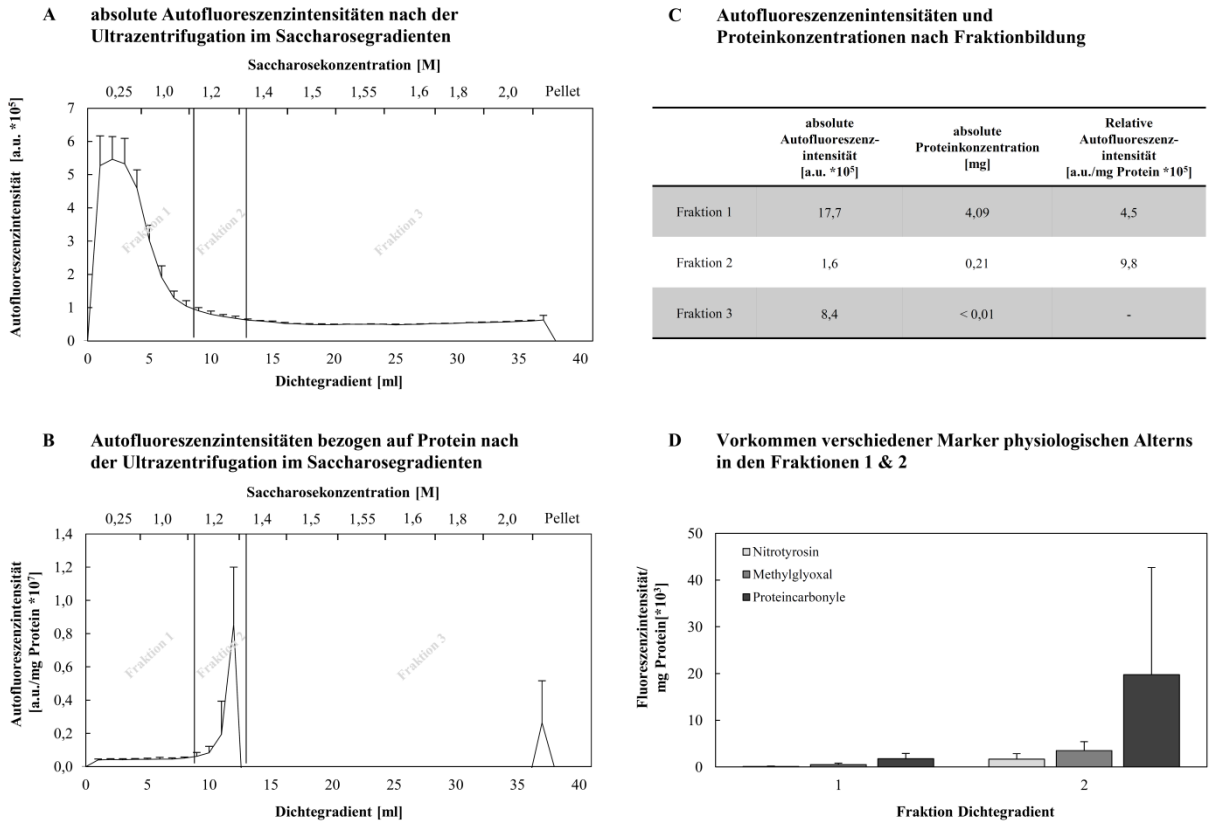

	absolute Autofluoreszenz-intensität [a.u. *10⁵]	absolute Proteinkonzentration [mg]	Relative Autofluoreszenz-intensität [a.u./mg Protein *10⁵]
Fraktion 1	17,7	4,09	4,5
Fraktion 2	1,6	0,21	9,8
Fraktion 3	8,4	< 0,01	-

Fig. 2.1: Exemplary Results of LF Isolation (Prof. T. Grune and Dr. J. König, Potsdam).
A. shows the auto-fluorescence intensities in the sucrose gradient after ultracentrifugation. Most of the autofluorescence was recovered after the centrifugation in the starting solution (0.25 M sucrose solution) and not separated. If one relates the auto-fluorescence intensities to the protein content of the samples. one recognises an accumulation of auto-fluorescent material in the 1.2 M sucrose fraction. **B**. Upon receipt of these data, the samples were pooled to form 3 fractions from the sucrose gradient: fraction 1 consisted of the first 8 ml, fraction 2 of millilitres 9-12 and fraction 3 formed the remainder of the gradient. **C**. Auto-fluorescence intensities and protein concentrations were also determined from these fractions. In addition, these fractions were assayed for the presence of nitrotyrosine, protein carbonyls and methylglyoxal by dot blot and appropriate antibodies. **D**. The intensities of the dots of the fractions were evaluated by an infrared detection system and standardised to protein contents. It was found that in fraction 2 over fraction 1 the amount of nitrotyrosine, methylglyoxal and protein carbonyls is increased. Since no signal of these parameters was detectable in fraction 3, it is not shown here.

2.6 Animals

For the present study, ~~wild-type~~ C57BL/6J mice were used. All mice came from the ZTE and were kept in our own animal facility. All experiments were performed in accordance with the ARVO Statement for the Use of Animals in Ophthalmic and Vision Research and the EU directive 2010/63/EU. They were approved by the local authorities (LANUV, Recklinghausen, Germany, file number 84-02.04. 2016. A395). Mice were held in ventilated cages at a 12 hours/12 hours' light/dark cycle with standard food and drinking water ad libitum.

Two groups of mice were used in this study. In the first group, designated as "young mice", animals were 3-6 months old, whereas mice of the second group were 14-24 months old ("old mice").

2.7 Subretinal Injection of LF Suspensions

Injections were performed in mice of approximately between 4 to 21 months. The animals were anaesthetised by inhalation anaesthesia with 2% isoflurane in oxygen. The eye of the mouse was pulled and rotated slightly. The conjunctiva was opened, and a sharp 30 g cannula is used to cut an opening in the sclera approximately half a millimetre behind the limbus. Through this opening, a blunt 33 g cannula is inserted almost tangentially to the globe and moved along the fundus along about 1.0 to 1.5 mm as close as possible to the back of the eye. Thereafter, a volume of 1 µl of the LF suspension is injected. As a negative control, a volume of 1 µl of the sterile PBS is injected. Sham intervention was performed by just inserting the needle into the eye beneath the retina without any injection. After another three to four seconds, the cannula is slowly pulled out of the eye and the eye is turned back to its original position. After the injection, mice were brought back into their cage and allowed to recover. Figure 2.2 shows the principle of subretinal injection.

In total, sham injection was performed in 8 young mice. All of them did not receive eye drops. PBS was injected intravitreally in 17 young and 18 old mice. Out of these animals, two young mice and four old mice received PBS eye drops, one young mouse received minocycline eye drops, and 2 mice received TKP eyedrops, three old mice received minocycline eye drops, and

three mice TKP eye drops. LF suspension was injected in 23 young mice and 27 old mice. Out of these animals, one young mouse and five old mice received PBS eye drops, two young mice and five old mice received minocycline eye drops, and two young mice and five old mice received TKP eye drops.

In figure 2.2, the principle of subretinal injection is outlined, and next to it an example of an eye of the mouse is shown, into which a suspension of fluorescent beads ("micro beads") was subretinally injected. It turns out that the subretinal injected fluid spreads over a larger area.

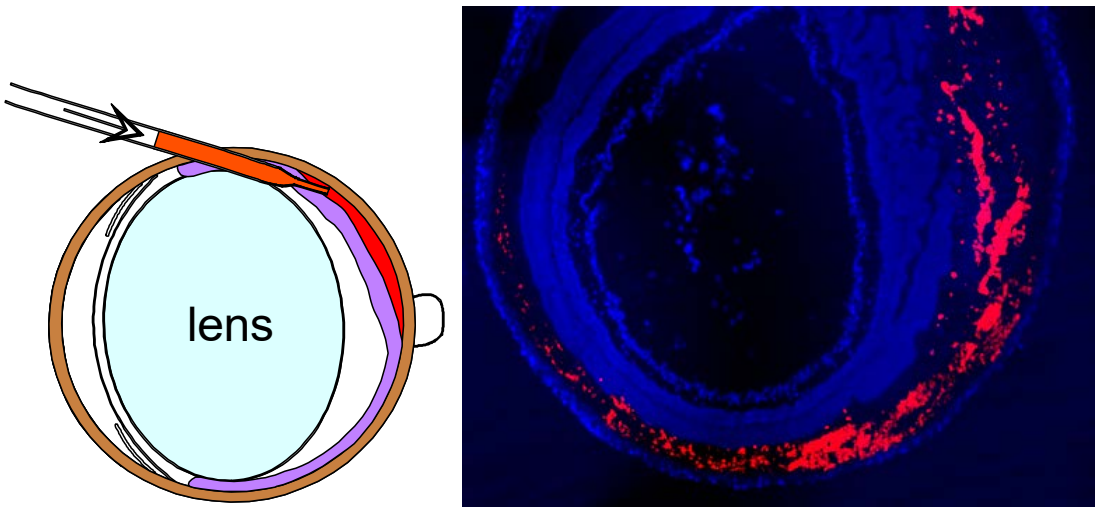

Fig. 2.2: Subretinal Injection.
Left: Schematic representation of the subretinal injection. Right: Frozen section of a mouse eye after subretinal injection of a suspension of fluorescent beads ("micro beads") used to test the injection procedure (Courtesy of Peter Heiduschka).

2.8 The Inhibitors of Microglia

Two different agents were used in this study. They are the tripeptide threonine-lysine-proline (TKP) (JPT Peptide Technologies GmbH, Berlin, Germany), and minocycline (Mino) (Sigma Aldrich, M9511).

In some of the animals injected with LF, 5 µl of PBS or solutions of 1 mg/ml of the peptide TKP or minocycline in PBS were applied topically daily on each eye.

2.9 Electroretinography (ERG)

For the ERG measurements, the animals were anaesthetised by an intraperitoneal injection of a mixture of 130 mg/kg ketamine and 2.7 mg/kg xylazine. The sleeping animals were placed on a heating pad. The pupils of mice were fully dilated with 1% tropicamide eye drops and 5% neosynephrine eye drops. The cornea was desensitised with proparacaine.

For the ERG measurement, the commercial measuring device RetiPort from Roland Consult (Brandenburg) was used. For the duration of the measurement, the animals were on a thermostated plate at 37°C to prevent cooling of the animals. For the measurement, gold ring electrodes were placed on the cornea of the eyes without damaging the cornea. As the reference electrode, another gold electrode was used, which was moistened with saline and placed into the mouth of the animals. After the measurement, the still sleeping animal was kept in a separate box and was brought back in the cage after awakening. Figure 2.3 shows the mouse on the platform of the ERG device during the measurement.

Fig. 2.3: ERG Measurement (Courtesy of Peter Heiduschka). Gold ring electrodes were placed onto the cornea of the eyes of the anaesthetised mouse that was placed on a heated platform of the ERG device during the measurement.

In this project, scotopic and photopic ERG were measured. Scotopic ERG was measured at six different light intensities (0.0003, 0.003, 0.03, 0.3, 3 and 30 cd·s/m²). Isolated oscillatory potentials were measured at 30 cd·s/m². Photopic ERG measurement was performed with a backlight of 25 cd/m² at four light intensities (1, 3, 10 and 100 cd·s/m²), isolated oscillatory potentials at 100 cd·s/m² and the 30 Hertz flicker ERG at 3 cd·s/m². In order to assess whether

and to what extent injection of LF and the use of inhibitors influence retinal function, the parameters of the different experimental groups resulting from the measurements were compared. For the evaluation, the amplitudes, and latencies of the a- and b-waves and the b/a ratio in the animals of the experimental groups were recorded, as well as the amplitudes and latencies of the oscillatory potentials and the amplitudes of the 30-Hertz flicker ERG.

2.10 *In vivo* Imaging by OCT

For *in vivo* imaging by OCT, mice were anaesthetised and the pupils dilated as described above. Then the mice were put in front of the "Spectralis" device from Heidelberg Engineering and were examined by optical coherence tomography (OCT) (see figure 2.4). Formation of cataract was delayed by dropping distilled water onto the eyes.

Fig. 2.4: Examination of the Mouse Eyes by OCT.
The anaesthetised mouse was placed on a platform in front of the OCT device with a 20D lens during the *in vivo* imaging.

2.11 Tissue Processing and Fluorescent Immunohistochemistry

Animals were killed by cervical dislocation and eyes were isolated at different time points after injection depending on kind of experiment (7, 14, 21 or 28 days with eye drops, or 0, 1 day, 3, 5, 7 days, or about 1 month, 6 months without eye drops, as indicated in the Results section).

At least two females and two male animals were used in every group, and typical examples are shown in the results section. Eyes were fixed in 4% paraformaldehyde for 1 hour, washed 2× in PBS pH 7.4 for 5 minutes and frozen in NEG-50™. Cryo sections (thickness 10 µm) were cut using a Cryostar NX70 cryostat (Thermo Fisher Scientific), placed on Starfrost Advanced Adhesive glass slides (Engelbrecht) and were stored at -20 °C until used for histology and immunohistochemistry.

Sections were blocked with Power Block™ reagent (HK085-5K, BioGenex) at room temperature for 6 minutes, then washed 3× with 0.1 M PBS and incubated overnight with primary antibodies at 4°C. The sections were then washed 3× with 0.1 M PBS and incubated with appropriate secondary antibodies for 1 hour at room temperature. Primary antibodies were diluted with 1% bovine serum albumin containing 0.1% Triton X-100, and secondary antibodies were diluted with 1% bovine serum albumin (BSA). The nuclei were counterstained for 7 minutes at room temperature with DAPI (4′6′-diamidino-2-phenylindole dihydrochloride) diluted with pure water 1:300. Finally, sections were washed 3× with 0.1 M PBS and mounted under glass coverslip using mounting medium (Immu Mount ™ Thermo Scientific).

We optimised dilutions of antibodies for best specific staining and lowest possible background fluorescence. For all secondary antibodies, so-called “negative controls” were performed, *i.e.*, staining procedures were performed where primary antibodies were omitted. Non-specific background staining was not seen in any case. All antibodies and their dilution used for immunohistochemistry are listed in Table 2.

Primary Antibodies

Specificity	Host	Supplier	Catalogue No.	Dilution
CD11b	rat	Serotec	MCA711	1:60
CD45	rat	Santa Cruz	sc-59071	1:20
GS	guinea pig	Synaptic Systems	367005	1:400
GFAP	Rabbit	Abcam	ab290	1:100
Iba1	guinea pig	Synaptic Systems	234 003	1:500
Iba1	Rabbit	Wako	019-19741	1:50
NeuN	guinea pig	Synaptic Systems	266 004	1:600
IL6	Rabbit	Abcam	ab6672	1:200
TNF-α	Rabbit	Abcam	ab6671	1:60
VEGF-R1	Rabbit	Abcam	ab32152	1:200
VEGF-R2	Rat	Abcam	ab51873	1:50
HIF-1α	Rabbit	Abcam	ab179483	1:50
CXCL2	Rabbit	Abcam	ab25130	1:500
P2rX4	Goat	Santa Cruz Biotechnology	sc-15187	1:10
VEGF-A^{164}	Goat	R+D System	AF-493-NA	1:10
FGF2	Goat	Santa Cruz	sc-1390	1:200

Secondary Antibodies

Specificity	Host	dye	Supplier	Catalogue No.	Dilution
Anti-Goat	Donkey	TexasRed AF594	Life technologies	A11058	1:200
Anti-Guinea pig	Goat	Alexa Fluor 488	Abcam	ab150185	1:400
Anti-Rabbit	Goat	Alexa Fluor 594 TR	Abcam	ab150080	1:800
Anti-Rabbit	Donkey	Alexa Fluor 488	Dianova	711-547-003	1:200
Anti-rat	Rabbit	Texas Red	Abcam	ab6732	1:600
Anti-rat	Goat	Alexa Fluor 488	Life technologies	A11006	1:200

Table 2: Antibodies Used in this Study

Negative controls were obtained by omitting the primary antibody during staining procedures.

For digital imaging, an epifluorescence microscope (EVOS fl, Advanced Microscopy Group, USA) was used to acquire images. Moreover, confocal microscopy was carried out using the Zeiss ELYRA/LSM 780 microscope (Carl Zeiss Microscopy, Jena, Germany) with 40× and 63× plan-apochromat oil-immersion objectives, a four-channel filter set (BP 420-488, BP 495-575, BP 570-650, LP 655) and an electron-multiplying CCD camera. Images were processed with ZEN imaging software. We made sure that filters in both microscopes showed only fluorescence of the appropriate fluorescent dye.

2.12 Counting the Cells in Histological Sections

Cells showing immunoreactivity for Iba1 and CD11b were counted in digital images of at least three different samples using Adobe Photoshop™, choosing at least three different images of every sample. Areas with a length of 400 μm and a height of 200 μm were selected in the images of retinal sections, and cells were counted using the counting tool of Photoshop. Cell counts are given as medians with median absolute deviation. Procedure of counting is demonstrated by an example given in figure 2.5.

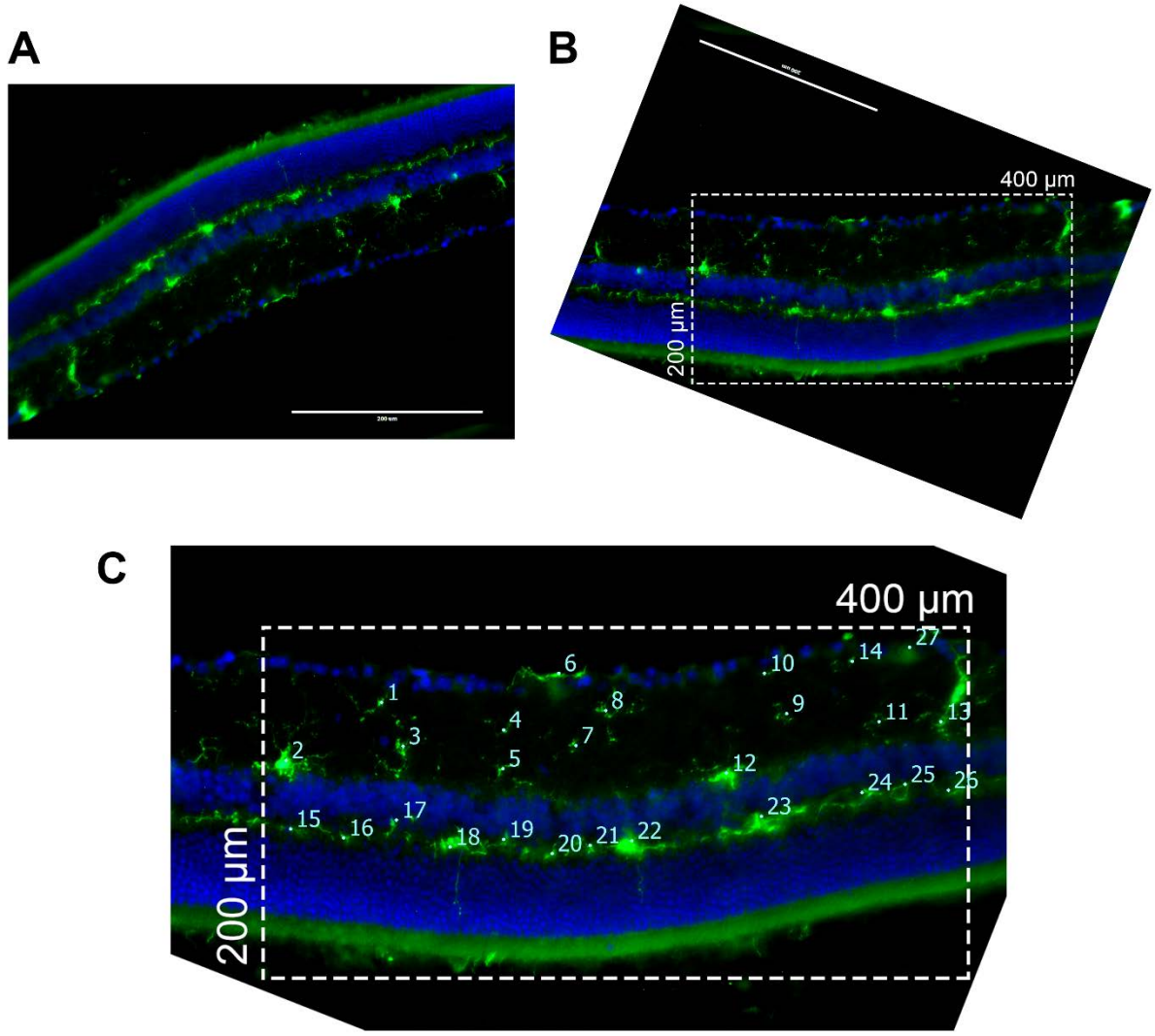

Fig. 2.5: Example for Counting Cells in Mouse Retina.

A) Original image Iba1 staining (green), 28 days after injection of LF, PBS eye drops. **B)** Rotation of the image to a horizontal orientation of retinal layers and definition of the rectangular area in which cells were to be counted. **C)** Use the counting tool in Photoshop, microglial cells (Iba1 positive cells, green) were counted.

2.13 Measurement of Thicknesses of RPE and Retina

Thicknesses of RPE and retina of mouse eyes were determined in both OCT images and digital images of untreated frozen sections using Adobe Photoshop™. For further explanation (see figure 2.5).

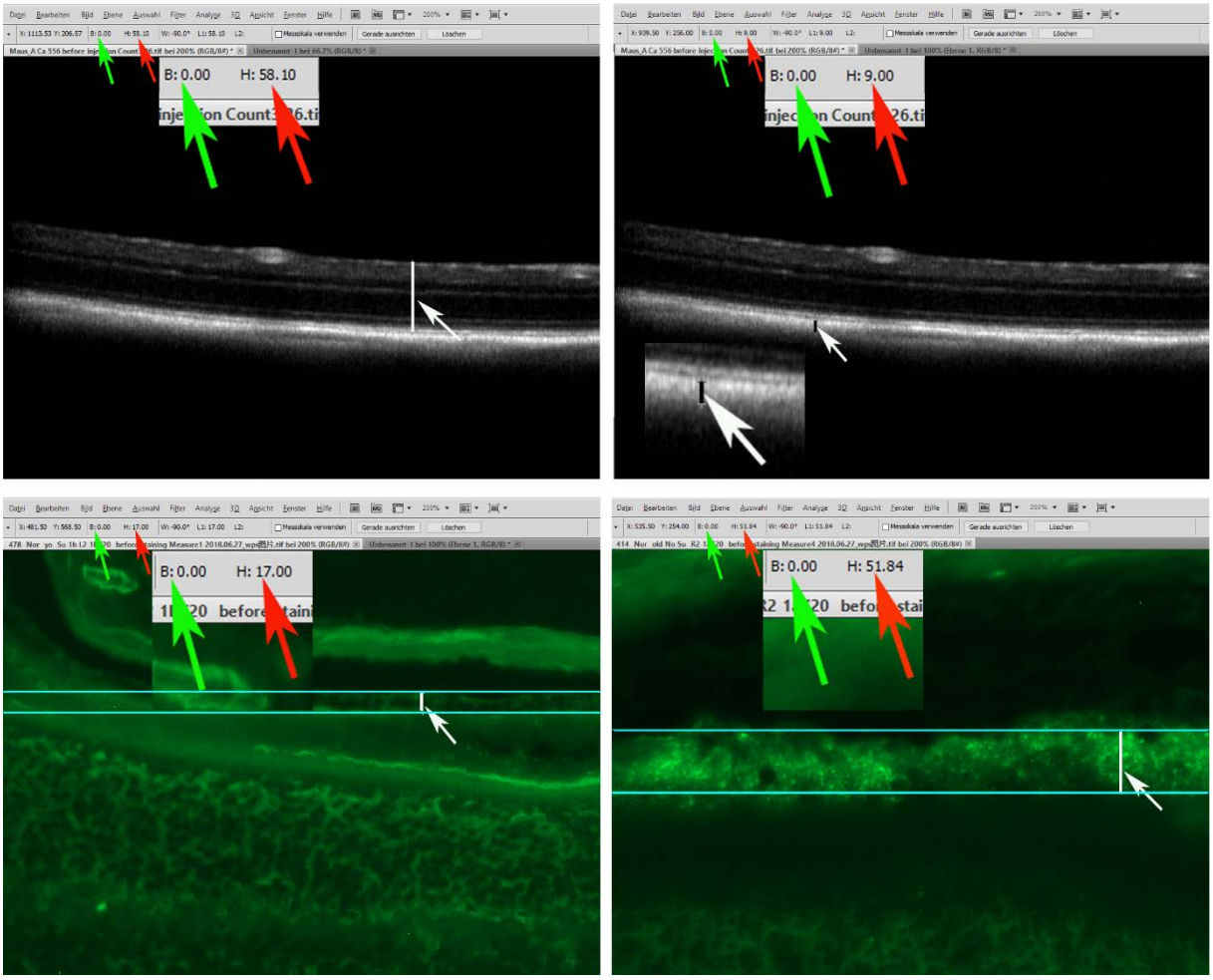

Fig. 2.6: The Thickness of RPE.

The top row shows OCT images. On the left side, determination of retinal thickness is shown, and on the right side determination of the thickness of RPE. The bottom row shows autofluorescent images of frozen sections before staining that were used for measurement of RPE thickness. On the left side, the retina of a young (4 months old) mouse is shown, on the right side a retina on an old (1.5 years old) mouse. The white arrows point to the position of the RPE, and the red arrows point to the number showing the thickness of the RPE. Green arrows point to the number of widths, which value of zero (B:0.00) indicates that the lines used for the thickness measurement (indicated by white arrows) are running exactly vertically.

2.14 Investigation of Gene Expression by Quantitative PCR

To prepare the material for qPCR, eyes of the mice were isolated and stored in PBS on ice before further processing not longer than 5 minutes. The retina and the RPE-choroid complex were isolated separately from the mouse eyes and put into 3.5 µl β-mercarptoethanol in 350 µl lysis buffer, so that the effects of the treatments on the retina and the RPE could be assessed separately.

The samples were stored at -80℃. The tissue was homogenised, and the total RNA was purified from the samples following routine procedures. The mRNA was isolated using the RNeasy® Mini Kit (50) (QIAGEN, cat. no. 74104, Hilden, Germany) with QIAshredder(250) REF 79656(QIAGEN) and RNase-free DNase Set(50) REF 79254(QIAGEN), according to the manufacturer's instructions. After determining the purity and the concentration of the obtained mRNA, it was rewritten into cDNA with the aid of the enzyme reverse transcriptase using the High Capacity cDNA Reverse Transcription Kit iScript^{TM} cDNA Synthesis Kit (BIO RAD), Cat.#170-8891, Applied Biosystems, Foster City, CA, USA. The Power SYBR® Green PCR Master Mix is used for the subsequent quantitative (real-time) PCR. A control without a template (cDNA) and an approach with RNase-free water instead of the template are carried out as controls. This is followed by the relative quantification of the expression of the target gene for the expression of the reference gene using the $2^{-\Delta\Delta Ct}$ method. This protocol is established in our laboratory and has also been used successfully in other projects. qPCR was performed with samples from injected mice. Eyes of some non-injected mice served as an additional control. For the characterisation of gene expression, primers of genes are listed in Table 3.

Gene Expression Assay	Order Number
Actb (beta Aktin) housekeeping gene	Mm02619580-g1
GapDh housekeeping gene	Mm99999915-g1
CCL2	Mm00441242-m1
FGF-2	Mm00433287-m1
IL-6	Mm01210733-m1
IL-1b	Mm99999061-mH
CXCL1(KC)	Mm04207460-m1
RPE-65	Mm00504133-m1
P2rx4	Mm00501787-m1
VEGF-α	Mm01281449-m1
VEGF-R1 (Flt1)	Mm00438971-m1
VEGF-R2 (Kdr)	Mm01222419-m1
TNF-α	Mm99999068-m1
HIF-1α	Mm00468869-m1

Table 3 Gene Expression Assays Used in this Study

2.15 Electron Microscopy

Electron microscopy was performed by Dr. Uwe Hansen (Institute for Experimental, University Hospital of Münster, Münster, Germany).

The eyes of treated and untreated mice were removed and immediately fixed in 2% (v/v) formaldehyde and 2.5% (v/v) glutaraldehyde in 100 mM cacodylate buffer, pH 7.4, at 4ºC overnight. After washing in PBS, the eyes were post fixed in 0.5% (v/v) osmiumtetroxide and 1% (w/v) potassium hexacyanoferrate (III) in 0.1 M cacodylate buffer for 2 h at 4ºC followed by washing with distilled water. After dehydration in an ascending ethanol series from 30 to 100% ethanol, specimens were incubated two times in propylenoxide each for 15 min and embedded in Epon. Ultrathin sections were cut with an ultramicrotome, collected on copper grids, and negatively stained with 2% uranyl acetate for 10 min. Electron micrographs were taken at 60 kV with a Phillips EM-410 electron microscope using imaging plates (Ditabis, Pforzheim, Germany). As LF was injected subretinally, we chose locations of typical appearance in the region of photoreceptors, RPE and Bruch's membrane.

2.16 Statistics

Using GraphPad ™ Prism 6 Software (GraphPad Software Inc., La Jolla, CA, USA), levels of significance were calculated and graphs were prepared. Levels of significance were calculated using unpaired Mann-Whitney or ANOVA with Kruskal-Wallis tests. P values of <0.05 were considered statistically significant.

3 Results

3.1 Synopsis

In this study, the effects of sub-retinal injection of human LF in murine retina are researched. It may be hypothesised that microglial cells or/and macrophages take up LF, become activated and elicit an inflammatory reaction that perhaps leads to a retinal pathology. After subretinal injection of LF, we observed the following phenomena: Firstly, microglial cells/macrophages positive for Iba1 are present in the subretinal space, as it was clearly shown in the results of immunostaining and the images of electron microscopy (EM). Secondly, some Iba1 positive cells contain LF granules, as it was clearly shown in the results of immunostaining. Thirdly, the Iba1 positive cells displayed phagocytosis, it results in an increase of some pro-inflammatory cytokines, as shown in the result of immunostaining and qPCR. Moreover, in the measurements of ERG, especially in the scotopic ERG, the amplitudes of a-waves and b-waves decreased two weeks after injection of LF. Fourthly, in the images of OCT, there was a significant difference in the subretinal structural integrity 13 days after LF or PBS injection. After injection of LF, mottled hyper-reflection is visible subretinally. However, after injection of PBS, only a dark area is seen in the subretinal space, which represents most probably liquid. Additionally, measurements of the thickness of the retina and the RPE layer in the OCT images revealed that they were significantly thinner after LF injection. In multi-colour images, reflections are visible only in infrared light 28 days after PBS and sham injection, whereas reflections are visible also in the green and blue channels 28 days after LF injection. In addition, a hyperreflective layer can be seen in OCT images in the same position as these reflections on top of the retina after LF injection, in contrast to sham and PBS injection.

Last but not the least, in the images of EM, it was shown that the labyrinth that is located at the basal side of the RPE loses its normal structure after LF injection. The RPE cells became thinner, some of them are dying, and the Bruch's membrane lost its uniform thickness. Some locations of it became thinner, some other locations much thicker. We also noticed some drusen-like granular deposits in the subretinal space in EM images. Moreover, the RPE cells lost some

melanin particles, and some new grey particles appeared in the RPE cells, most probably LF granules. The microvilli of RPE cells lost their ordered structure and became shorter, and their number decreased. The quite similar phenomenon also occurred with the photoreceptors when LF was injected. At some locations, a big portion of the photoreceptors was lost, and only vaguely see the remnants of few photoreceptors.

3.2 *In vivo* Imaging OCT (Optical Coherence Tomography)

Using the "Spectralis" device from Heidelberg Engineering, we attempted to visualise the subretinally injected LF by its auto-fluorescence, although the chances of success were low due to the low concentration of LF in the injected suspension. In addition, we examined by means of optical coherence tomography (OCT) whether the area of sub-retinal injection can be found by retinal detachment. We also examined the differences among injection of LF or PBS and the sham injection by multi-colour imaging and OCT. Figure 3.1 shows example of imaging of the untreated mouse eye using OCT.

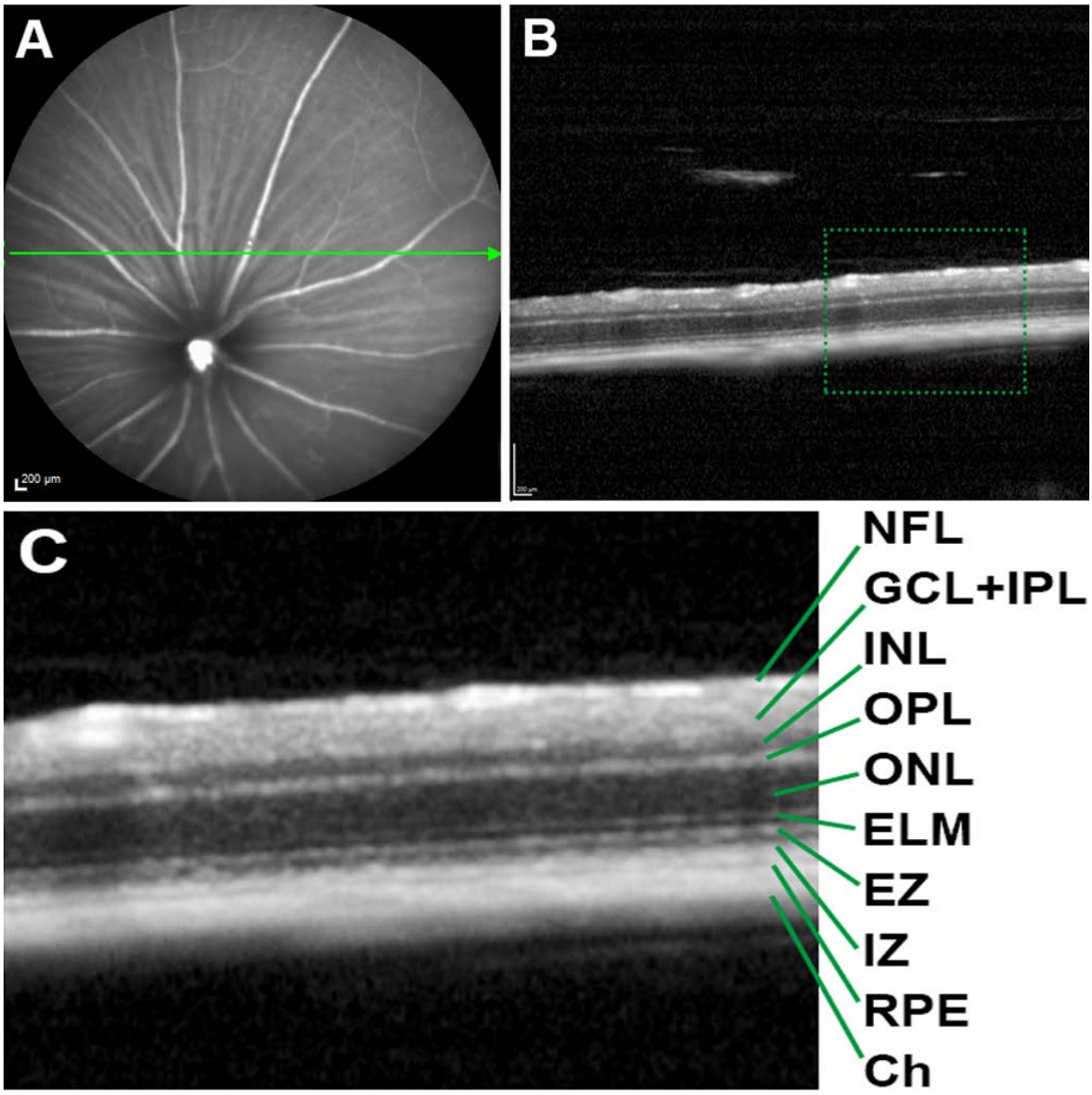

Fig. 3.1: Examples of *in vivo* Imaging of the Untreated Mouse Eye by OCT.

A) was the infrared fundus image of the eye. B) is the OCT sectional image of the retina. The green light line on image A) indicates the location of the OCT scan. C) The individual layers of the retina are clearly visible. Image C was an enlargement of the green square of image B. Abbreviations: NFL- nerve fibre layer, GCL-ganglion cell layer; IPL-inner plexiform layer; INL-inner nuclear layer; OPL-outer plexiform layer; ONL-outer nuclear layer (nuclei of the photoreceptors); ELM: external limiting membrane; EZ: ellipsoid zone; IZ: interdigitation zone; RPE-retinal pigment epithelium; Ch-choroid.

3.2.1 The Detachment of the Retina after Injection

Following sub-retinal injection of lipofuscin, the areas where injection was made were clearly visible in *in vivo* imaging. Dark shadows indicated detachment of the retina, which was also evident in the OCT slice image, see pictures below, figure 3.2.

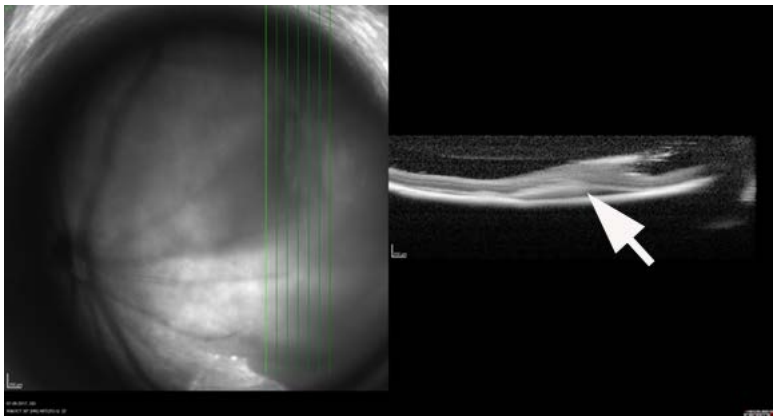

Fig. 3.2: Example of an OCT Image 1 Day after a Sub-retinal Injection.
The detachment of the retina can be seen in the cross-sectional image, which appears in the SLO image as shading (white arrow points to retinal detachment).

Figure 3.3 shows an example of the condition of an eye scarce a month after the injection of lipofuscin. It can clearly be seen that the retina is lifted off over a wide area, while the RPE appears largely intact. As evidenced by OCT cross-sectional images, the RPE is not detached. It should be noted that this was a one and half year-old mouse.

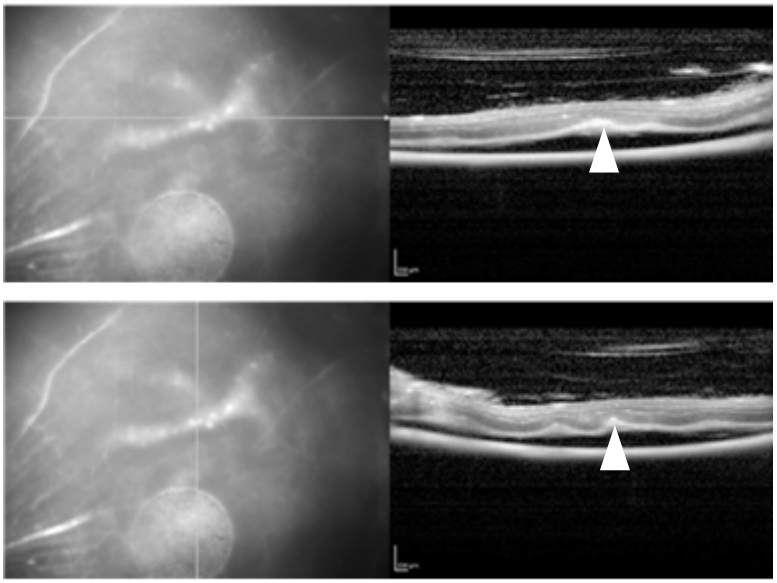

Fig. 3.3: Examples of the Retinal Detachment.
In *vivo* imaging of a one and half year-old mouse 27 days after the subretinal injection of lipofuscin. The white arrowheads point to the gap in the sub-retinal space caused by retinal detachment.

3.2.2 The Auto-Fluorescence of LF in Retina

By raising the amplification in the settings of the device, the injected LF could be visualised by its auto-fluorescence in some mice (see figure 3.4).

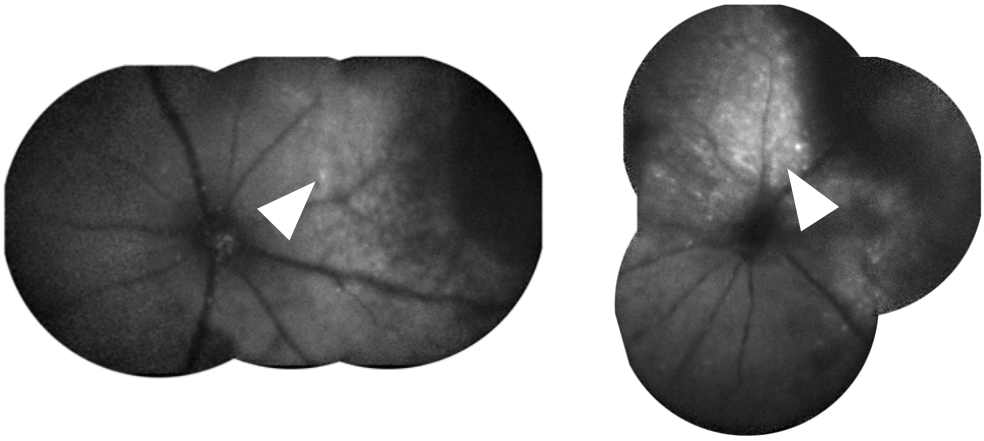

Fig. 3.4: Examples of Auto-fluorescence shortly after Subretinal Injection of LF.
The arrowheads point to the area of enhanced fluorescence.

3.2.3 The Difference between the LF and PBS Injection

The shading in infrared SLO images indicates a detachment of the retina, but the LF seems to have spread further. *In vivo* imaging was also repeated at later times. Here no auto-fluorescence of the injected LF could be detected. The detachment of the retina around the site of injection, however, persisted for a longer period, especially after LF was injected. However, even after the injection of PBS, certain distortions in the structure of the retina remained visible, even if the retina had reattached (see figure 3.5)

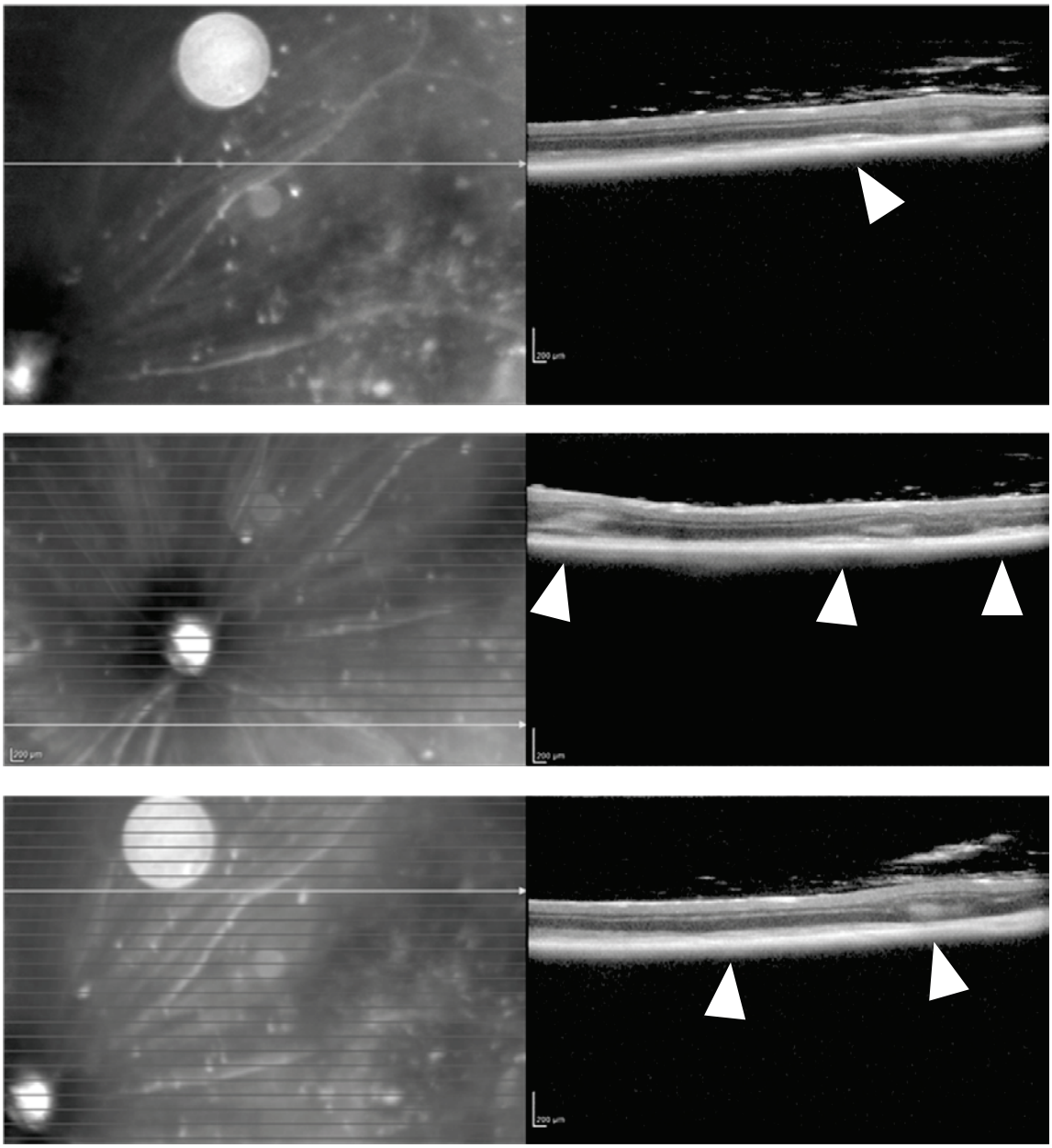

Fig. 3.5: Examples of Changes in the Retinal Structure 6 Days after Sub-retinal Injection of PBS. The white arrowheads point to dislocations of retinal layers.

Interestingly, there was a significant difference in the sub-retinal structure 13 days after LF and PBS injection. In the former, mottled hyper reflection is visible subretinally. In the latter case, only a dark area is seen in the subretinal space, most probably liquid (see figure 3.6).

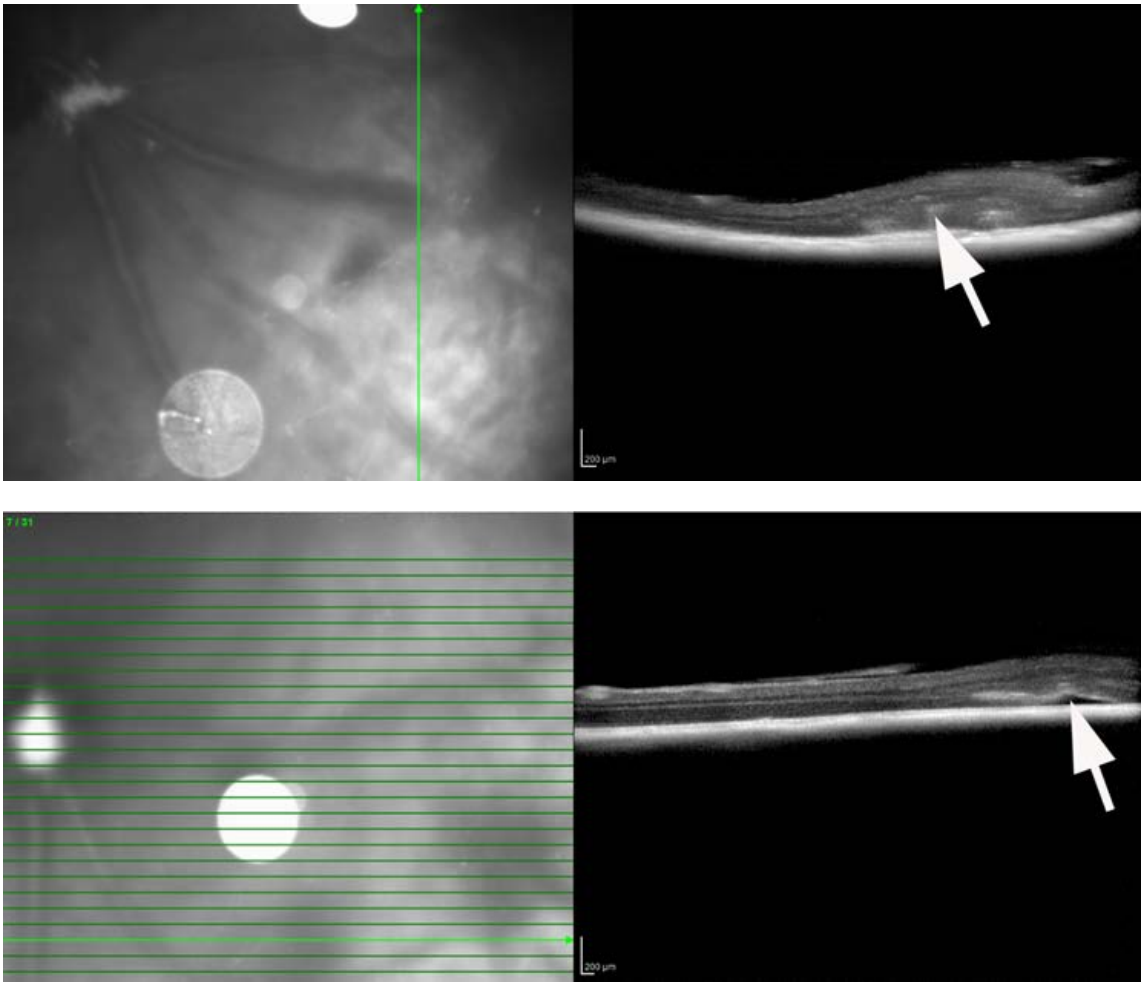

Fig. 3.6: Difference between LF and PBS Injection 13 Days.
First row OCT shows after LF injection d13. Second row OCT shows after PBS injection d13. Both are one and half year-old mice. The arrows point to the sub-retinal area.

3.2.4 The Difference among the Sham, PBS and LF Injection is Visible in Multicolour Images and OCT

The multi-colour images show clear reflections only in the infrared channel after PBS and sham injection, and a slight reflection in the blue and green channels after PBS injection. In contrast, clear reflections are visible also in blue and green channels after LF injection, indicating autofluorescence 14 and 28 days after LF injection. After sham treatment (insertion of the needle) or after intravitreal injection of PBS or lipofuscin, reflection is seen in the area of injection in the infrared channel. The size and intensity of this reflection decrease clearly in the sham-treated eye or after injection of PBS, whereas it remains clearly visible after injection of

lipofuscin. No autofluorescence is visible in green and blue channels after sham treatment or PBS injection, whereas a gradually increase of autofluorescence can be seen after injection of lipofuscin (see figure 3.7).

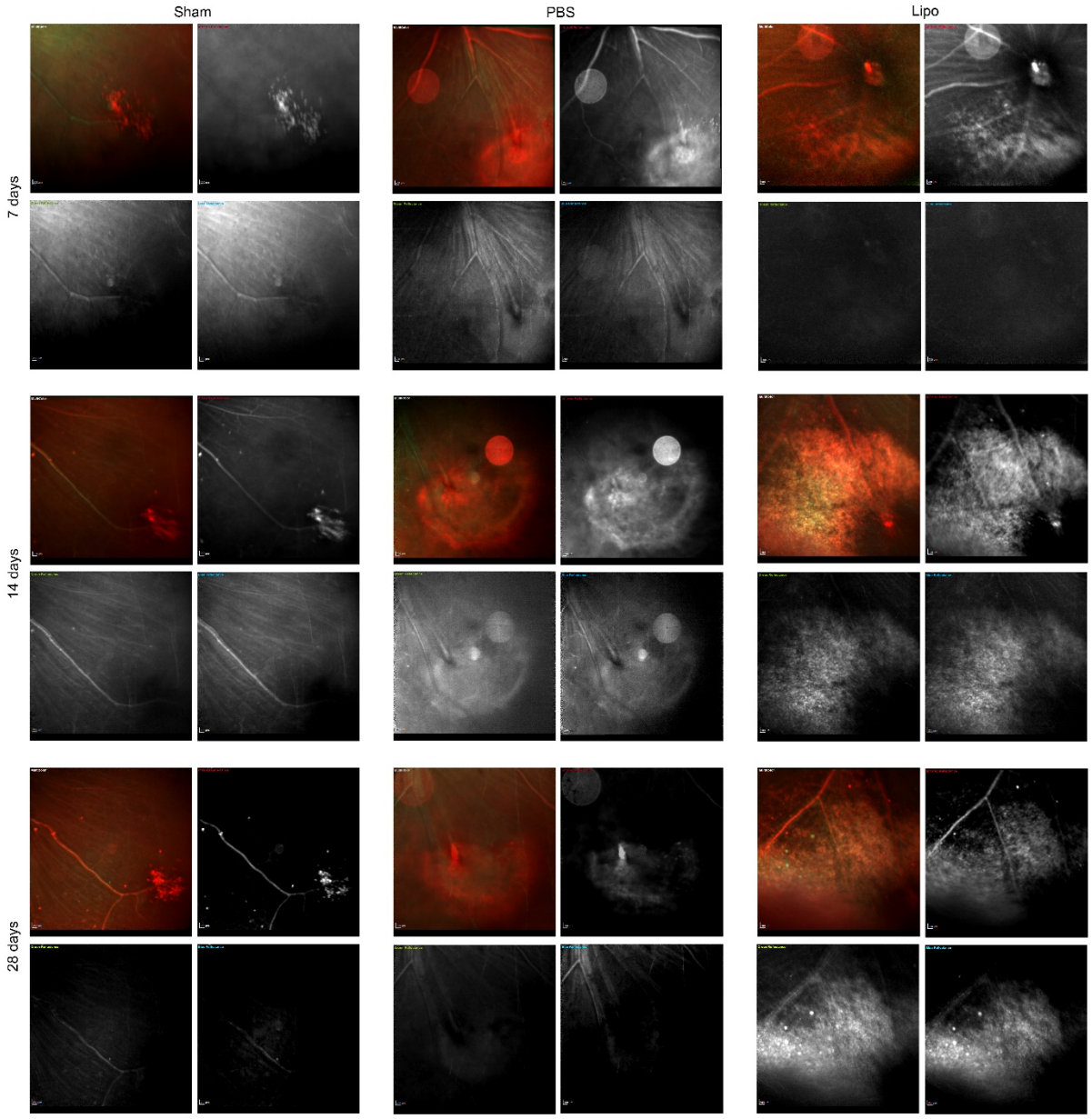

Fig. 3.7: Multi-colour Images Obtained 7 Days, 14 Days, and 28 Days after Subretinal Injection of PBS or Lipofuscin, or after a Sham Injection as Indicated.
Whereas some reflection in the infrared channel remains after all treatments, autofluorescence in green and blue channels is visible only after injection of LF.

In OCT images, the hyperreflective layer on top of the retina can be seen in the same position as the injection site after LF injection. However, it cannot be seen after sham and PBS injection (see figure 3.8)

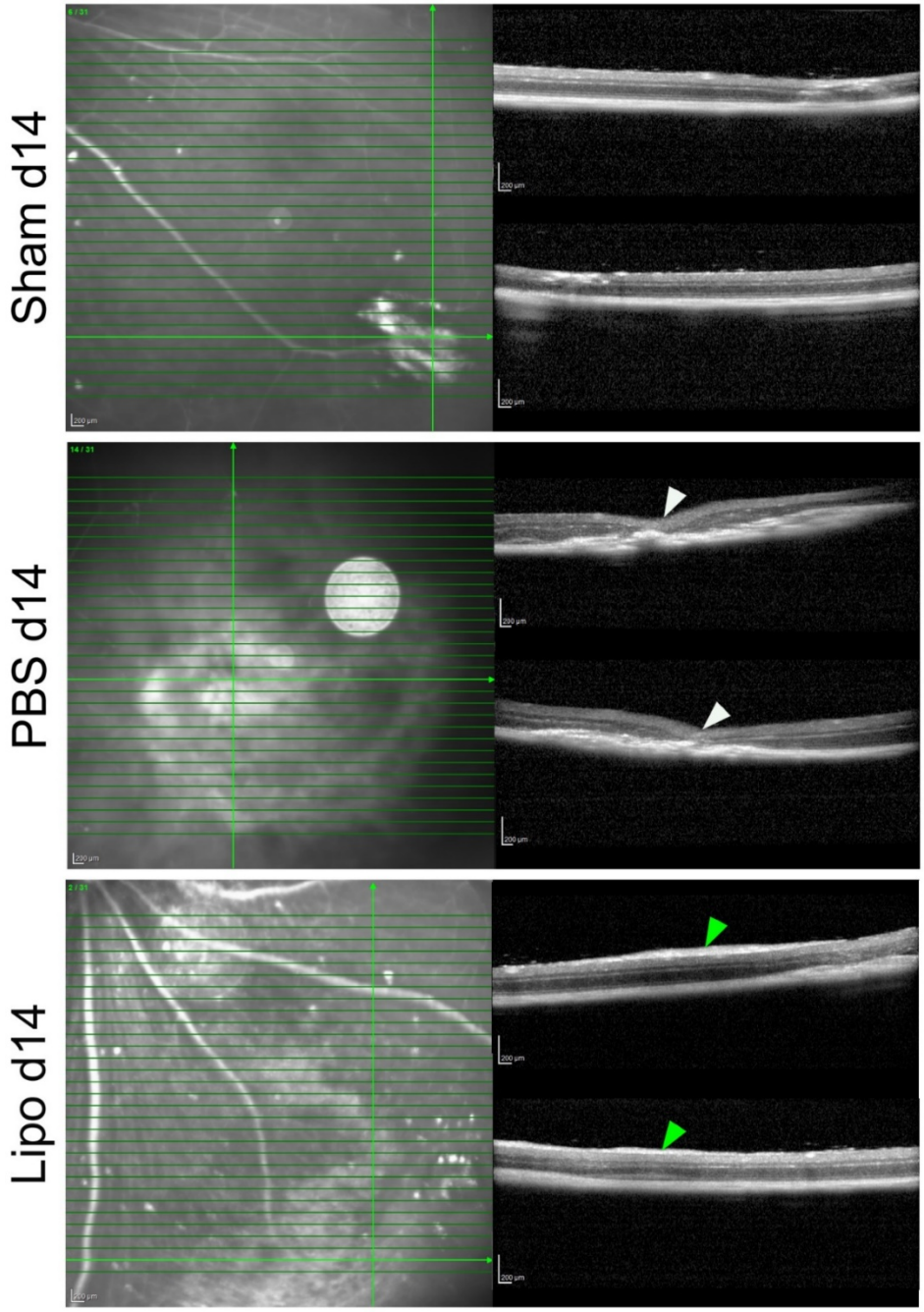

Fig. 3.8: OCT Images Obtained 14 Days after Subretinal Injection of PBS or Lipofuscin, or after a Sham Injection as Indicated.

The white arrowheads in PBS injection show local depression, *i.e.*, PBS injection position. The green arrowheads in LF injection show the hyper reflective layer on top of the retina. The top rows in all these three images are horizontal scan, the bottom rows show vertical scan.

3.2.5 The Thickness of RPE and Retina Measured in OCT Images

The thickness of RPE and retina was determined in the OCT scans using Adobe Photoshop™. OCT scans were taken at three different positions, exactly through the optic nerve, in a distance of approximately two times the diameter of the optic nerve head, and through the injection site, named in the following diagrams centre, nearby the optic nerve, and injection site, respectively (see figures 3.9, 3.10 and 3.11). Number of animals for these three figures is given in legend of figure 3.9.

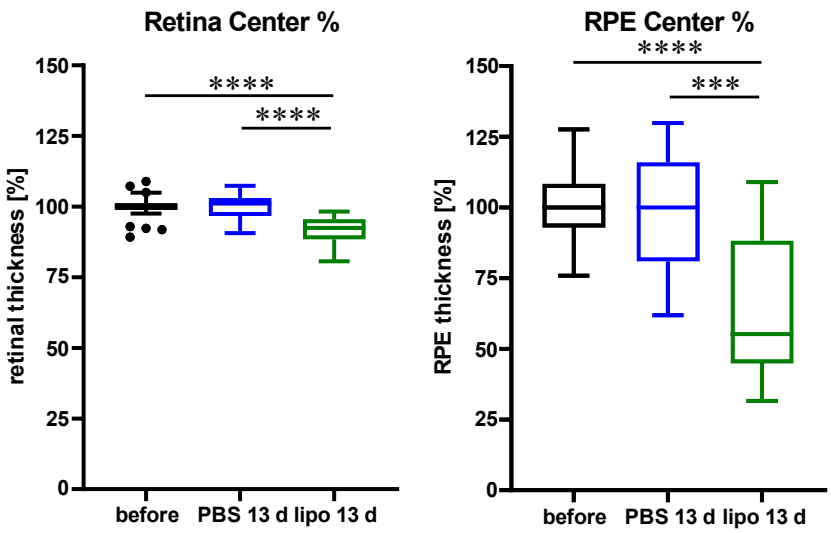

Fig. 3.9: The Thickness of Retinal and RPE in Centre.
Comparison of retinal and RPE thickness in the centre position before injection and 13 days after injection of PBS or LF as indicated. Thickness of the retina and the RPE is significantly smaller after LF injection than before injection and 13 days after injection of PBS. There is no significant change between retina and RPE thicknesses before injection and 13 days after injection of PBS. 45 images of six control mice and 19 images of three mice 13 days after injection of PBS and 19 images of three mice 13 days after injection of LF were analysed. Data are presented as box plots by the method of Tukey in this and the following diagrams. Statistical significance of the differences between the groups are indicated by *=$p<0.05$, **=$p<0.01$, ***=$p<0.001$, ****=$p<0.0001$ in this and all following diagrams.

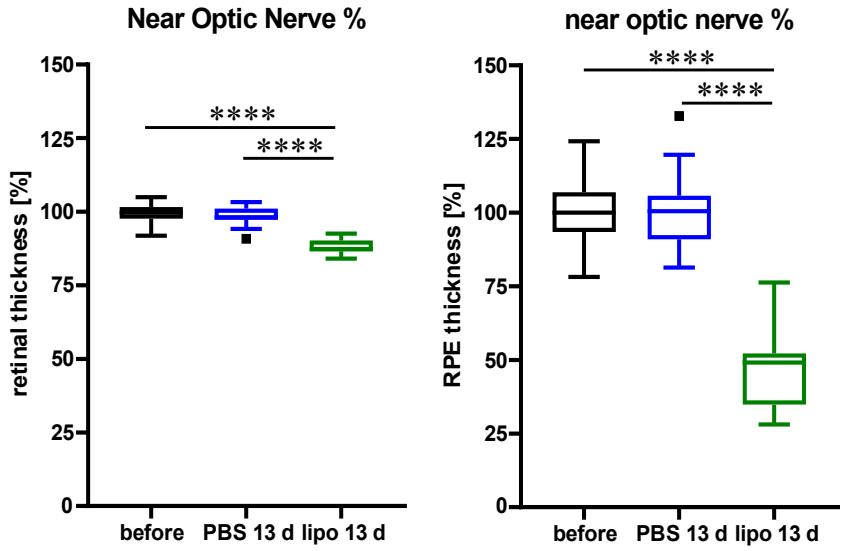

Fig. 3.10: The Thickness of Retinal and RPE Near Optic Nerve.

Comparison of retinal and RPE thickness of near the optic nerve before injection and 13 days after injection of PBS or LF as indicated. Thickness of the retina and the RPE is significantly smaller after LF injection than before injection and 13 days after injection of PBS. There is no significant change between retina and RPE thicknesses before injection and 13 days after injection of PBS.

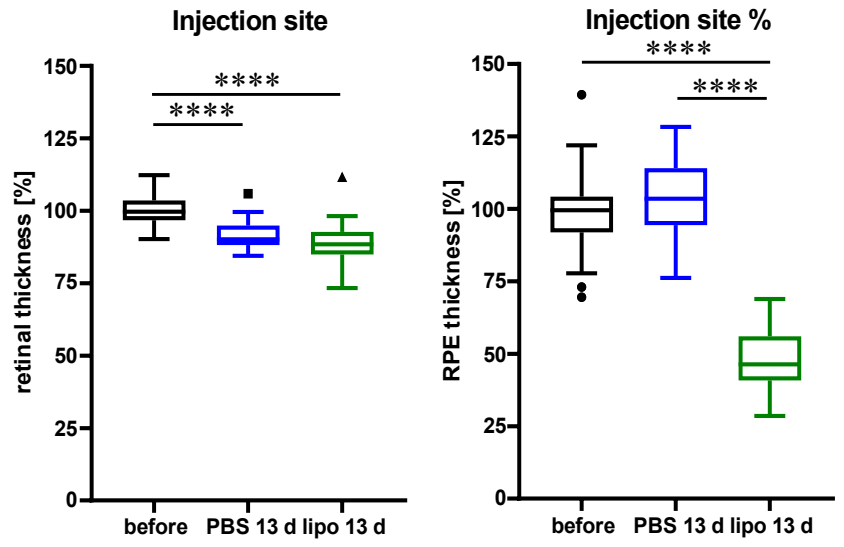

Fig. 3.11: The Thickness of Retinal and RPE in Injection Site.

Comparison of retinal and RPE thickness at the injection site before injection and 13 days after injection of PBS or LF as indicated. There is no significant change between retina thickness 13 days after PBS injection and LF injection, whereas thickness of the retina is significantly smaller after LF and PBS injection 13 days than before injection. However, thickness of the RPE is significantly smaller 13 days after LF injection than before injection and 13 days after PBS injection, and thickness of the RPE 13 days after PBS injection is significantly bigger than before injection.

3.2.6 The Difference among the Sham, PBS, and LF Injection Detected by OCTA

There is no big difference in the appearance and density of blood vessels in the superior layers and the deep layers after sham, PBS, and LF injection near the injection site. No vessels are visible in the avascular zone near the injection site.

At the injection site, there are again only slight differences in the superior and deep layers between the groups. The avascular zone appears to be normal in the sham group, whereas some blood flow is visible after PBS and LF injection (see figure 3.12).

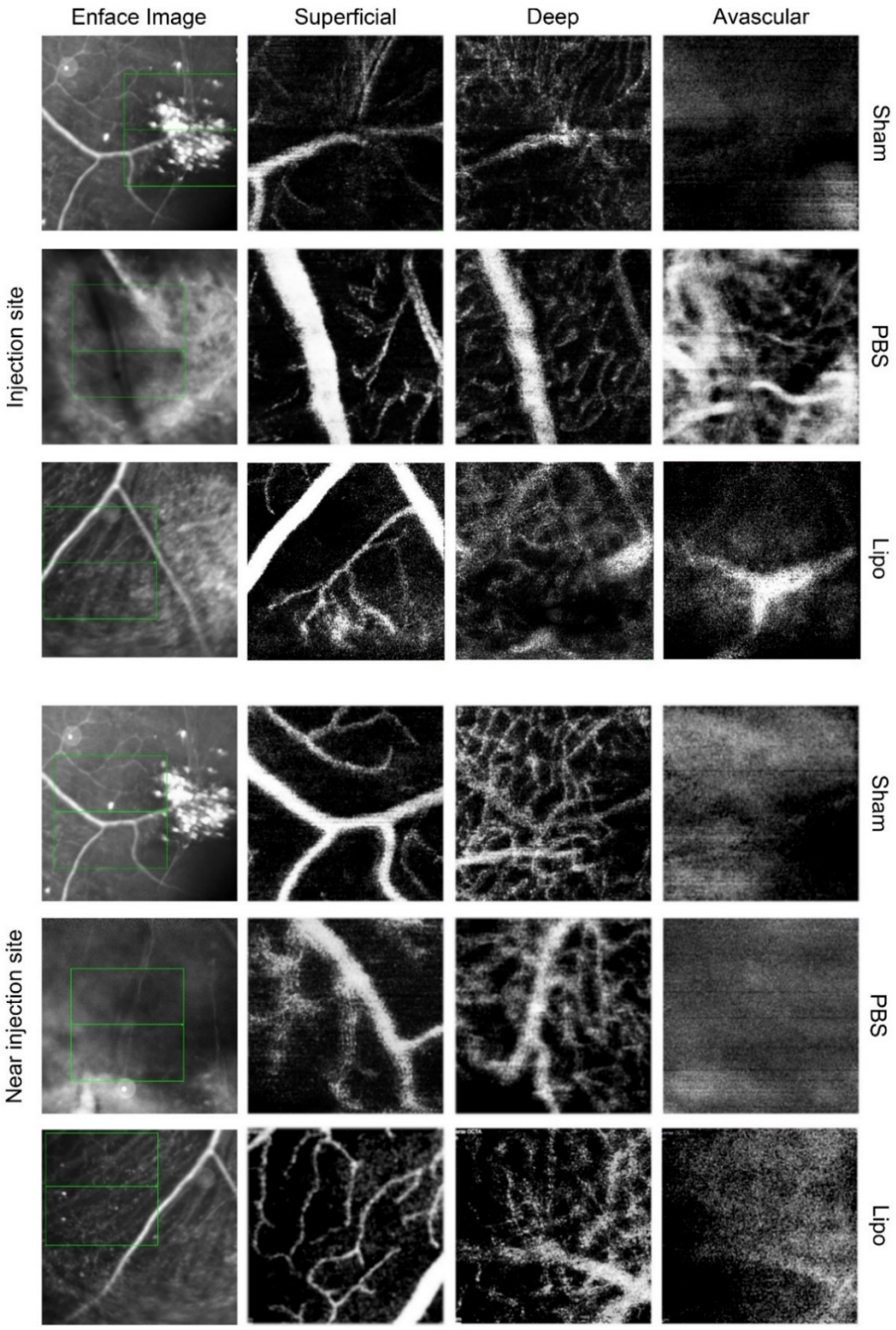

Fig. 3.12: OCTA Images Obtained 28 Days after Subretinal Injection of PBS or LF, or after a Sham as Indicated.

At the injection site, some blood flow is visible after PBS and LF injection in the avascular zone, whereas no blood flow is present in the sham group. Near the injection site, there is no big difference after sham and after PBS or LF injection.

3.3 Investigation of the Function of the Retina Measured by ERG

Electroretinography (ERG) is the standard procedure and the only procedure available for the objective testing of retinal function.

In order to assess whether and to what extent injection of LF and use of the inhibitors influence retinal function, the parameters of the different experimental groups resulting from the measurements were compared. The following figures (figure 3.13, 3.14 and 3.15) are examples of some photopic ERG traces, left side is a young mouse and right one is an older mouse.

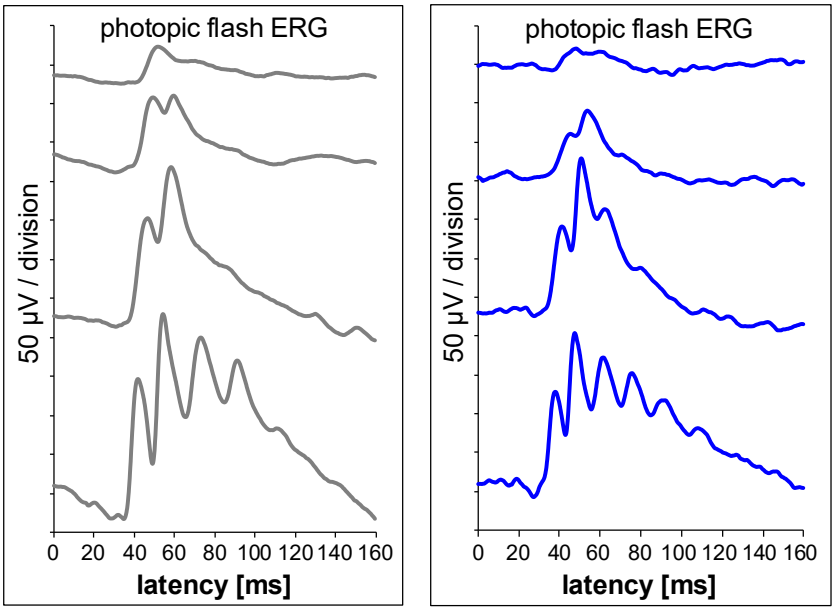

Fig. 3.13: An Example of some ERG Traces.
These four curves result from the four intensities of stimulation mentioned above. At the weakest intensity one hardly recognises an a-wave and only a weak b-wave, whereas at the highest intensity the a-wave is clearly visible and the b-wave is high, additionally superimposed by the oscillatory potentials. Left side: young mouse, right side: old mouse.

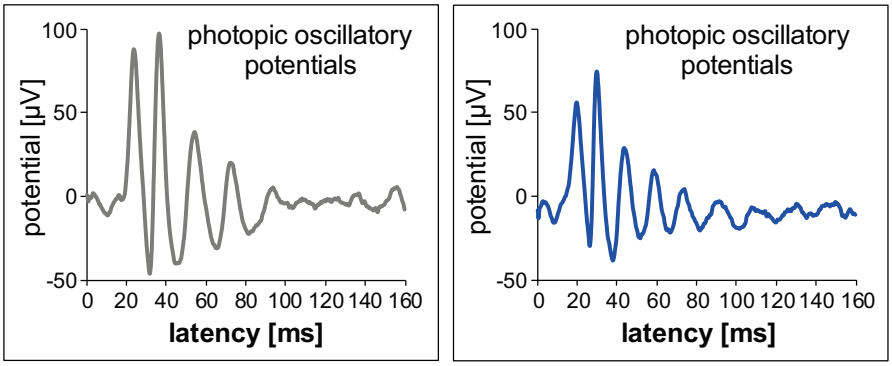

Fig. 3.14: Typical Waveform of Oscillatory Potentials.
By changing the setting of the amplifier's frequency filter from 1-200 Hertz to 50-500 Hertz, the oscillatory potentials can be displayed and evaluated in isolation. The amplitudes and latencies of the first four oscillations are used. Left side: young mouse, right side: old mouse.

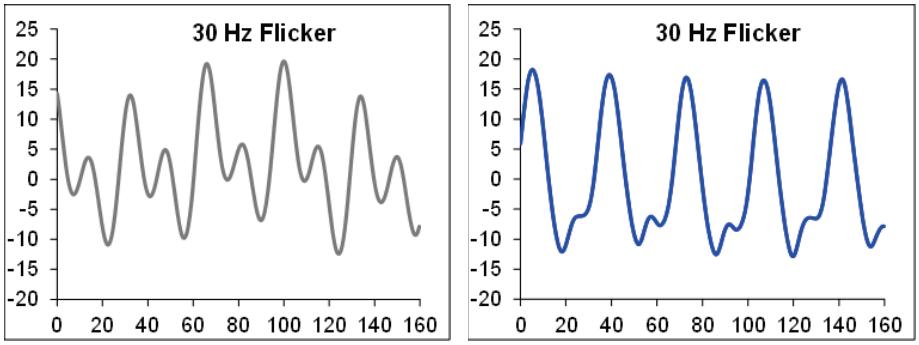

Fig. 3.15: Typical Waveforms of a 30 Hertz Flicker ERG.
By this method, post-receptoral response to cone activity upon a 30-Hertz stimulation can be demonstrated. Left side: young mouse, right side: old mouse.

ERG measurements were carried out before and at certain times after the subretinal injection. The resulting parameters obtained one or two weeks after sham or injection of PBS or LF are shown as an example in figure 3.16. These experiments were carried out in younger animals. The latencies in scotopic ERG were in a similar range. Because of the inevitable spread of results, most error bars overlap and it is difficult to make stringent statements about differences between the groups. In contrast, the amplitudes of a-waves first decreased after one week. After two weeks, the amplitudes of a-waves recovered slightly in the sham group, whereas such a recovery was almost not notable after PBS injection. Amplitudes of a-waves decreased even more two weeks after the LF injection. A similar picture could be found in the amplitudes

of b-waves, with the slight recovery two weeks after PBS injection better visible than in the a-wave amplitudes (see figure 3.16).

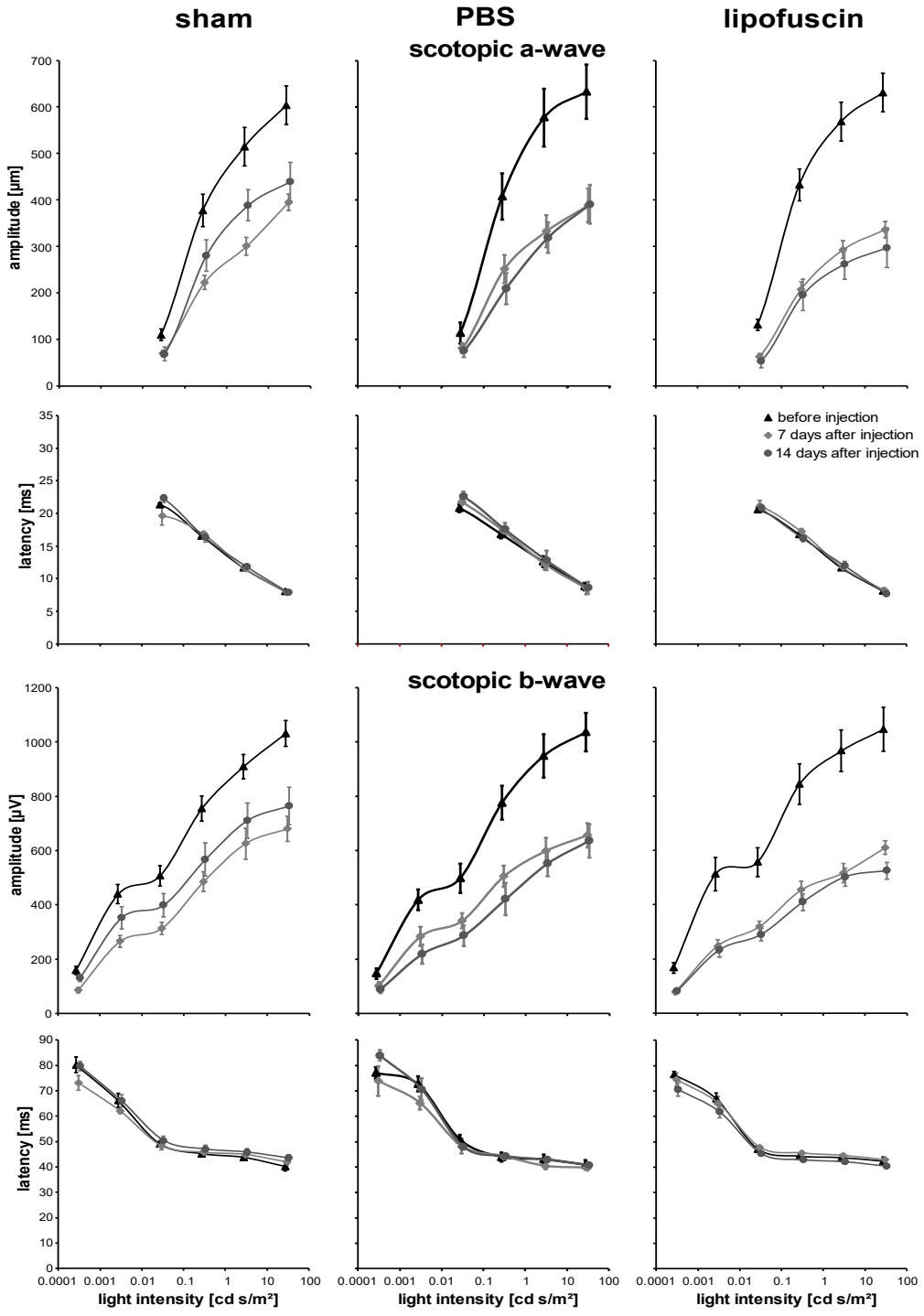

Fig. 3.16: Scotopic Amplitudes and Latencies before Injections and after 7 and 14 Days.
Data are shown as mean values and standard deviations. Number of animals in the sham, PBS, and LF groups: before treatment n=5, n=6 and n=6, after one week n=5, n=6 and n=6, after two weeks: n=5, n=3 and n=6, respectively.

Similar to the situation in the scotopic ERG, the latencies in the photopic ERG were in a similar range in all three groups before treatment and one or two weeks later.

In sham injection group, no stringent statements can be made about changes of a-wave amplitudes after treatment. However, it is clear that the amplitudes of b-wave first decreased one week after the sham injection and then recovered two weeks after injection. In PBS injection group, the amplitudes of a-wave first decreased one week after the injection and then decreased more two weeks after injection, whereas the amplitudes of b-wave first decreased after one week the injection and recovered slightly after two weeks. In the LF injection group, the amplitudes of a-waves first decreased one week after the injection and then recovered slightly two weeks after injection; however, amplitudes of b-wave first decrease one week after the injection and almost did not recover two weeks after injection (see figure 3.17).

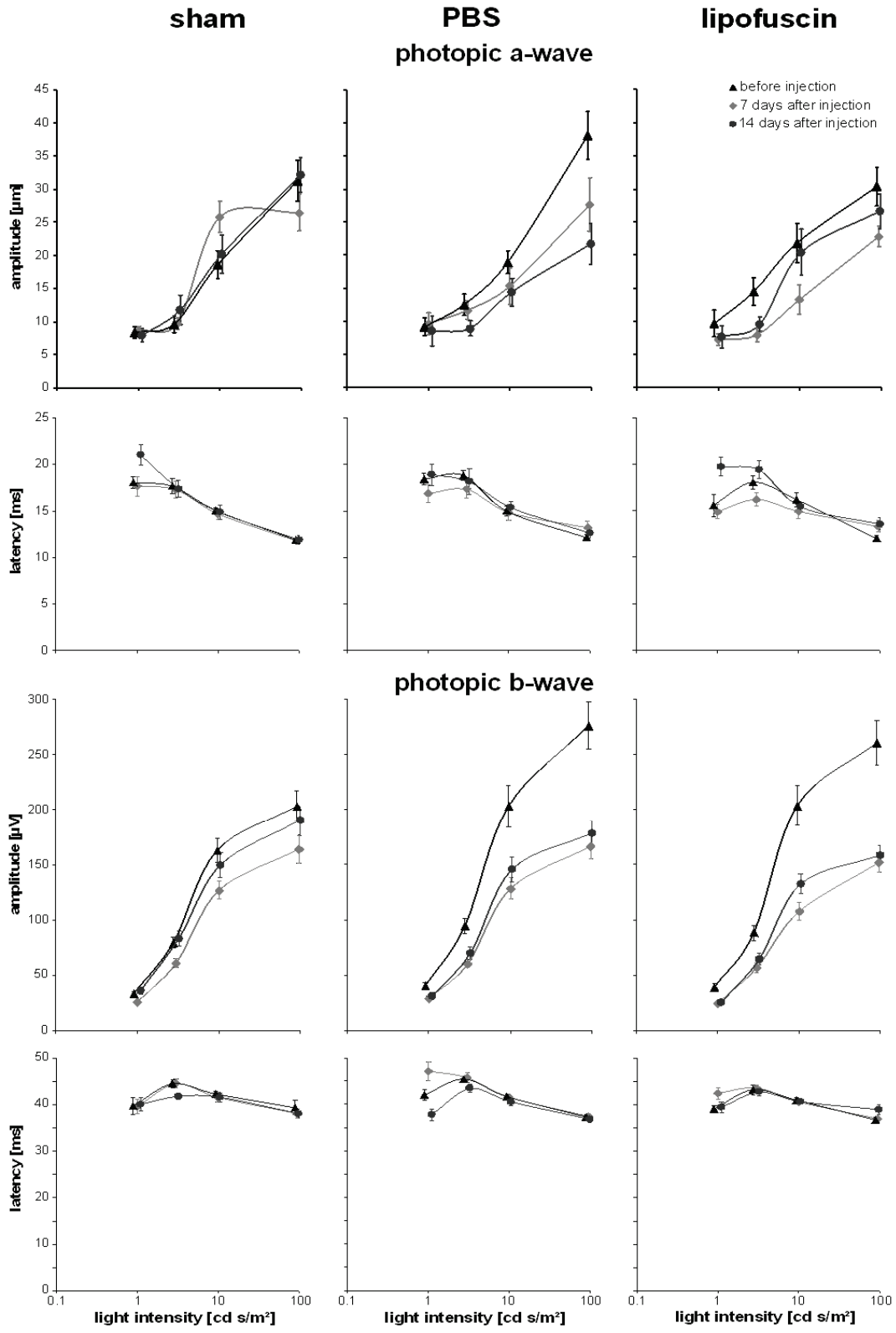

Fig. 3.17: The Photopic Amplitudes and Latencies of before Injections and after 7 or 14 Days. Number of animals in the sham, PBS, and LF groups: before treatment n=6, n=14 and n=11, after one week n=6, n=7 and n=8, after two weeks: n=5, n=8 and n=8, respectively. Mean values are shown, with error bars showing S.E.M.

All changes of amplitudes in photopic and scotopic ERG at highest intensities of light stimulus are summarised in figure 3.18. In the photopic ERG, a reduction of a-wave amplitudes was found after injection of PBS. Amplitudes of b-waves and oscillatory potentials were significantly smaller after injection of PBS or LF, and a slight recovery after two weeks was found only in the amplitudes of oscillatory potentials. There was no difference of the parameters between PBS and LF injections. And yet, there was a significant difference of the parameters between 14 days after sham and LF injections in the photopic b-wave.

Scotopic ERG amplitudes were reduced after sham treatment or injection of PBS or LF, except for the oscillatory potentials of the sham group, which decreased only slightly and were found to be recovered after two weeks. The decrease of all other scotopic parameters was significant, and no clear recovery could be observed. There was no significant difference of the parameters between PBS and LF injections. However, there was a significant difference of the parameters between 14 days after sham and LF injection (see figure. 3.18).

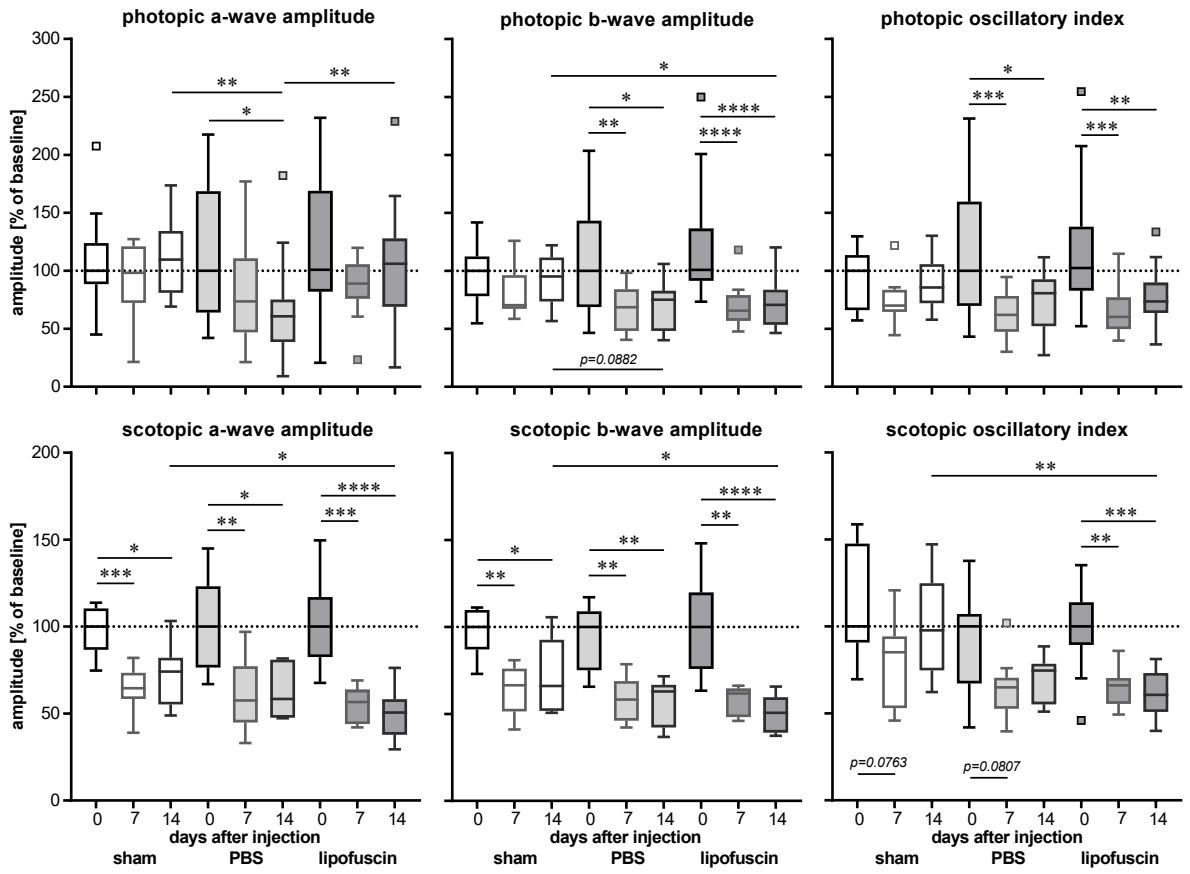

Fig. 3.18: Parameters of Photopic and Scotopic ERG before treatments and after 7 and 14 Days. Box plots after Tukey are shown. In top line (photopic), number of animals in the sham, PBS, and LF groups: before treatment n=6, n=14 and n=11, after one week n=6, n=7 and n=8, after two weeks: n=5, n=8 and n=8, respectively. In bottom line (scotopic), number of animals in the sham, PBS, and LF groups: before treatment n=5, n=6 and n=6, after one week n=5, n=6 and n=6, after two weeks: n=5, n=3 and n=6, respectively. Levels of significance were calculated with ANOVA and Kruskal-Wallis test. Statistical significance of the differences between the groups is indicated by *=p<0.05, **=p<0.01, ***=p<0.001, ****=p<0.0001.

Typical waveforms of the scotopic flash ERG in a mouse before injection and 7 days and 14 days after injection of the LF suspension are shown in figure 3.19. Light intensities of light flashes are indicated on the right side.

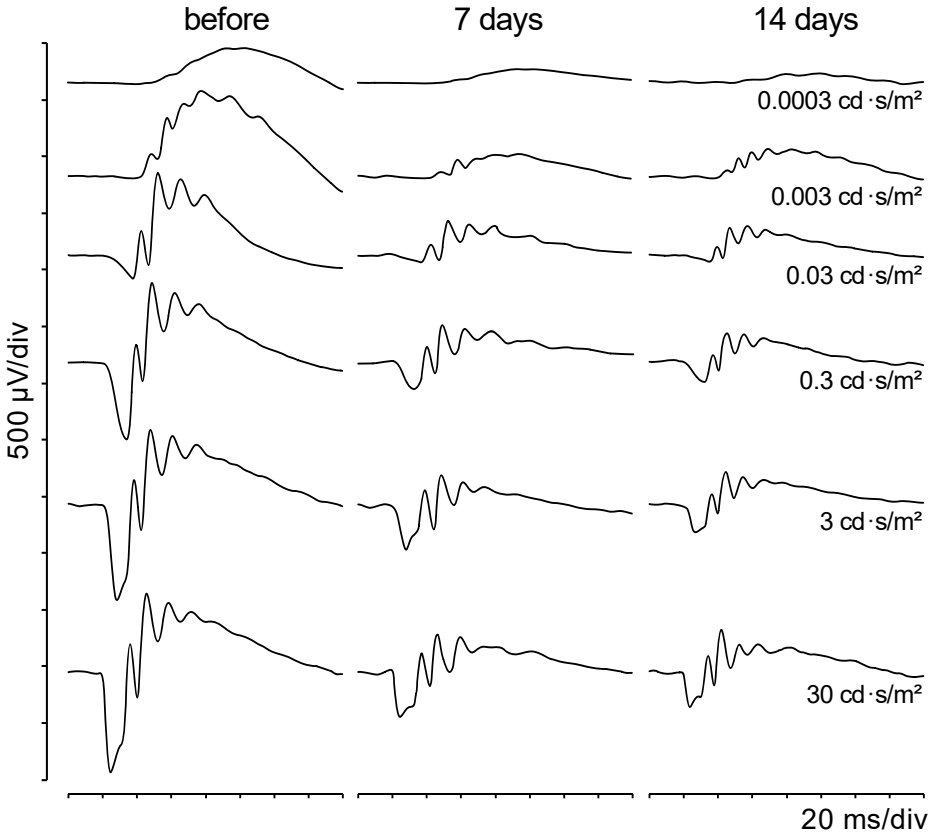

Fig. 3.19: Examples of Waveforms for the Scotopic Flash ERG.
Typical waveforms obtained at different light intensities as indicated are shown for a mouse before injection and 7 days and 14 days after injection of LF.

3.4 Histology

All histological studies were performed on frozen sections.

3.4.1 Distribution of LF Histology

The eyes were examined one, two and four weeks after injection of LF, and the injected LF was to be detected as in the *in vivo* imaging by its auto-fluorescence by exciting the histological samples with 488 nm wavelength light. Significant traces of the injected LF were found in the frozen sections of the eyes, isolated one week after the injection. By contrast, auto-fluorescent LF particles were practically undetectable in the eyes two and four weeks after the injection.

One example is shown in figure 3.20. Many small bright spots are visible in the layer of the inner and outer segments of the photoreceptors, but most are in the RPE. This means that after the injection, LF particles distribute from the sub-retinal space into these layers. Due to which mechanism, it remains to be seen, probably by diffusion. The RPE shows a slight fluorescence. Obviously, RPE cells have also taken up LF, which corresponds to the finding emphasised in the introduction that LF is accumulating naturally in the RPE.

Over time, the level of LF recognisable by its autofluorescence decreases in the retina, and virtually no increased auto-fluorescence was seen in the frozen sections of the eyes two and four weeks after the injection (see figures 3.20, 3.21).

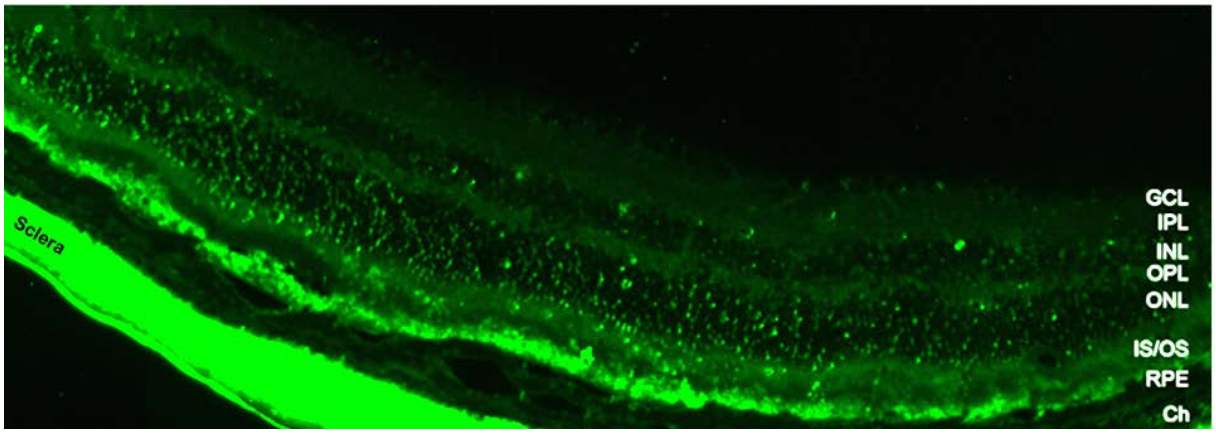

Fig. 3.20: Fluorescence Image of a Frozen Section.
Composite fluorescence image of a frozen section of an eye one week after the sub-retinal injection of lipofuscin. To avoid leaching of the LF particles, further staining of the preparation *e.g.*, with DAPI, was waived. For orientation, the individual retinal layers were labelled using the following abbreviations, and these abbreviations are used also in the following figures: GCL-ganglion cell layer; IPL-inner plexiform layer; INL-inner nuclear layer; OPL-outer plexiform layer; ONL-outer nuclear layer (nuclei of the photoreceptors); IS/OS-inner and outer segments of the photoreceptors; RPE-retinal pigment epithelium; Ch-choroid.

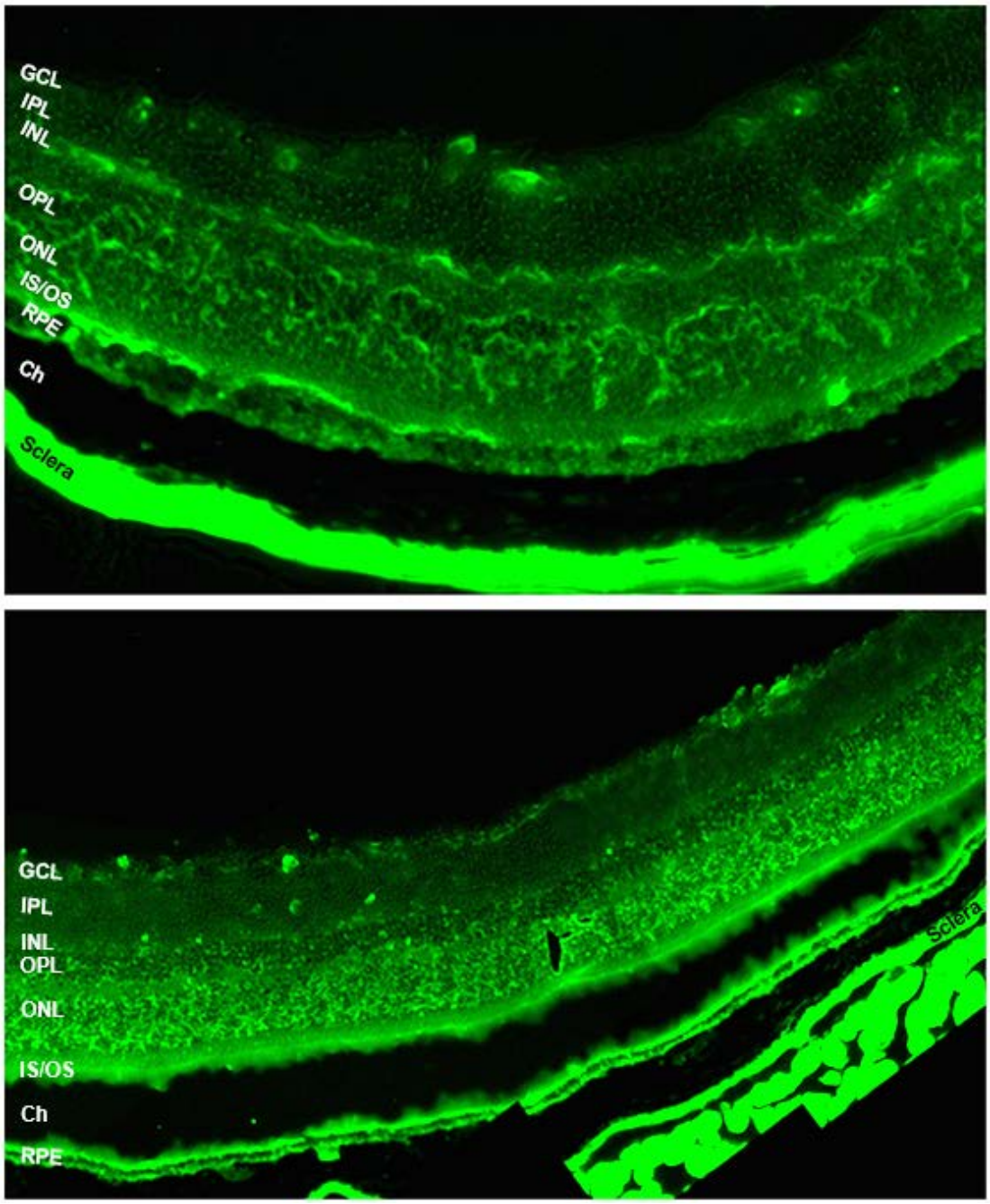

Fig. 3.21: Fluorescence Image of the Other Frozen Section.

Composite fluorescence images of frozen section of one eye two (top) and four (bottom) weeks after sub-retinal injection of lipofuscin. To avoid leaching of the LF particles, further staining of the preparation, *e.g*., with DAPI, waived. In the retina and the RPE very few dots indicating auto-fluorescent LF are to be seen. The granules' size of auto-fluorescent LF is bigger than they are in the retina of one week after sub-retinal injection of lipofuscin. The bright structures on the right side of the lower image are cross-cut auto-fluorescent eye muscles. For abbreviations, see Fig.3.20.

3.4.2 The Behaviour of Microglia

The microglia show a clear reaction to the injection of LF. On the one hand, this manifests itself in a change in the morphology of the microglial cells, in that the processes become shorter and thicker until some of the cells show a pure amoeboid shape. It is also noticeable that several microglial cells are also present in the subretinal space or in the layer of the inner or outer segments of the photoreceptors. This means that these microglial cells must have migrated from their original locations in the inner layers of the retina to the outer layers. As a result, microglial cells can also be seen in places in the outer nuclear layer *i.e.*, they are on the way from the outer plexiform layer to the subretinal space. Later, four weeks after the subretinal injection of LF, most of the microglial cells have returned to their normal location and their normal ramified morphology, and they are found only sporadically in the subretinal space. At this time point, the reaction of the microglia to the injected LF has obviously subsided, especially since, as described above, no more LF was found in the frozen sections (see figure 3.22).

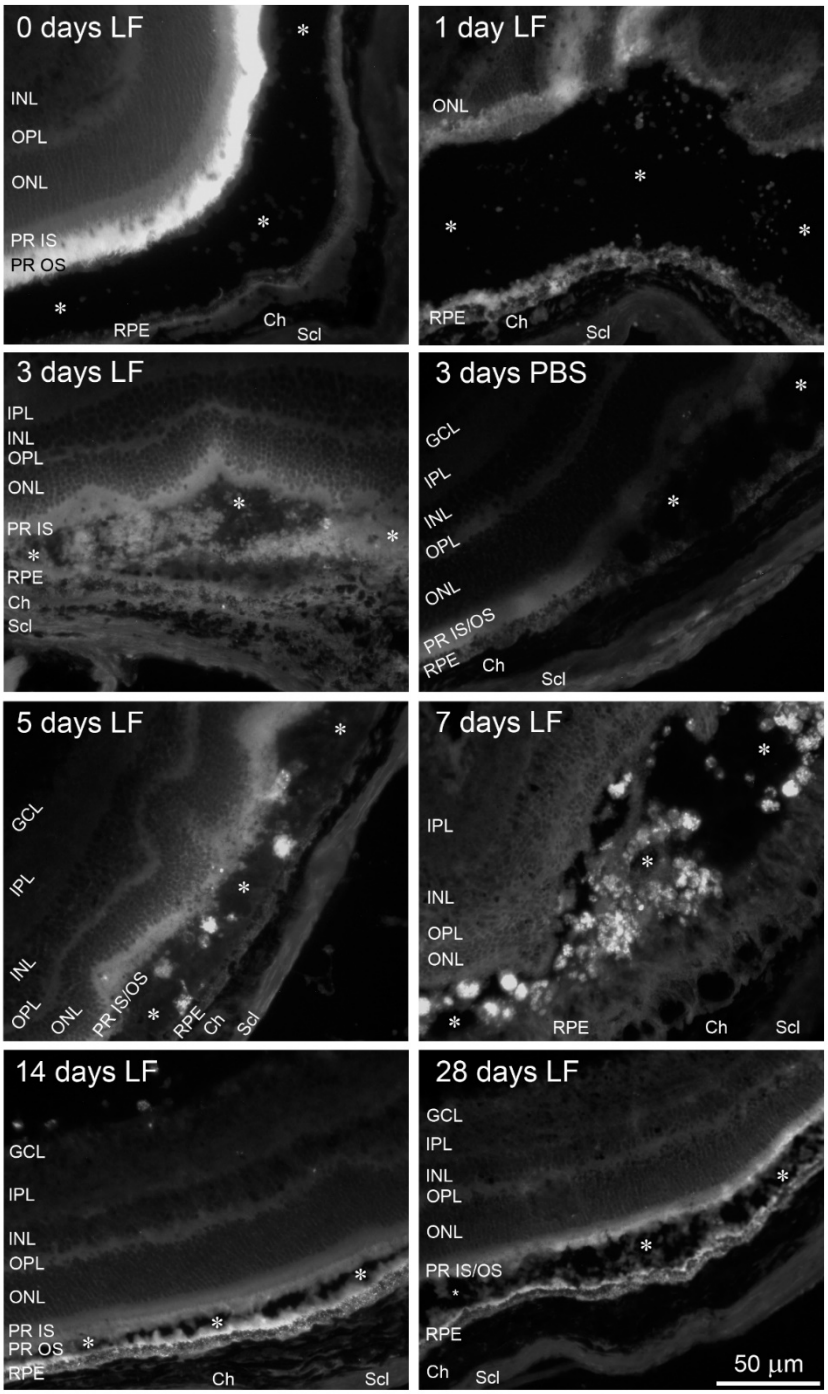

Fig. 3.22: Unstained Sections Obtained on Different Time Points after Subretinal Injection of LF. The figure shows unstained frozen sections of the eyes of older mice at the indicated time points after a subretinal injection of LF. Initially, LF is distributed diffusely in the subretinal space (asterisks), including in the layer of the photoreceptors. After five days, it is concentrated in cells that are in the subretinal space, most likely phagocytic, macrophage-like microglial cells. Later on, the situation calms down and a lot of auto-fluorescence can be seen in the RPE. For abbreviations, see Fig. 3.20. Scale bar: 50 µm.

To make sure which kind of cells containing LF is gathering in the subretinal space, we performed immunohistochemical staining against CD11b. The positive CD11b staining of these cells shows that these are microglia cells and/or macrophages, see figure 3.23.

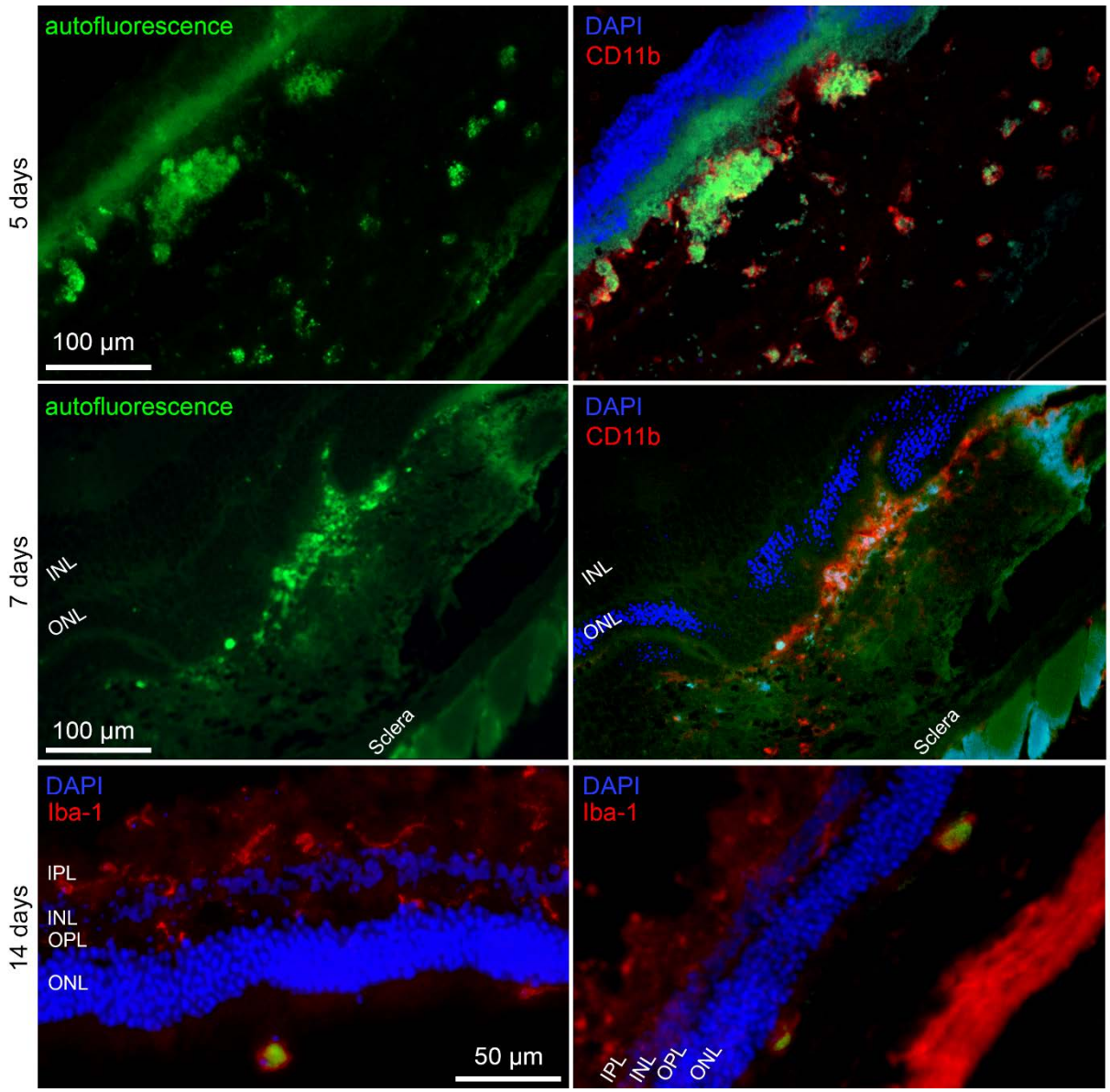

Fig. 3.23.: Freeze Sections of the Microglia Cells Contain Lipofuscin.
Top and middle: auto-fluorescent cells in the subretinal area of the eyes of older mice after injection of LF 5 and 7 days. The positive CD11b (red) staining of these cells shows that these are microglia cells and/or macrophages, the cell nuclei with DAPI (blue). Scale bar: 100 µm. Bottom: an eye of a young mouse two weeks after injection of LF. The microglial cells were stained against Iba1 (red), the cell nuclei with DAPI (blue). In the subretinal space, some Iba1 positive cells can be seen in which there is a lot of green fluorescent material most likely LF. IPL-inner plexiform layer; INL-inner nuclear layer; OPL-outer plexiform layer; ONL-outer nuclear layer (nuclei of the photoreceptors); Scale bar: 50 µm.

Figure 3.24 shows Iba1 positive cells in the eyes of young mice that contain LF 14 days after injection (top image), and auto-fluorescent cells in the sub-retinal area of the eyes of older mice 5 and 7 days after the injection of LF (bottom line).

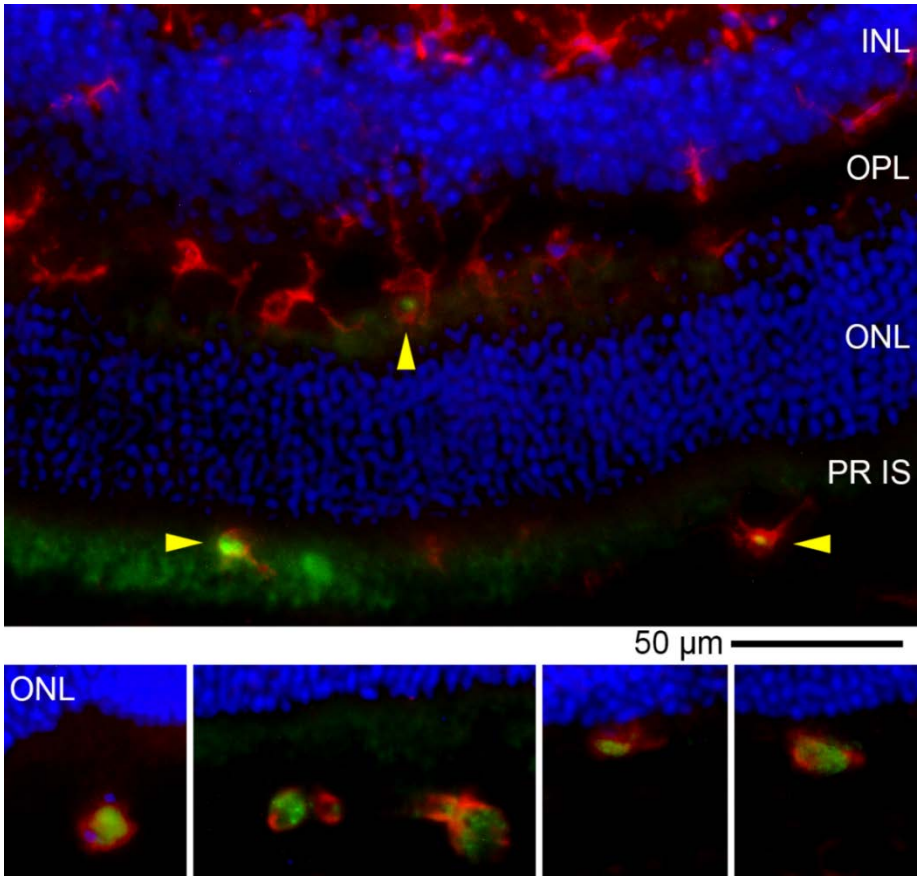

Fig. 3.24: Iba1 Positive Cells Contain LF Granules.
Cryosections of an eye 14 days after injection of LF (top). Microglial cells were labelled with an antibody against Iba1 (red). The yellow arrow heads and the lower images show Iba1-positive cells containing LF granules (green). INL-inner nuclear layer; OPL-outer plexiform layer; ONL-outer nuclear layer; PR IS-inner segments of the photoreceptors. Scale bar: 50 µm.

3.4.3 Microglia Inhibitors and Immumohistochemical Staining

In the present work, we also investigated the effects of the microglia-inhibiting substances minocycline and tripeptide TKP. It is of interest whether these substances inhibit the migration of microglia into the subretinal space, whether the phagocytosis of LF is slowed down by the microglia, and whether any production of pro-inflammatory cytokines is reduced. For this

purpose, the animals were treated with solutions of the substances after the injection of LF over the experimental period by a daily drop of these solutions was applied to the eyes.

Firstly, it was found that the morphology and migration of the microglial cells were not significantly affected by the treatment with the inhibitors. Similar to the situation without the inhibitors, the morphology of the microglial cells initially changed towards an activated state, *i.e.*, with shorter or completely missing processes and an amoeboid shape. In addition, migration to the subretinal space was observed with both inhibitors. However, it was somewhat slower than without these inhibitors. The slowdown in migration was particularly evident in terms of the return of microglial cells to the inner layers of the retina, as even four weeks after the injection, a considerable number of microglial cells remained in the subretinal space or the inner and inner layers out-segments of the photoreceptors was seen (see figure 3.25).

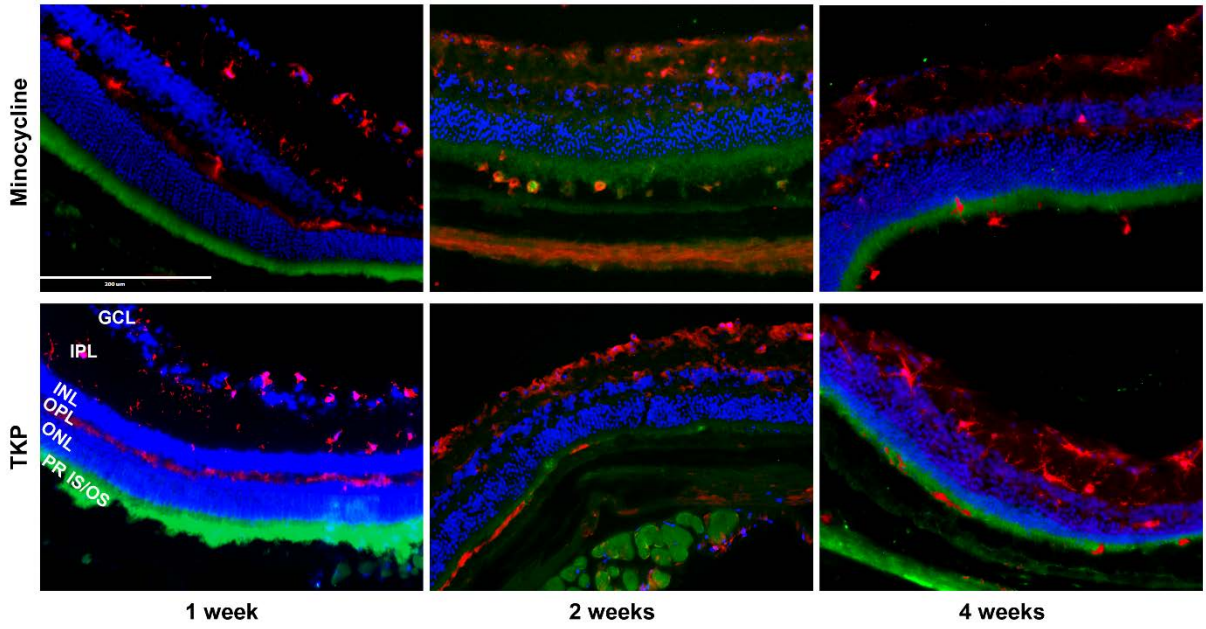

Fig. 3.25: Examples of Immunohistochemical Staining Against the Microglia Marker Iba1.
Iba1-positive (red) cells in frozen sections of the retina of the older mouse eye. The cell nuclei were stained with DAPI (blue). In order to detect any auto-fluorescence of the lipofuscin, excitation was also carried out with light of the wavelength of 488 nm (green). GCL-ganglion cell layer; IPL-inner plexiform layer; INL-inner nuclear layer; OPL-outer plexiform layer; ONL-outer nuclear layer (nuclei of the photoreceptors); PR IS/OS-inner and outer segments of the photoreceptors. Scale bar: 200 µm.

3.4.4 Double Staining of Microglia and some Pro-inflammatory Cytokines

Immunohistochemical staining was carried out against the cytokines IL-6, TNF-α and CXCL2; transcription factor HIF-α; growth factor VEGF as well as the receptors VEGF-R1, VEGF-R2 and P2X4 in frozen sections of eyes treated with minocycline and TKP, and simultaneously against Iba1 as a marker for the microglia cells. For comparison, frozen sections were stained from eyes that were treated with phosphate-buffered saline (PBS) instead of with the inhibitors. It is clear that the microglial cells are activated after LF injection (with larger soma and a reduced length, number, and ramification of their processes) compared with normal retina.

3.4.4.1 Double Staining of Microglia and IL-6

It can be seen in the sections stained against Iba1 and against IL-6 that in the case of treatment with PBS there is a clear immunoreactivity against IL-6 in the whole retina, especially in the GCL and photoreceptor inner segments. Immunoreactivity (IR) for IL-6 is significantly weakened after 7 days when the inhibitors were applied, especially the tripeptide TKP. With minocycline, IR for IL-6 slightly increased after 14 days, and its IR is increasing more after 28 days, particularly in the ganglion cell layer. In the retina treated with PBS, IL-6 IR was almost on the same increased level over all three time points. The localisation of IL-6 IR was almost the same as that of Iba1, so it can be assumed that the microglial cells produce IL-6. A slight IR for IL-6 can also be observed in the RPE and in the photoreceptor inner segments.

As noted above, microglia cells are still present in the subretinal space after treatment with minocycline or the tripeptide TKP. However, they no longer show IR for IL-6.

In the eyes that were treated with PBS or with minocycline, there have been other retinal areas with a slight IR for IL-6 besides the photoreceptor inner segments and the RPE, which is not co-localised with that for Iba1. The cellular assignment is not yet clear here (see figure 3.26).

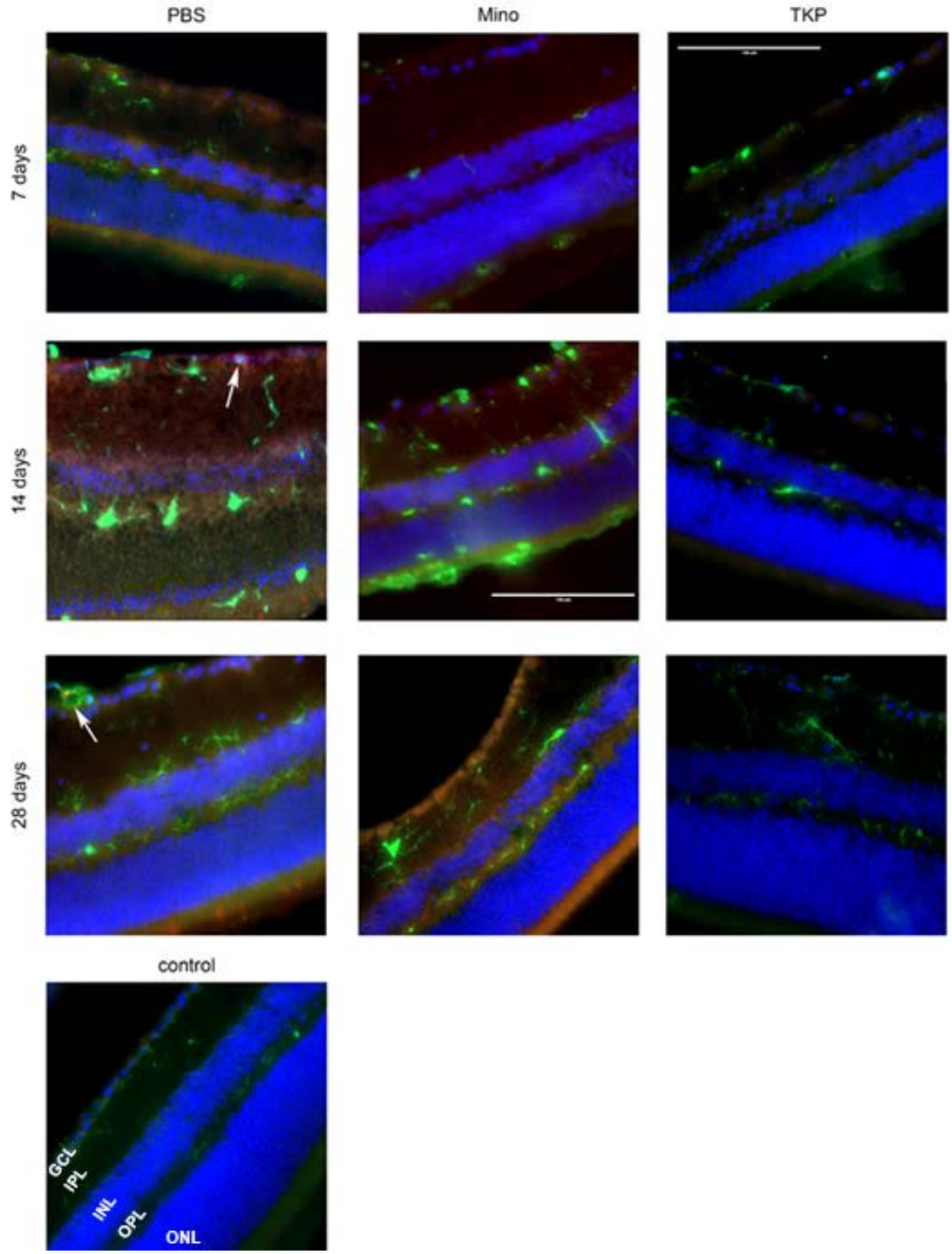

Fig. 3.26: Immunohistochemical Staining Against IL-6 and Iba1.

The cytokine IL-6 (red) and the microglial marker Iba1 (green) on frozen sections of the retina of the mouse eye one week, two weeks and four weeks after the subretinal injection of LF as indicated. A normal retina without any treatment served as a negative control. For abbreviations, see Fig. 3.25. The cell nuclei were stained with DAPI (blue). The white arrows show the co-localisations of IR for IL-6 and Iba1. Scale bar: 100 µm.

3.4.4.2 Double Staining of Microglia and TNF-α

A comparable effect of treatment with the inhibitors was observed in the immunoreactivity (IR) of TNF-α. While IR for TNF-α was found in many areas of the retina in the case of treatment with PBS, it was drastically attenuated after treatment with minocycline or TKP (see figures 3.27 and 3.28).

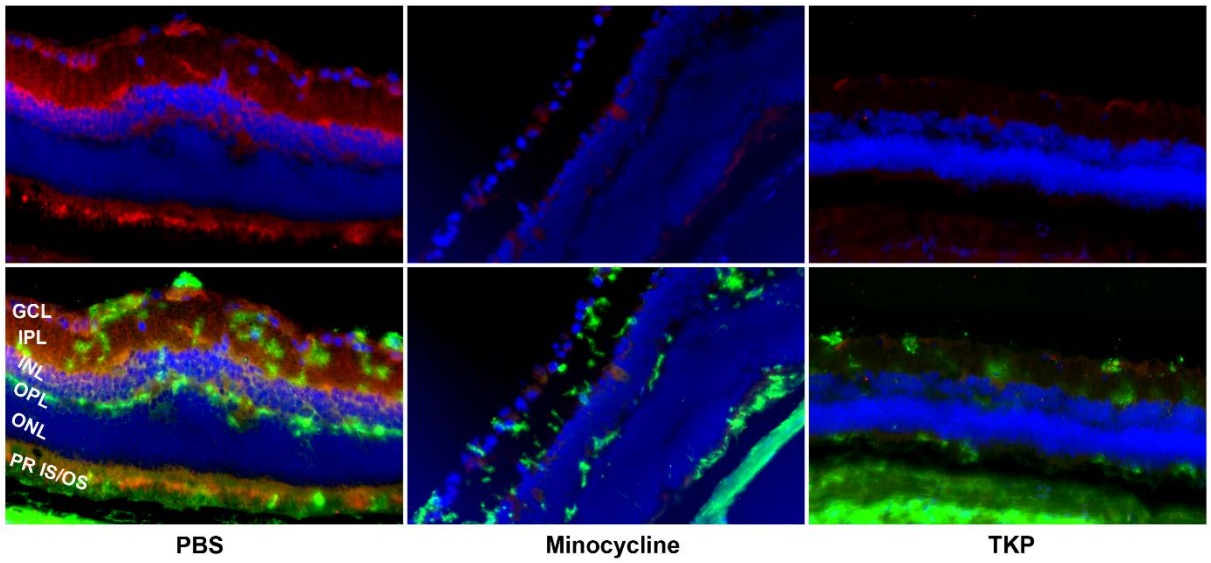

Fig. 3.27: Examples of Immunohistochemical Staining Against TNF-α and CD11b.
The cytokine TNF-α (red) and the microglia marker CD11b (green) in frozen sections of the retina of the mouse eye one week after the subretinal injection of LF. The cell nuclei were stained with DAPI (blue). For better visibility of the TNF-α staining, the CD11b staining has been hidden in the top row. GCL-ganglion cell layer; IPL-inner plexiform layer; INL-inner nuclear layer; OPL-outer plexiform layer; ONL-outer nuclear layer (nuclei of the photoreceptors); PR IS/OS-inner and outer segments of the photoreceptors. The scale bar: 200 µm.

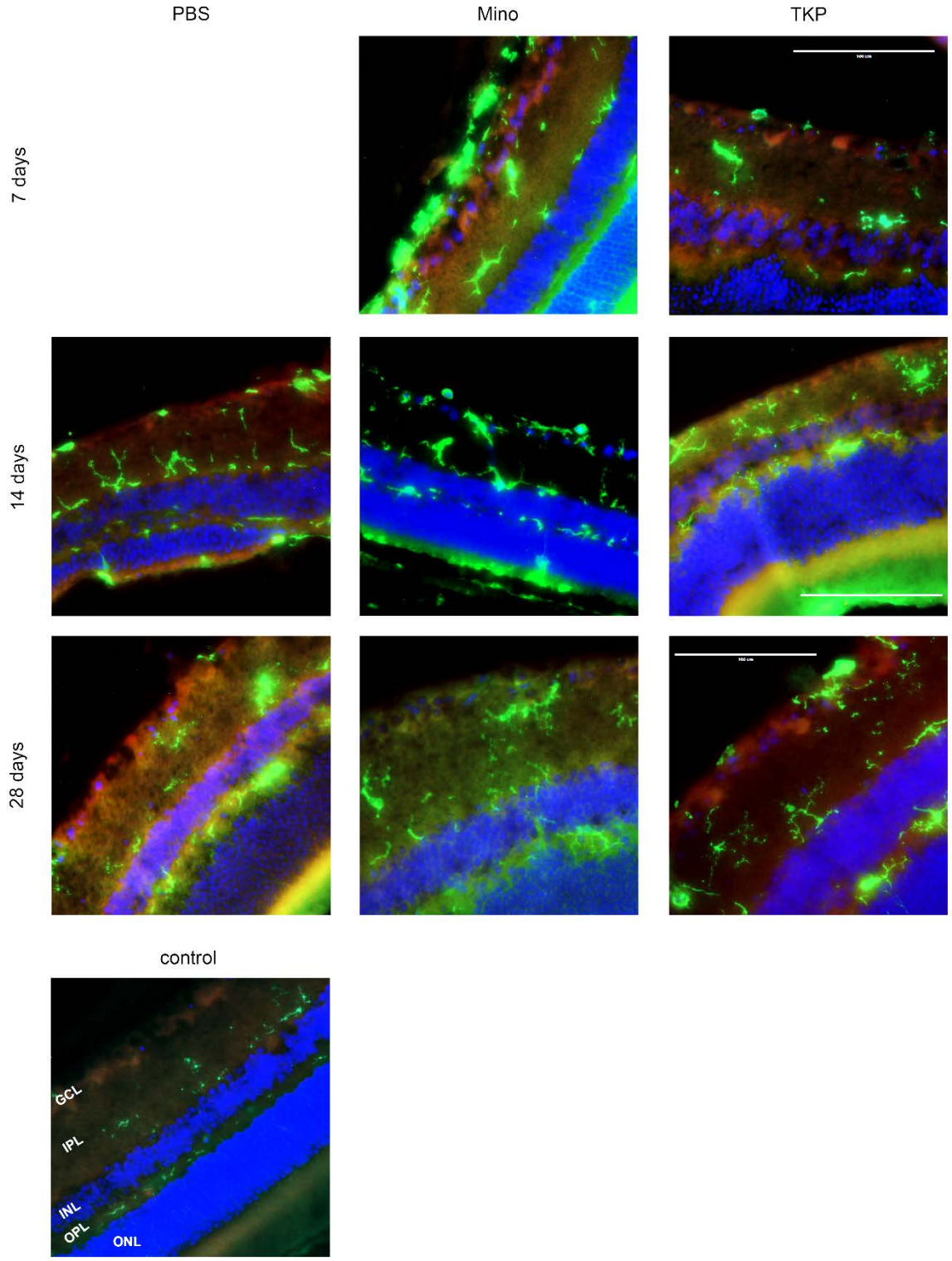

Fig. 3.28: Immunohistochemical Staining Against TNF-α and Iba1.

The cytokine TNF-α (red) and the microglia marker Iba1 (green) in frozen sections of the retina of the mouse eye one week, two weeks and four weeks after the subretinal injection of LF as indicated. A normal retina without any treatment served as a negative control. The cell nuclei were stained with DAPI (blue). For abbreviations, see Fig. 3.27. Scale bar: 100 µm.

3.4.4.3 Double Staining of Microglia and CXCL2

Immunohistochemical staining was carried out against CXCL2 in the frozen sections of the eyes treated with minocycline and TKP, and simultaneously against Iba1 as a marker for the microglia cells. For comparison, frozen sections were stained from eyes that were treated with phosphate-buffered saline (PBS) instead of inhibitors. A normal eye without any treatment served as a control.

CXCL2 IR was seen mainly in the ganglion cell layer. In the retina treated with minocycline, CXCL2 IR was decreased after 7 days, increased after 14 days, and decreased again after 28 days. In the retina treated with PBS, CXCL2 IR was slightly increased after 28 days, whereas almost no IR for CXCL2 was found in the retina treated with TKP (see figure 3.29).

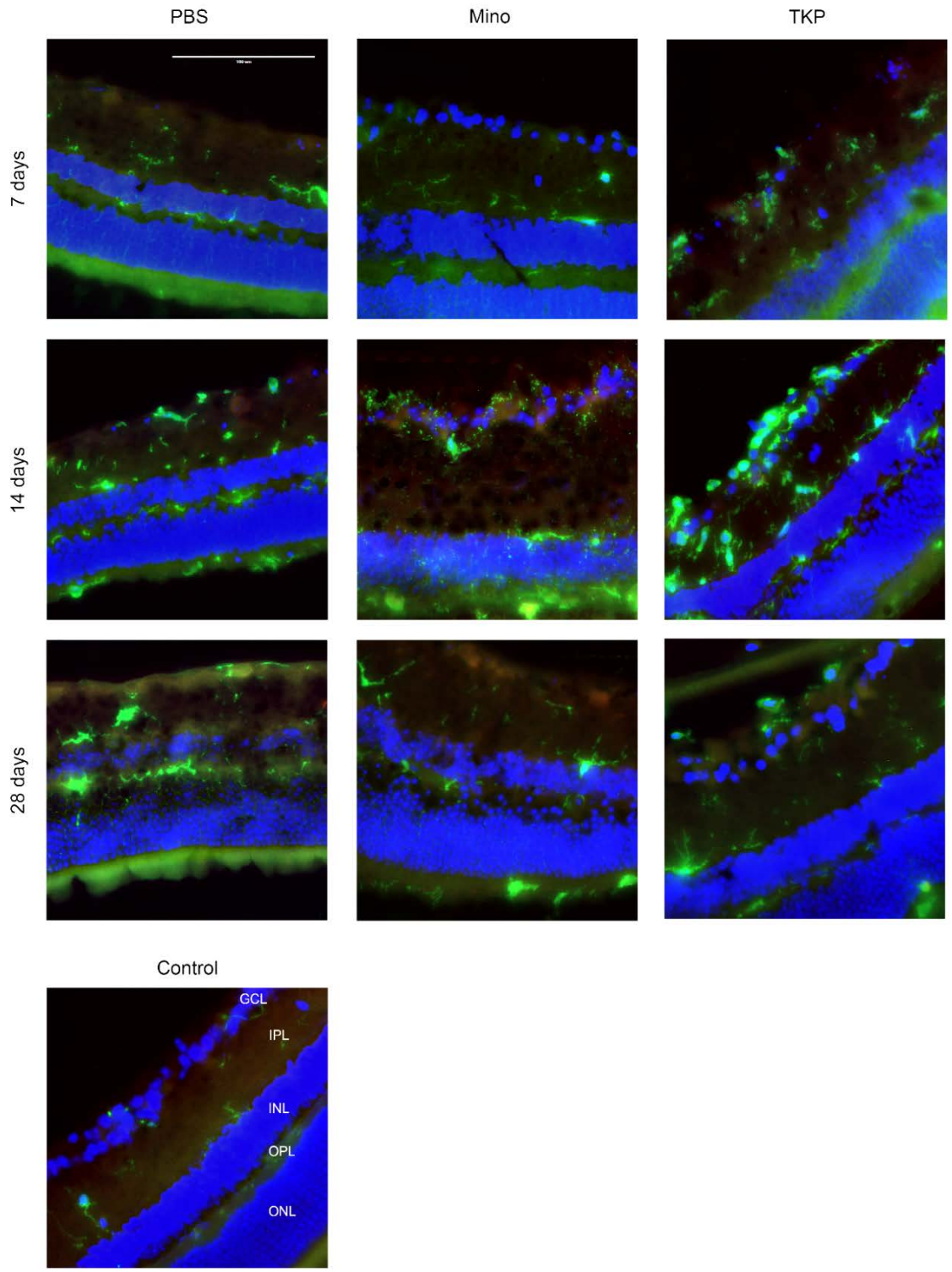

Fig. 3.29: Immunohistochemical Staining Against CXCL2 and Iba1.

The cytokine CXCL2 (red) and the microglia marker Iba1 (green) in frozen sections of the retina of the mouse eye one week, two weeks, four weeks after the subretinal injection of LF as indicated. A normal retina without any treatment served as a negative control. The cell nuclei were stained with DAPI (blue). GCL-ganglion cell layer; IPL-inner plexiform layer; INL-inner nuclear layer; OPL-outer plexiform layer; ONL-outer nuclear layer (nuclei of the photoreceptors). Scale bar: 100 µm.

3.4.4.4 Double Staining of Microglia and HIF-1-α

Immunohistochemical staining was carried out against the transcription factor HIF-1-α in the frozen sections of the eyes treated with minocycline and TKP, and simultaneously against Iba1 as a marker for the microglia cells. For comparison, frozen sections were stained from eyes that were treated with phosphate-buffered saline (PBS) instead of inhibitors. A normal eye that was without any treatment served as a control.

A clear although not strong IR for HIF-1α was found in the ganglion cell layer and in the inner nuclear layer in all groups and at all studied time points, except in the TKP group 28 days after LF injection, where HIF-1α IR is diminished (see figure 3.30).

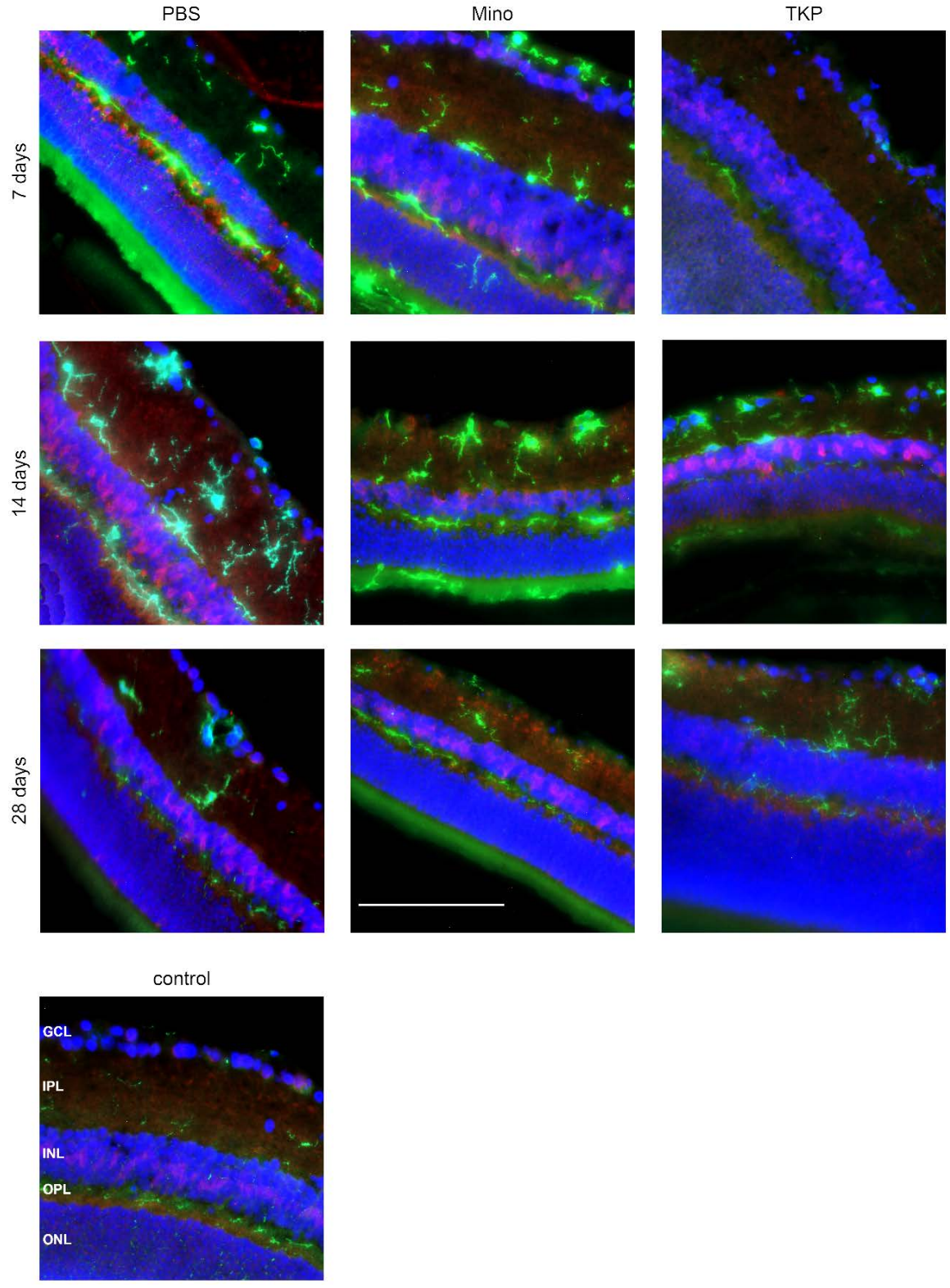

Fig. 3.30: Immunohistochemical Staining Against HIF-1-α and Iba1.

The transcription factor HIF-1-α (red) and the microglia marker Iba1 (green) in frozen sections of the retina of the mouse eye one week, two weeks, four weeks after the subretinal injection of LF as indicated. A normal retina without any treatment served as a negative control. The cell nuclei were stained with DAPI (blue). For abbreviations, see Fig. 3.29. The scale bar: 100 µm.

3.4.4.5 Double Staining of Microglia and P2X4

A clear effect of the treatment with the inhibitors was observed in the IR for the receptor P2X4. While IR for P2X4 was found in the ganglion cell layer of the retina in the case of treatment with PBS, it was drastically attenuated after treatment with minocycline, it was almost gone after treatment with TKP (see figure 3.31).

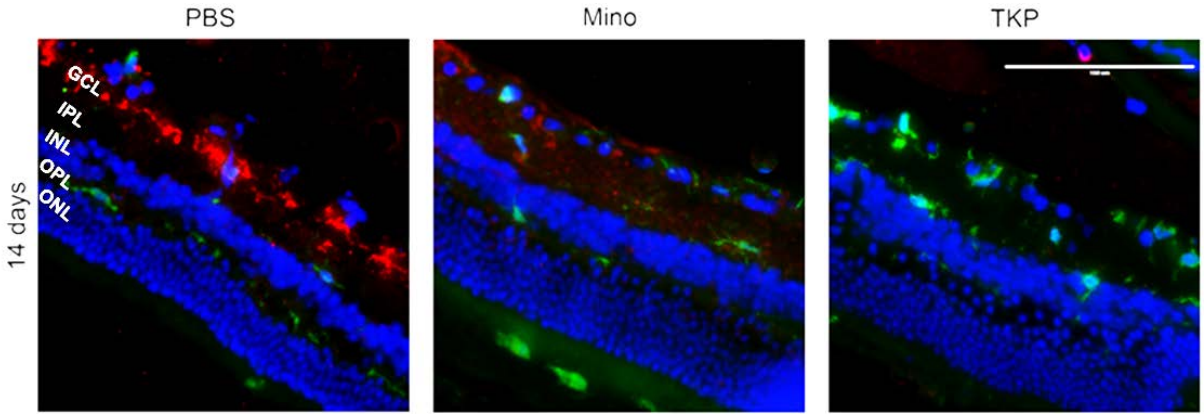

Fig. 3.31: Immunohistochemical Staining Against P2X4 and Iba1.
The receptor P2X4 (red) and the microglia marker Iba1 (green) in frozen sections of the retina of the mouse eye two weeks after the subretinal injection of lipofuscin. The cell nuclei were stained with DAPI (blue). For abbreviations, see Fig. 3.29. Scale bar: 100 µm.

3.4.4.6 Double Staining of Microglia and VEGF-R1

Immunohistochemical staining was carried out against the receptor VEGF-R1 in frozen sections of the eyes treated with minocycline and TKP, at the same time against Iba1 as a marker for the microglial cells. For comparison, frozen sections were stained from eyes that were treated with phosphate-buffered saline (PBS) instead of inhibitors. A normal eye without any treatment served as a control.

Compared to the control, all injected retinas at all time points showed an elevated IR for VEGF-R1 in the two plexiform layers and photoreceptor inner segments, except for the minocycline-treated eyes 7 and 14 days after injection of LF (see figures 3.32 and 3.33).

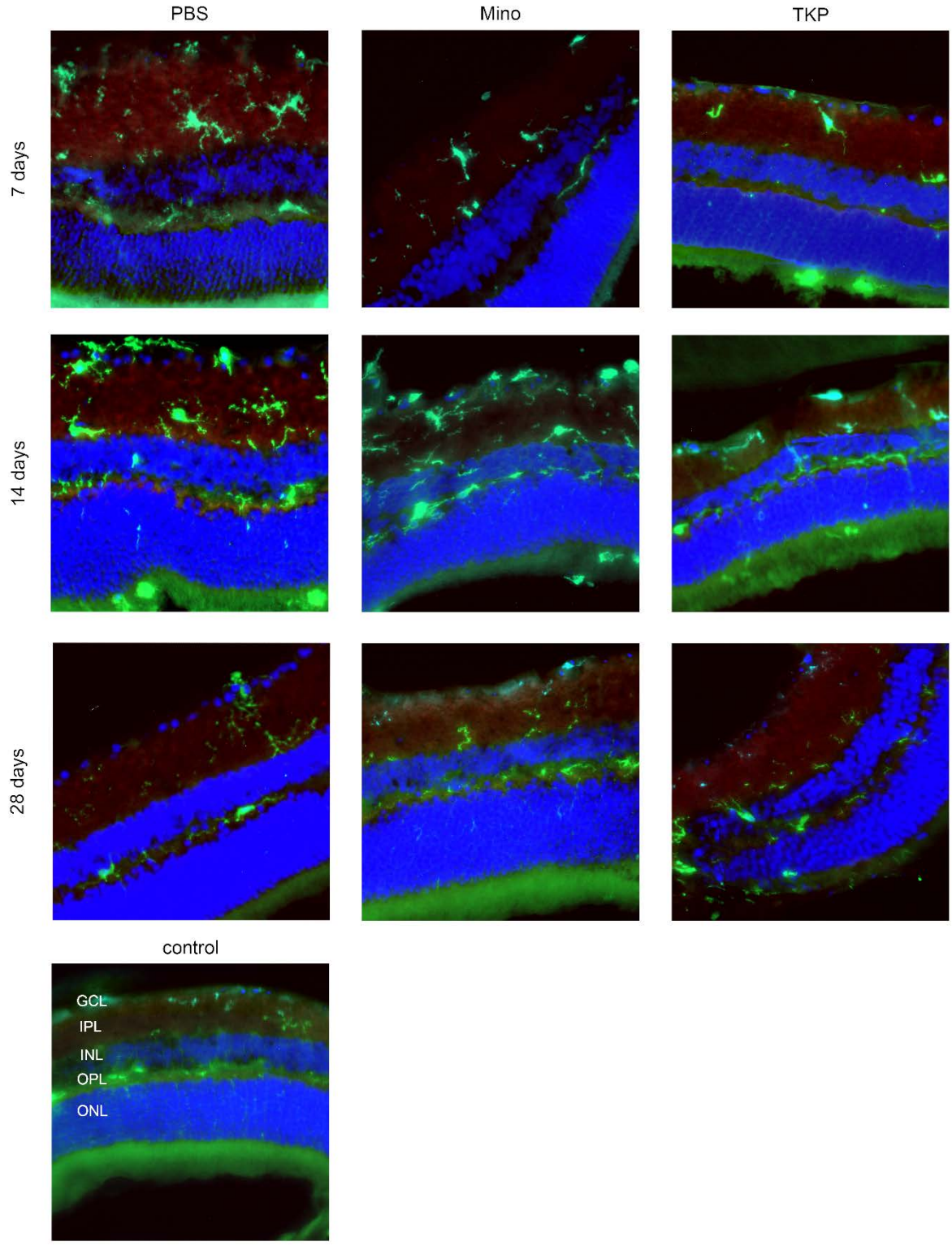

Fig. 3.32: Immunohistochemical Staining Against VEGF-R1 and Iba1.
The receptor VEGF-R1 (red) and the microglia marker Iba1 (green) in frozen sections of the retina of the mouse eye one week, two weeks, four weeks after the sub-retinal injection of LF as indicated. A normal retina without any treatment served as a negative control. The cell nuclei were stained with DAPI (blue). For abbreviations, see Fig. 3.29. Scale bar: 100 µm.

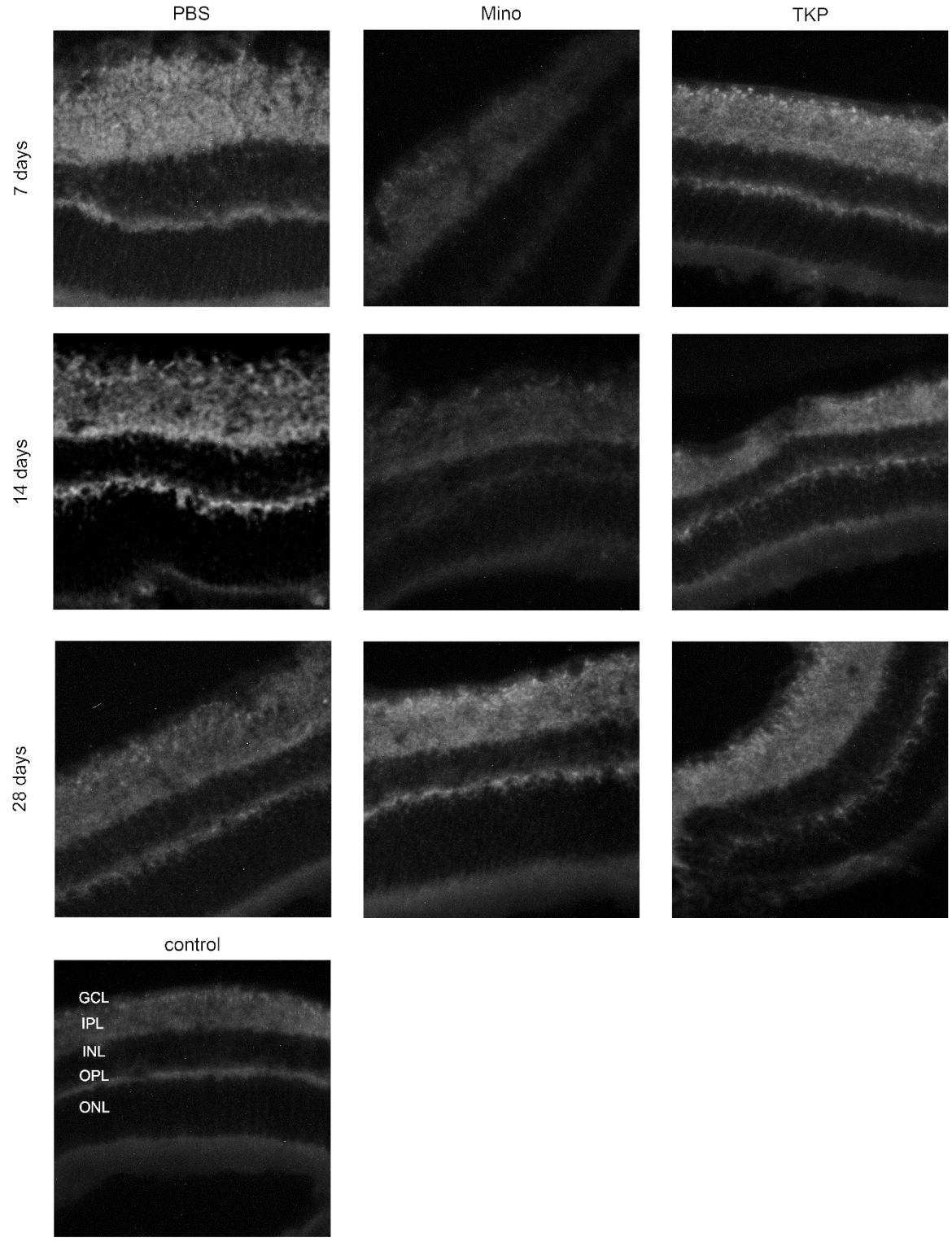

Fig. 3.33: Same Staining as Fig. 3.32 only Showing Red Channel (VEGF-R1 staining).
The green channel was very strong compared to the red one. To show the red channel more clearly, it is presented separately in the black-white images. GCL-ganglion cell layer; IPL-inner plexiform layer; INL-inner nuclear layer; OPL-outer plexiform layer; ONL-outer nuclear layer (nuclei of the photoreceptors). Scale bar: 100 µm.

3.4.4.7 Double Staining of Müller Cells and VEGF-R2

Immunohistochemical staining was carried out against the receptor factor VEGF-R2 in the frozen sections of the eyes treated with minocycline and TKP, and simultaneously against GS as a marker for the Müller cells. For comparison, frozen sections were stained from eyes that were treated with phosphate-buffered saline (PBS) instead of inhibitors. A normal eye without any treatment served as a control.

IR for VEGF-R2 is found in the normal retina, particularly in the Müller cells, and slightly in the photoreceptor inner segments. Similar to normal retina, IR for VEGF-R2 was visible in the eyes treated with PBS at all time points. In the eyes treated with minocycline or TKP, almost no IR for VEGF-R2 was found in the Müller cells. As the green channel of GS staining was very strong, we decided to present in addition the black-white images, showing only the red channel (see figures 3.34 and 3.35).

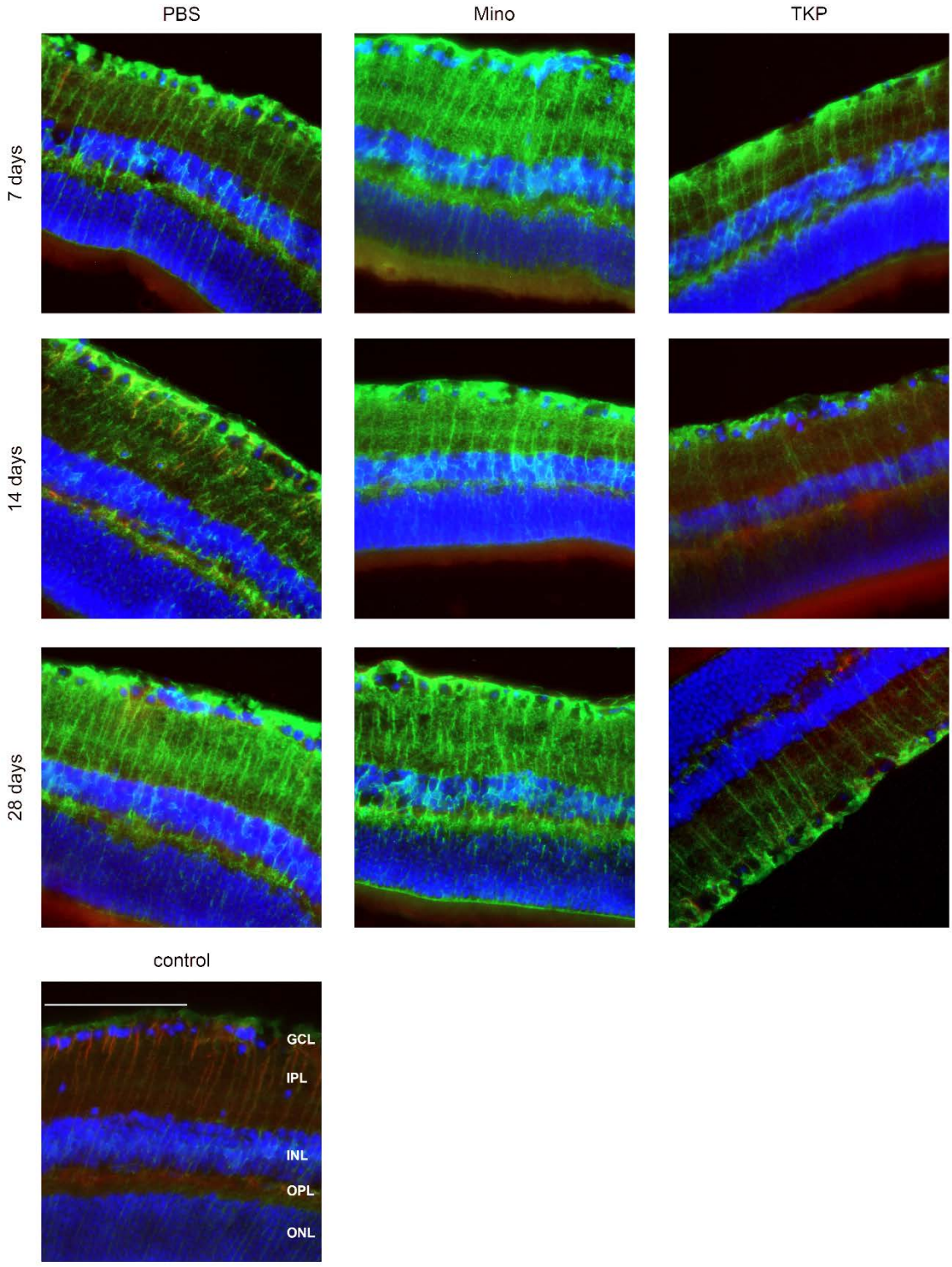

Fig. 3.34: Immunohistochemical Staining Against VEGF-R2 and GS.
The receptor VEGF-R2 (red) and the Müller cells marker (green) in frozen sections of the retina of the mouse eye one week, two weeks, four weeks after the subretinal injection of LF as indicated. A normal retina without any treatment served as a negative control. The cell nuclei were stained with DAPI (blue). For abbreviations, see Fig. 3.33. Scale bar: 100 µm.

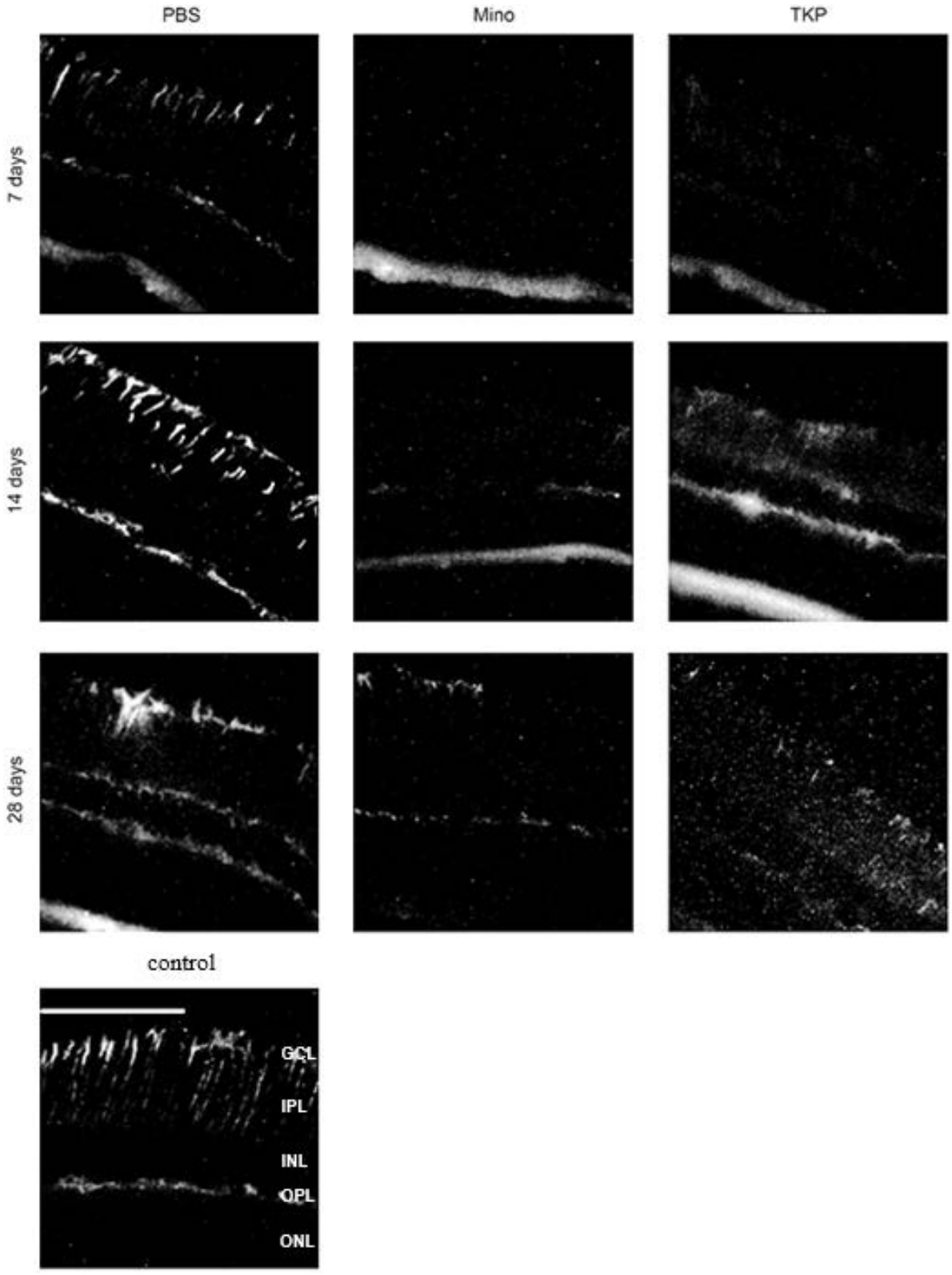

Fig. 3.35: Same Staining as Fig. 3.34 only Showing Red Channel (VEGF-R2 staining).
The green channel was very strong compared to the red one. To show the red channel more clearly, it is presented separately in the black-white images. GCL-ganglion cell layer; IPL-inner plexiform layer; INL-inner nuclear layer; OPL-outer plexiform layer; ONL-outer nuclear layer. Scale bar: 100 μm.

3.4.4.8 Double Staining of Microglia and VEGF

A clear effect of treatment with the inhibitors was observed on the IR of VEGF. IR for VEGF was found in the GCL and IPL of the retina in the case of treatment with PBS and minocycline 7 days and 14 days after injection. 28 days after injection, it was not present in the PBS group, and in the minocycline group only in the GCL. There was almost no IR for VEGF present in the TKP group after 7 days, and it appeared gradually in the GCL and IPL 14 days and 28 days after LF injection (see figure 3.36).

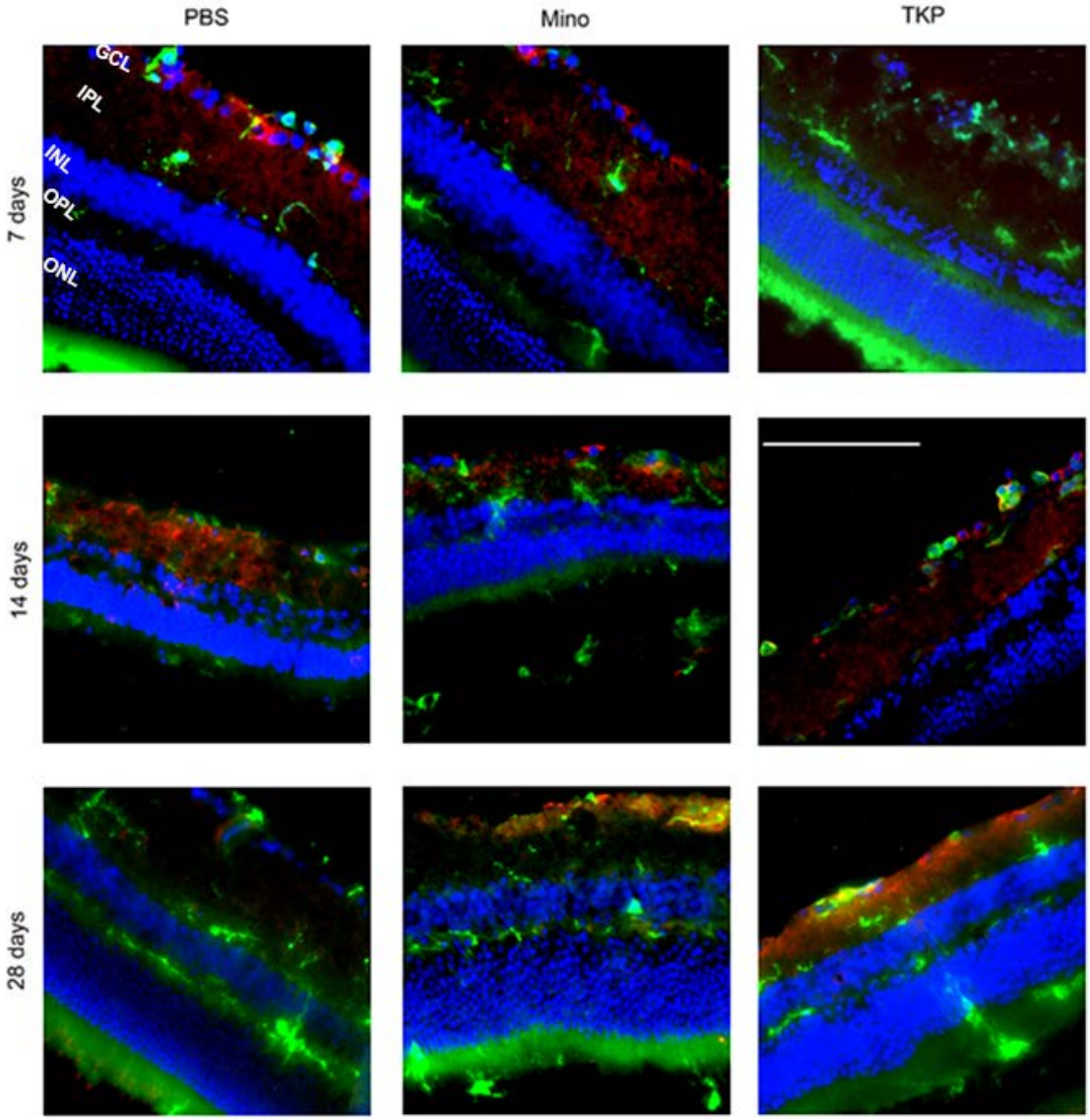

Fig. 3.36: Immunohistochemical Staining Against VEGF and Iba1.
The growth factor VEGF (red) and the microglia marker Iba1 (green) in frozen sections of the retina of the mouse eye one week, two weeks, four weeks after the subretinal injection of LF as indicated. The cell nuclei were stained with DAPI (blue). For abbreviations, see Fig. 3.35. Scale bar: 100 µm.

3.4.4.9 Double Staining of Ganglion Cells and IL-6 or TNF-α

Ganglion cells were stained using an antibody against the marker NeuN. It is clearly seen that 28 days after LF injection, the IR for IL-6 in INL slightly higher than in the normal retina, but in the GCL it was almost the same. No obvious difference was seen in the IR for TNF-α. Some RGC were positive for IL-6 or TNF-α (see figure 3.37).

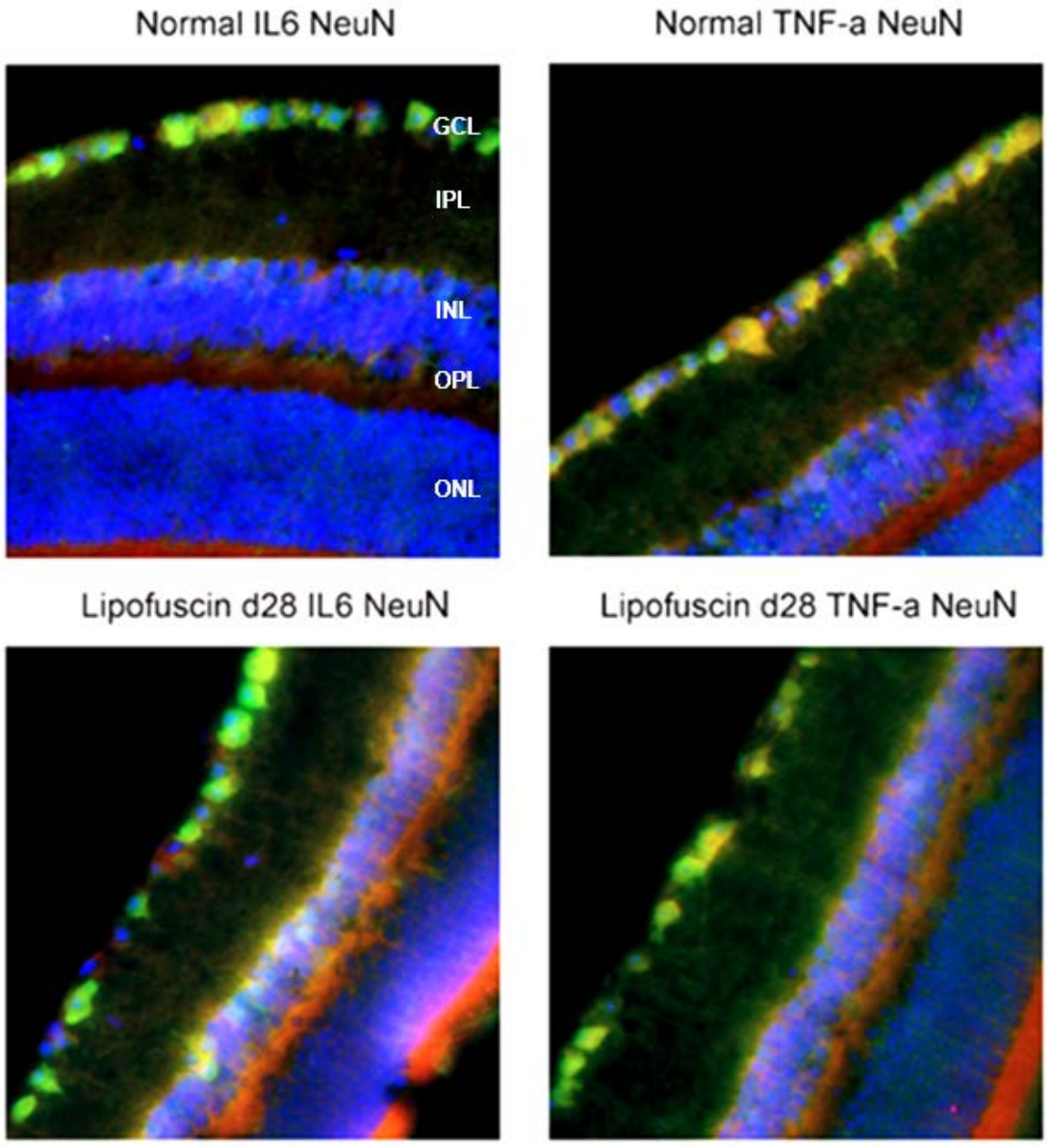

Fig. 3.37: Immunohistochemical Staining Against IL6 or TNF-α and NeuN.
The cytokines IL-6 (red, left side) and TNF-α (red, right side) and the ganglion cell's marker NeuN (green) in frozen sections of the retina of the mouse's eye four weeks after the subretinal injection of LF as indicated. A normal retina without any treatment served as a negative control. The cell nuclei were stained with DAPI (blue). For abbreviations, see Fig. 3.35.

3.4.4.10 The Cell Number of Microglial Cells in Subretinal Space and the Inner Retina

One week after LF injection, the number of microglial cells in retina and subretinal space increases compared to the untreated control without any injection and after topical treatment with PBS. However, if the eyes are treated topically with solutions of minocycline or TKP, the number of microglial cells does not increase, it is slightly smaller compared to the control. In the subretinal space, the number of MG increased compared to the control, however, this increase was much smaller in the TKP or minocycline treatment group compared to the PBS group one and two weeks after injection. There is no obvious difference between the groups 4 weeks after the injection **(**see figure 3.38).

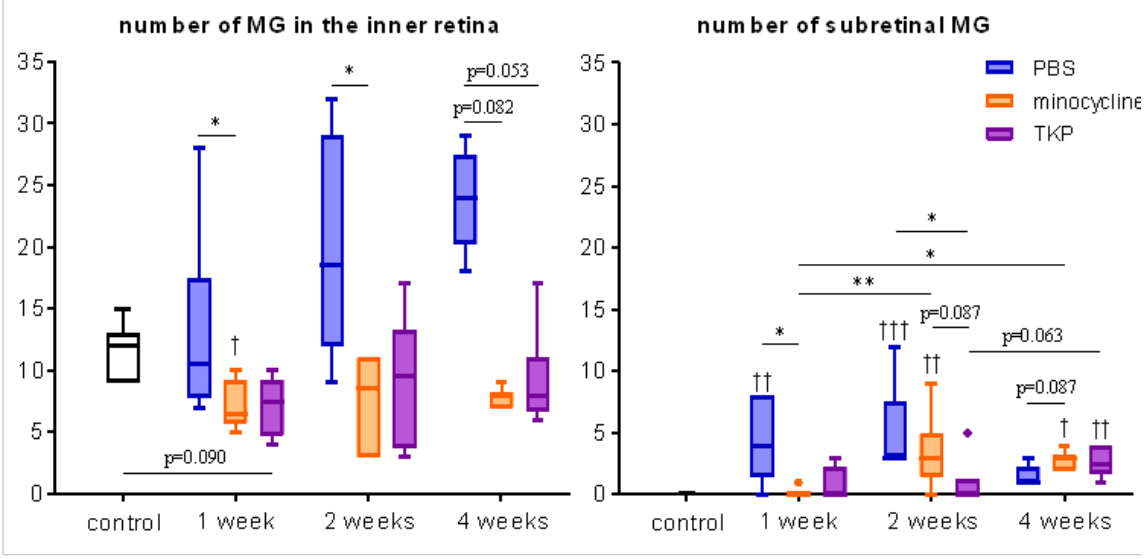

Fig. 3.38: The Number of Microglial Cells in the Inner Retina (left side) and Subretina (right side). The asterisks indicated significances of differences among PBS treatment, minocycline and TKP treatment. The crosses indicate significances of differences compared to the control.

3.5 Analysis of Retinal Structure in Histological Sections

We analysed some histological sections a longer time, *i.e.*, five weeks, after subretinal injection. We found some cells nearby the RPE layer that contained melanin after PBS and LF injection. The difference between these two groups was that after PBS injection the RPE displays a normal appearance, whereas some RPE cells lost their normal structure and released some melanin after LF injection (see figure 3.39).

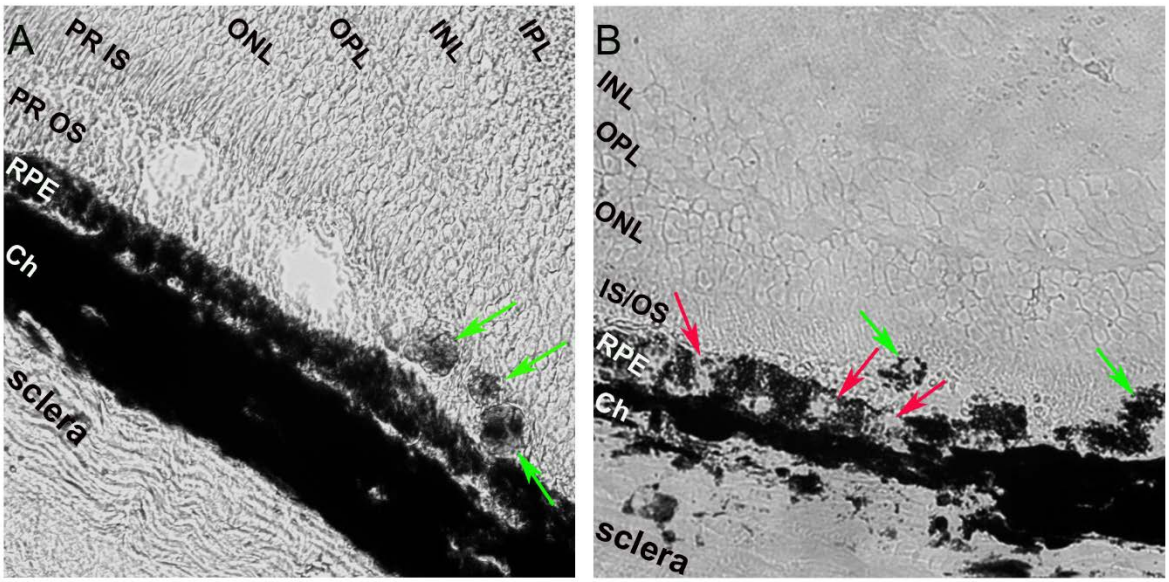

Fig. 3.39: Longer Time after Injection.
A) Transmission light images of cryosections of mouse eyes 35 days after PBS injection. Green arrows point to some cells contain melanin. **B**) 21 days after injection of LF, some RPE lost melanin (red arrows), and there are several cells in the subretinal space containing melanin (green arrows). GCL-ganglion cell layer; IPL-inner plexiform layer; INL-inner nuclear layer; OPL-outer plexiform layer; ONL-outer nuclear layer (nuclei of the photoreceptors); IS/OS-inner and outer segments of the photoreceptors; RPE-retinal pigment epithelium; Ch-choroid.

To assess the nature of melanin-containing cells, we performed staining against Iba1. Iba1 positive cells that contain melanin show an almost round shape. In contrast, those cells that do not contain melanin still have some processes (see figure 3.40).

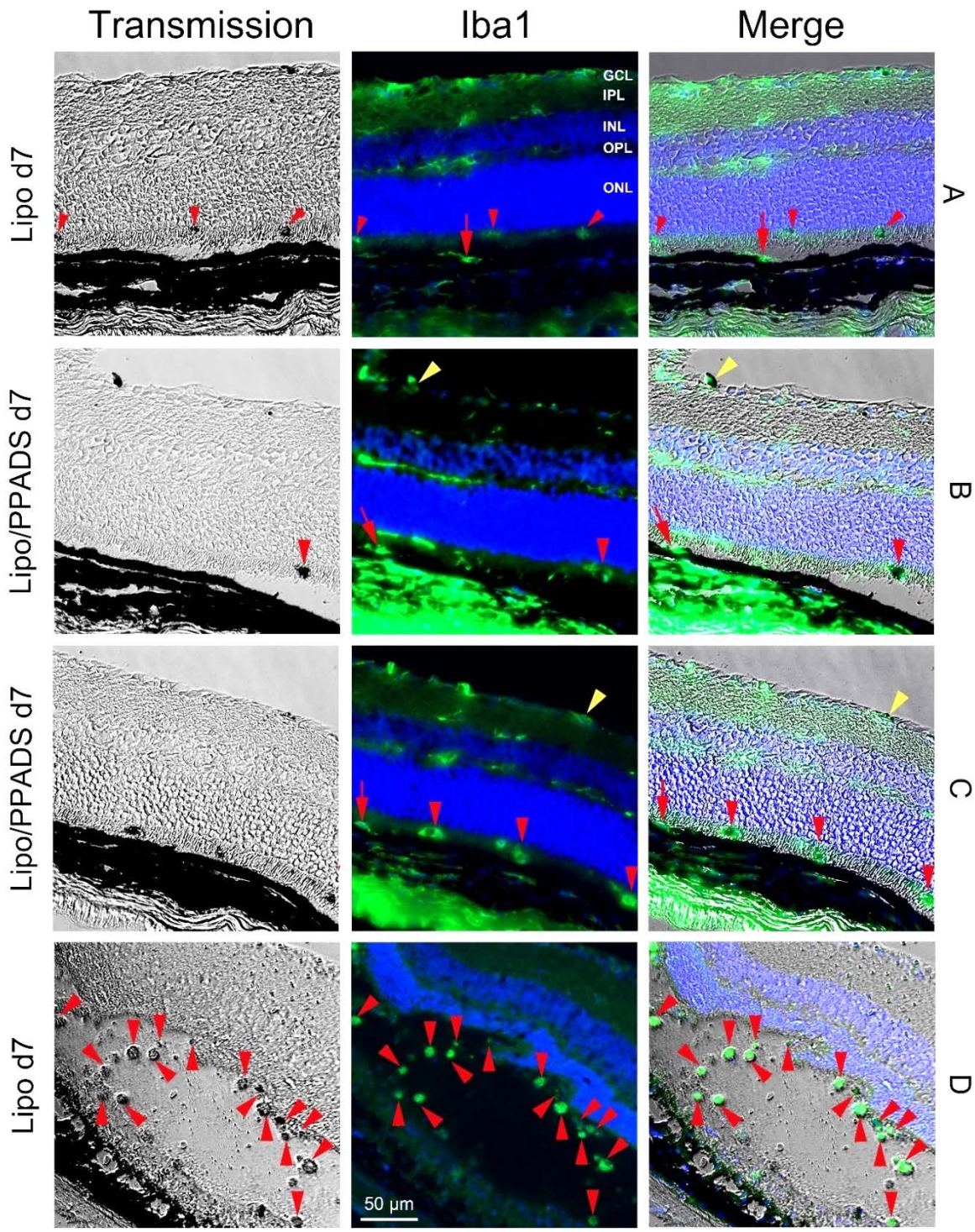

Fig. 3.40: Iba1 Positive Cells Contain Melanin 7 Days after LF Injection.
Red arrowheads in all the images point to Iba1 positive cells in the subretinal space containing melanin. A particular high number of Iba1 positive cells in the subretinal space containing melanin is seen in image D. Red arrows in images A and C point to Iba1 positive cells on top of the RPE layer, and the red arrow in image B points to Iba1 positive cells in the RPE layer. The yellow arrowheads in images B and C point to Iba1 positive cells on top of the retina that contain melanin. For abbreviations, see Fig. 3.35. Scale bar: 50 µm.

3.6 The Thickness of the RPE

RPE thickness was measured in frozen sections using Adobe Photoshop. In elder mice, RPE was found to be significantly thicker than in younger mice (see figure 3.41).

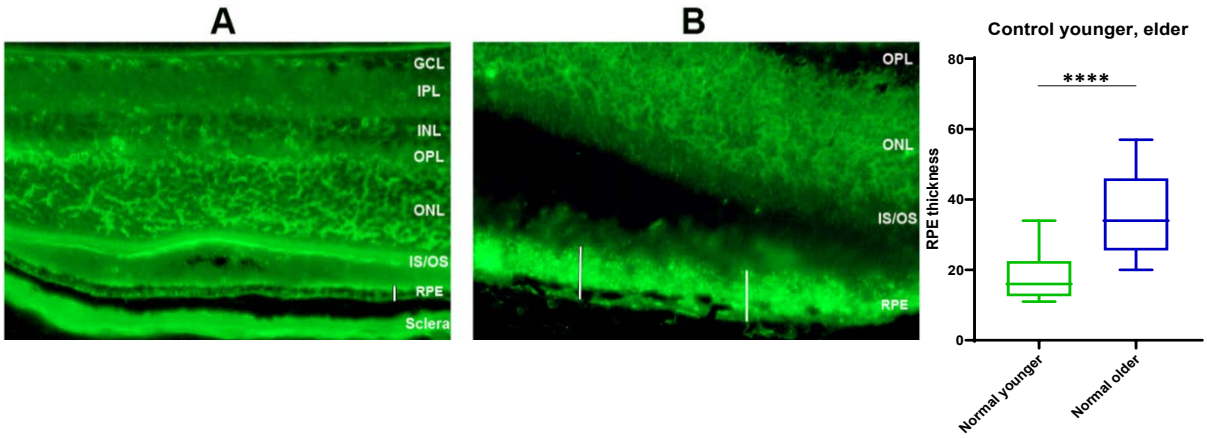

Fig. 3.41: Comparison of RPE Thickness in Younger and Elder Mice.

RPE in typical cryosections of younger mouse (4 months, **A**) and elder mouse (1.5 years, **B**). Vertical lines show position and thickness of the RPE. Diagram shows results of thickness measurement in images of retinal cryosections obtained from 5 young mice and 4 old mice. The asterisks indicate high significance of difference between the younger mice and the elder mice. GCL-ganglion cell layer; IPL-inner plexiform layer; INL-inner nuclear layer; OPL-outer plexiform layer; ONL-outer nuclear layer (nuclei of the photoreceptors); IS/OS-inner and outer segments of the photoreceptors; RPE-retinal pigment epithelium.

3.7 Examination of mRNA Levels Using Quantitative PCR

To study the effects of LF injection, retina and RPE/choroid were isolated from treated mice. The homogenates were examined for the gene expression of the abovementioned proteins, and it was compared with the expression of untreated eyes. In the diagrams showing results for the retina and the RPE/choroid complex (RPE/Ch), the identical scales were used on the y-axis for a better comparability.

In order to see the different expression of IL6, TNF-α, CCL-2, IL-1β, CXCL1, FGF-2, VEGF-A at different time points after PBS and LF injection, their mRNA levels were determined one, three, seven and 14 days after the injection in old mice, repeated 3 times. The results are shown in the following diagrams.

One day after subretinal injection, we have found a clear increase of gene expression of inflammatory cytokines in both the retina and the RPE/choroid complex. During the next days, expression levels of the cytokines decreased sharply in the retina and were hardly detectable two weeks after the injection, whereas they remained on a higher level in the RPE/choroid. complex. Again, it can be seen that the pro-inflammatory cytokines are primarily expressed by the RPE/choroid complex. The levels of gene expression of the inflammatory cytokines in the retina and in the RPE/choroid complex were higher in both cases after LF injection than after PBS injection, especially 1 day after injection in most cases (see figures 3.42 and 3.43, please note the different scales).

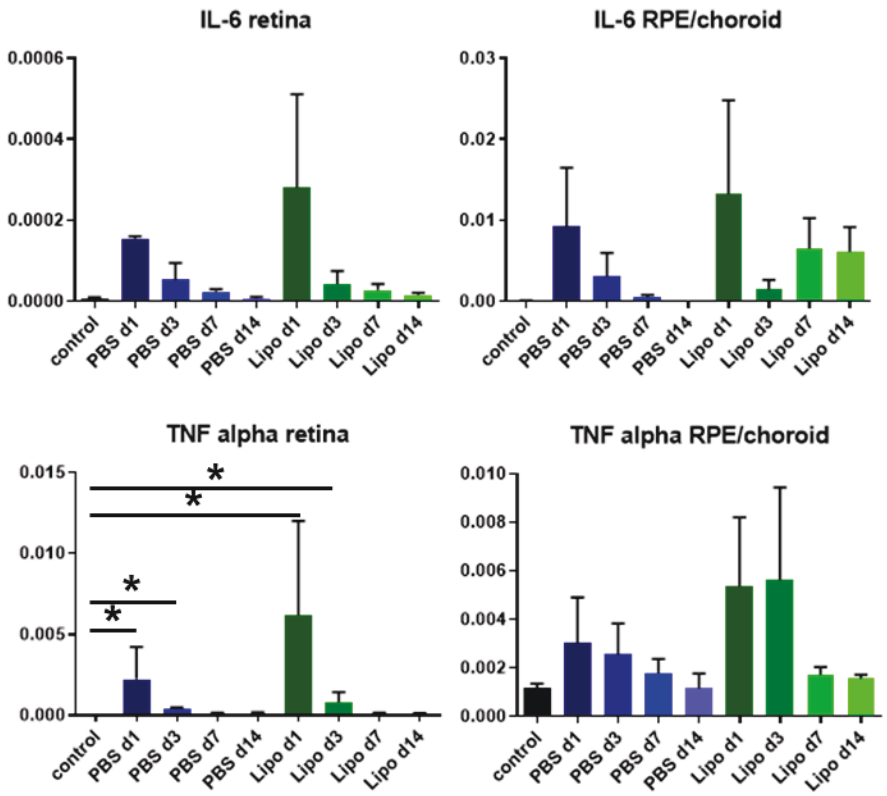

Fig. 3.42: IL-6 and TNF-α mRNA Levels in the Retina and RPE/Choroid Complex after injections and in the controls.

After injection of PBS and Lipofuscin, mRNA levels show a transient increase compared to the controls, in particular in the RPE and after injection of lipofuscin (n=3 for each group). Mean values ± SEM are shown. Asterisks show statistical significance between the control and the single groups after injection: * $p<0.05$.

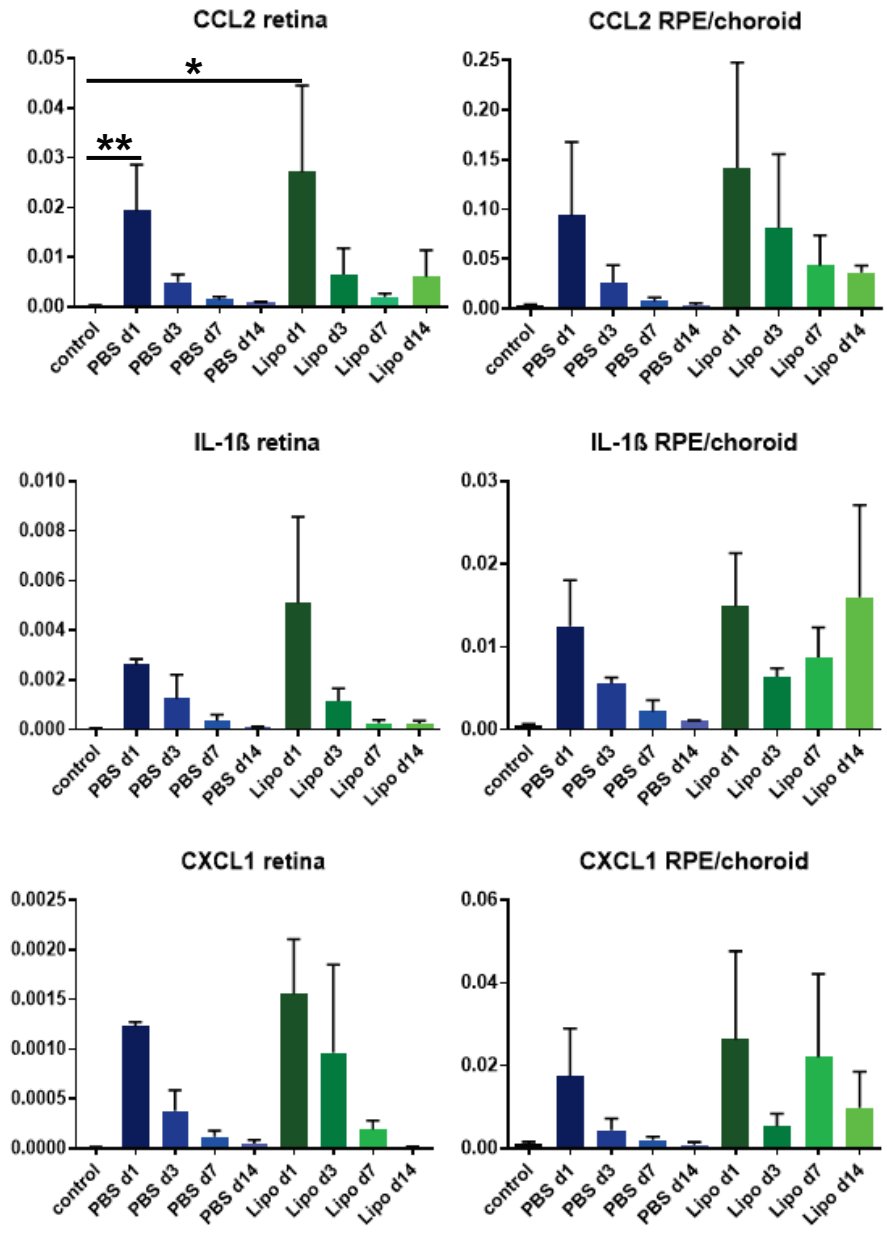

Fig. 3.43: CCL2, IL-1β and CXCL1 mRNA Levels in the Retina and RPE/Choroid Complex after injections and in the controls.

After injection of PBS and Lipofuscin, mRNA levels show a transient increase compared to the controls, in particular after injection of lipofuscin and in the RPE for CCL2, IL-1β and CXCL1 (n=3 for each group). Mean values ± SEM are shown. Asterisks show statistical significance between the control and the single groups after injection: * $p<0.05$, ** $p<0.01$.

A different picture was found for the growth factors VEGF-A and FGF-2 (see figure 3.44). FGF-2 gene was expressed primarily in the retina, and its expression remains high over the entire observation period compared to the control in the retina, no matter if PBS or LF was

injected. On the other hand, FGF-2 gene expression in the RPE/choroid complex was in total much lower than in the retina. 7 days after injection, it started to increase and was even higher 14 days after injection, especially if LF was injected.

We found a relatively high gene expression level of VEGF-A in the retina of the controls. It did not change very much during the first days after PBS or LF injection, and it decreased 7 and 14 days after injections. In the RPE/choroid complex, VEGF-A gene expression did not change very much except a transient increase after PBS injection (see figure 3.44).

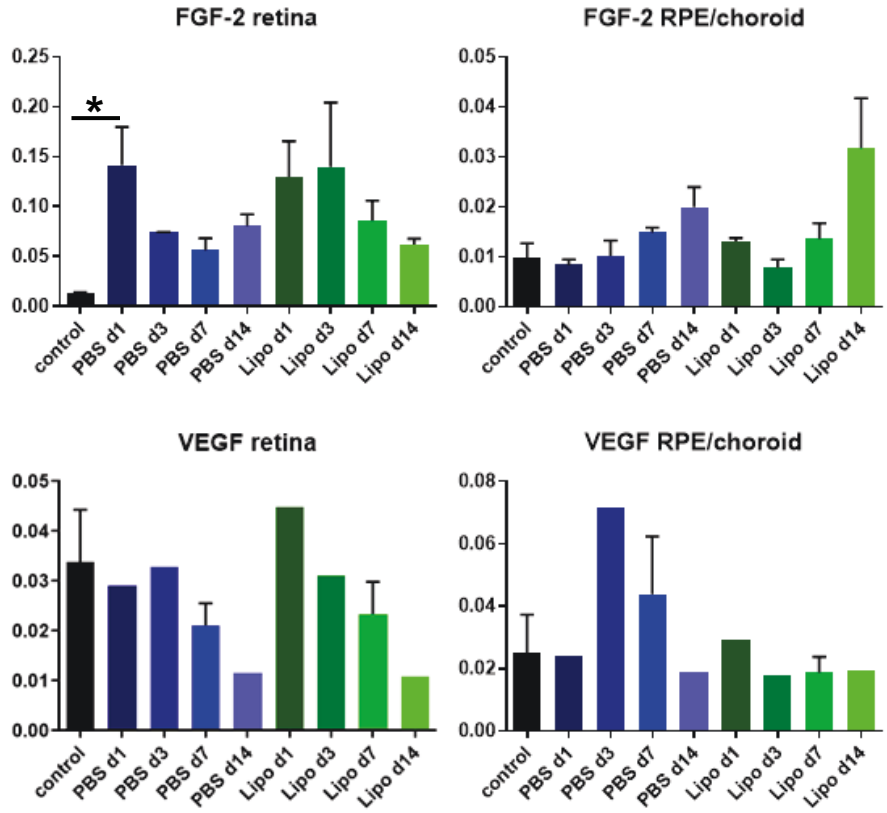

Fig. 3.44: FGF-2 and VEGF-A mRNA Levels in the Retina and RPE/Choroid Complex after injections and in the controls.

After injection of PBS and Lipofuscin, mRNA levels show a longer lasting increase for FGF-2 and a transient increase for VEGF-A compared to the controls, in both the retina and the RPE. While mRNA levels are higher in the retina after injection of lipofuscin, this is not the case in the RPE (n=3 for each group). Mean values ± SEM are shown. Asterisks show statistical significance between the control and the single groups after injection: * $p<0.05$.

3.8 Ultrastructural Evaluation

Appearance of Bruch's membrane (BM), RPE cells, labyrinth which is located between the BM and RPE layer, as well as the microvilli of RPE cells was inspected using electron microscopy (EM) in ultrathin epon sections of mouse eyes after sham, PBS, and LF injection. The eyes were examined one and three weeks after injection of PBS and LF, and three weeks after sham injection.

3.8.1 Macrophages in the Subretinal Space

After LF injection, we found some macrophages in subretinal space and even between the RPE cells, which is consistent with Iba1 positive cells in the subretinal space in immuno-staining, as we described above (see figures 3.45 and 3.23).

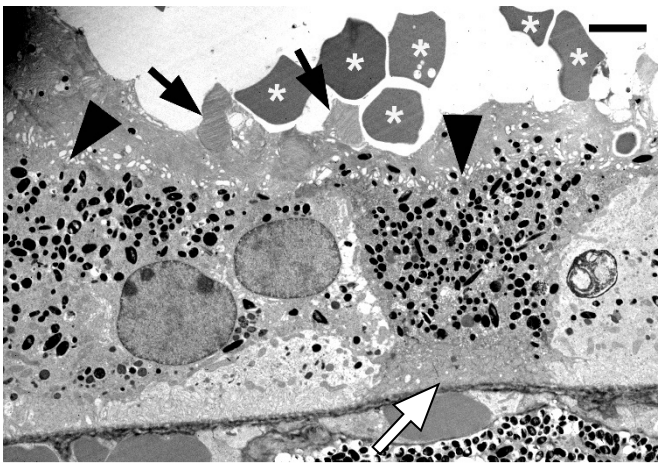

Fig. 3.45: 7 Days after LF Injection
The arrowheads point to macrophages. The white arrow points to the pseudopodium of a macrophage that is in close contact to Bruch's membrane. This macrophage is located between two RPE cells. The black arrows point to parts of photoreceptor outer segments. The asterisks indicate some LF granules.
Scale bar: 200 nm.

3.8.2 The Effect of LF on Structure of RPE Cells and the BM

Injected LF granules were detected one week after LF injection in the subretinal space nearby the RPE. By contrast, in the eyes three weeks after the injection of LF, these granules were not detectable. This is consistent with the observation we made in frozen sections.

The thickness of BM one week after LF injection became thinner compared to control and sham PBS injection. Three weeks after LF injection, thickness of BM is uneven and differs along its length in the EM images. On the other hand, there is almost no difference in the thickness of BM between untreated controls without any injection and after sham as well as PBS injection.

Moreover, some dark particles appear in RPE cells one and two weeks after LF injection, which were not seen after sham and PBS injection (see figure 3.46).

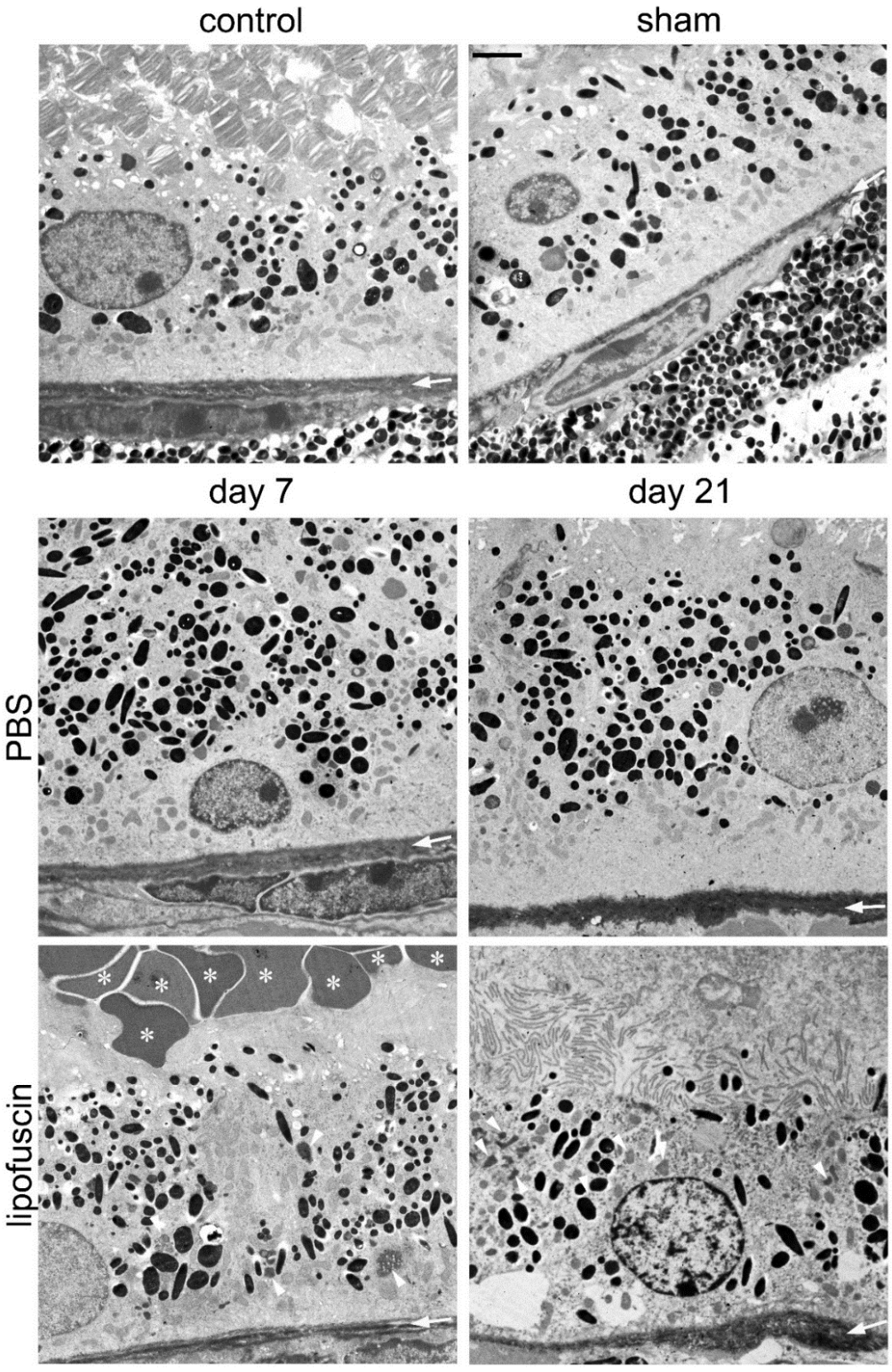

Fig. 3.46: EM Images of Eyes of Control and 21 Days after Sham Injection, and 7 and 21 Days after PBS and LF Injection

The white arrows point to Bruch's membrane (BM), white asterisks in LF injection day 7 show some examples of LF granules, white arrow heads point to the dark particles in RPE cells that are only visible after injection of lipofuscin. Scale bar: 600 nm.

In an enlargement of the above image of the eye 21 days after LF injection, the dark particles mentioned above are visibly better. Several cystic membranous degradations can be seen as vacuoles near the BM that are present only after injection of lipofuscin (see figure 3.47).

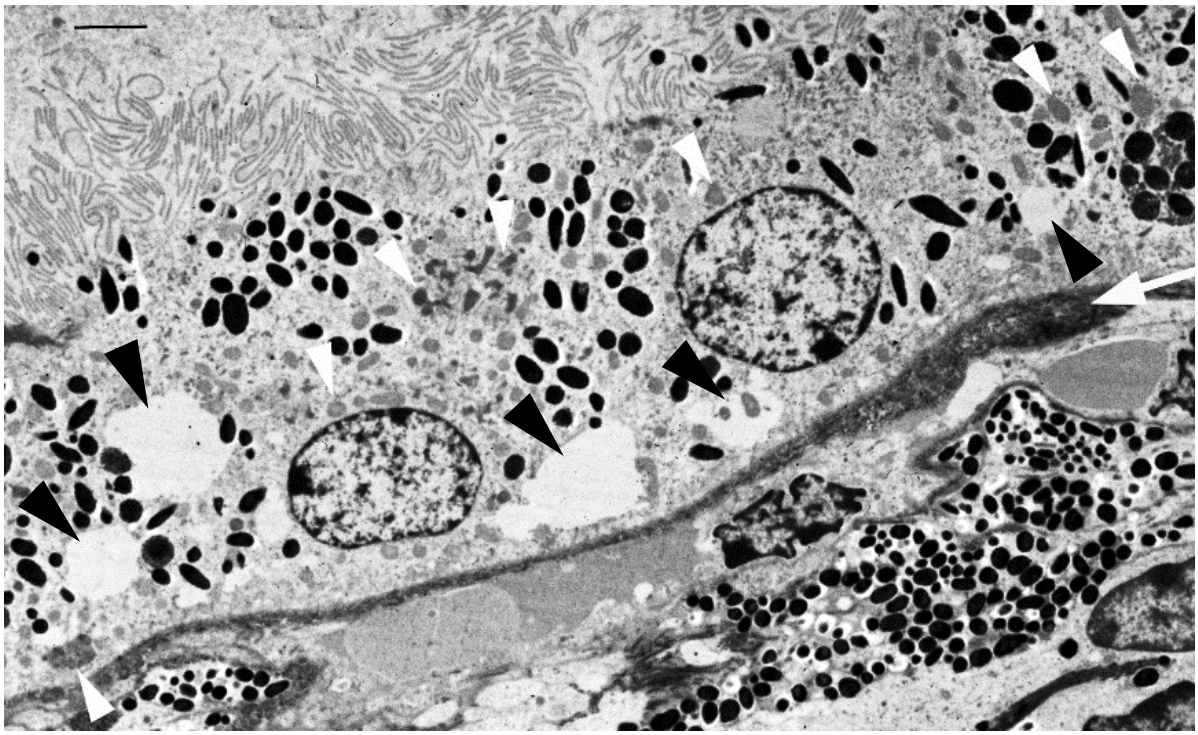

Fig. 3.47: EM Image 21 Days after LF Injection
The arrow on the right-side points to a thicker region of Bruch's membrane. White arrowheads point to dark particles in the RPE cells. Black arrowheads point to sites of cystic membranous degradation of the RPE. Scale bar: 1 μm.

3.8.3 The Effect on Structure of the Labyrinth

On their basal side, RPE cells form many invaginations in their cell membrane that are called the "labyrinth". We checked the structure of the labyrinth after in eyes 20 days after sham injection and in eyes 7 days and 20 days after PBS and LF injection.

Seven days after PBS or LF injection, a slight disorder was seen in the labyrinth compared to the control (see figure 3.48).

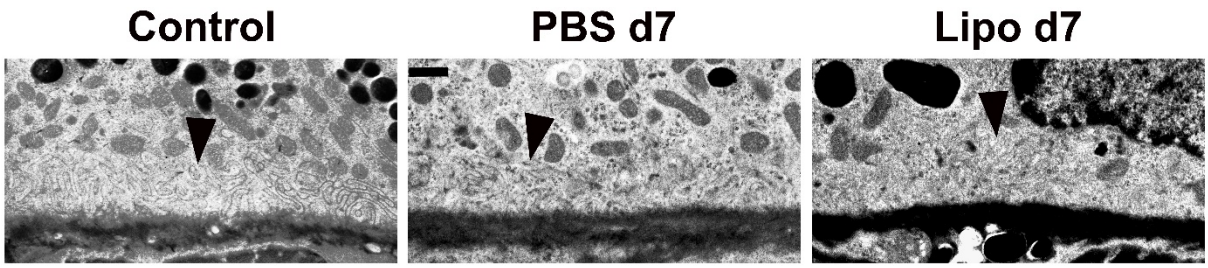

Fig. 3.48: The Labyrinth in Eyes of Control and 7 Days after PBS and LF Injection
The arrowheads point to the labyrinth. Scale bar in the PBS 7 days image: 1 µm.

The structure of the labyrinth showed no big differences between the controls and 20 days after sham and PBS injection. By contrast, the labyrinth lost its normal structure 20 days after LF injection, and it was very difficult to identify its structure at all. This finding may indicate that PBS injection had only a short-term effect on the labyrinth, which had recovered later, while the effect of LF injection on the labyrinth continued to aggravate (see figure 3.49).

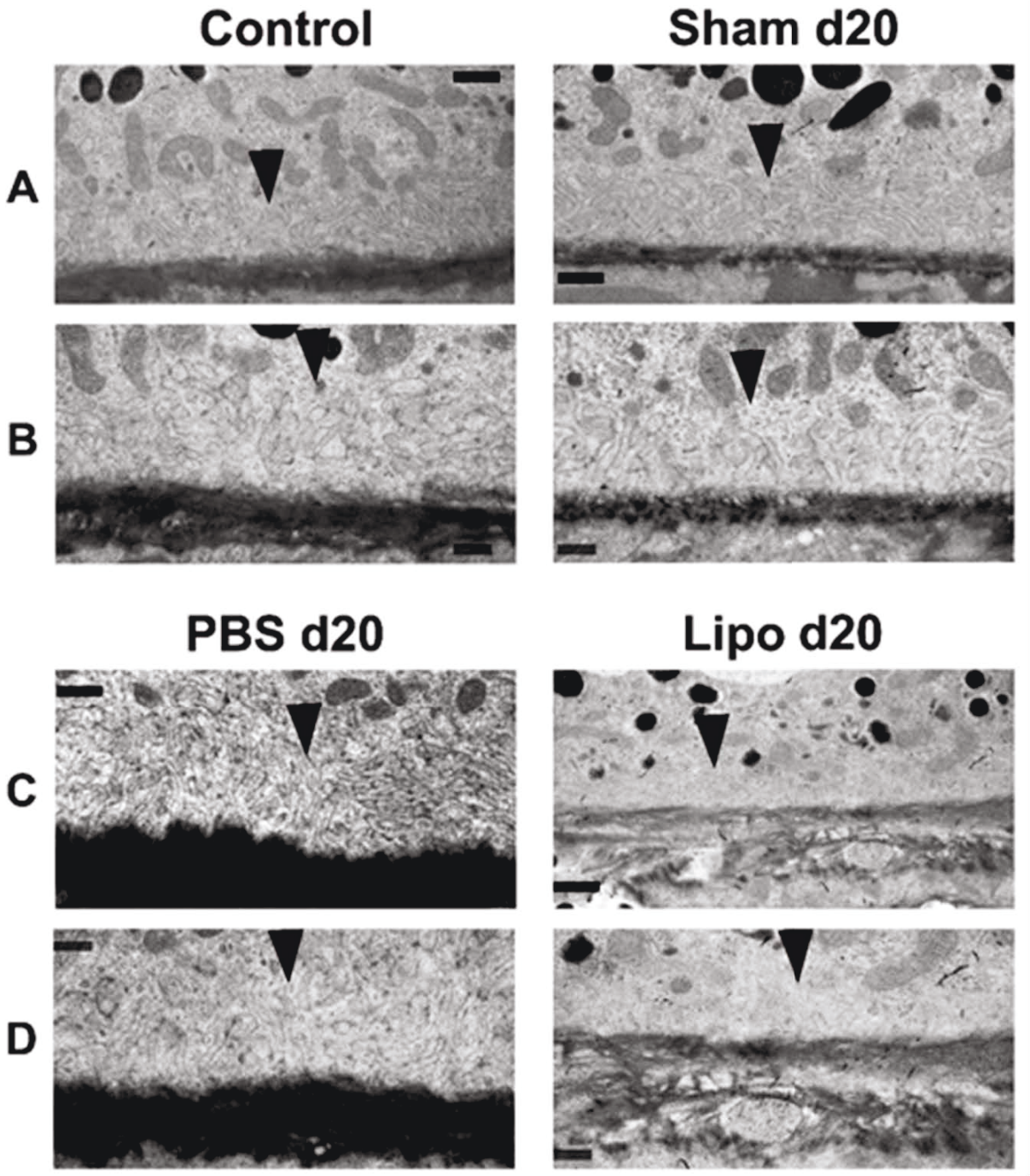

Fig. 3.49: The Labyrinth of Control, Sham, PBS, and LF 20 Days after Injection
The arrowheads point to the labyrinth. A and C, scale bars: 1 μm. B and D scale bars: 600 nm.

3.8.4 The Effect on Structure of the RPE Cells and Microvilli

To study the structure of RPE cells and the microvilli after sham injection, PBS and LF, the eyes were examined 21 days after injection. It can be clearly seen that the RPE cells not only lost some melanin 21 days after injection of LF, some of them also shrank and are on the verge of dying. The microvilli of some RPE cells lost their normal structure, became shorter, and their obviously decreased. In contrast, the structure of RPE cells and the microvilli did not exhibit big differences in the sham and PBS injected eye compared to the control (see figures 3.50, 3.51, and 3.52).

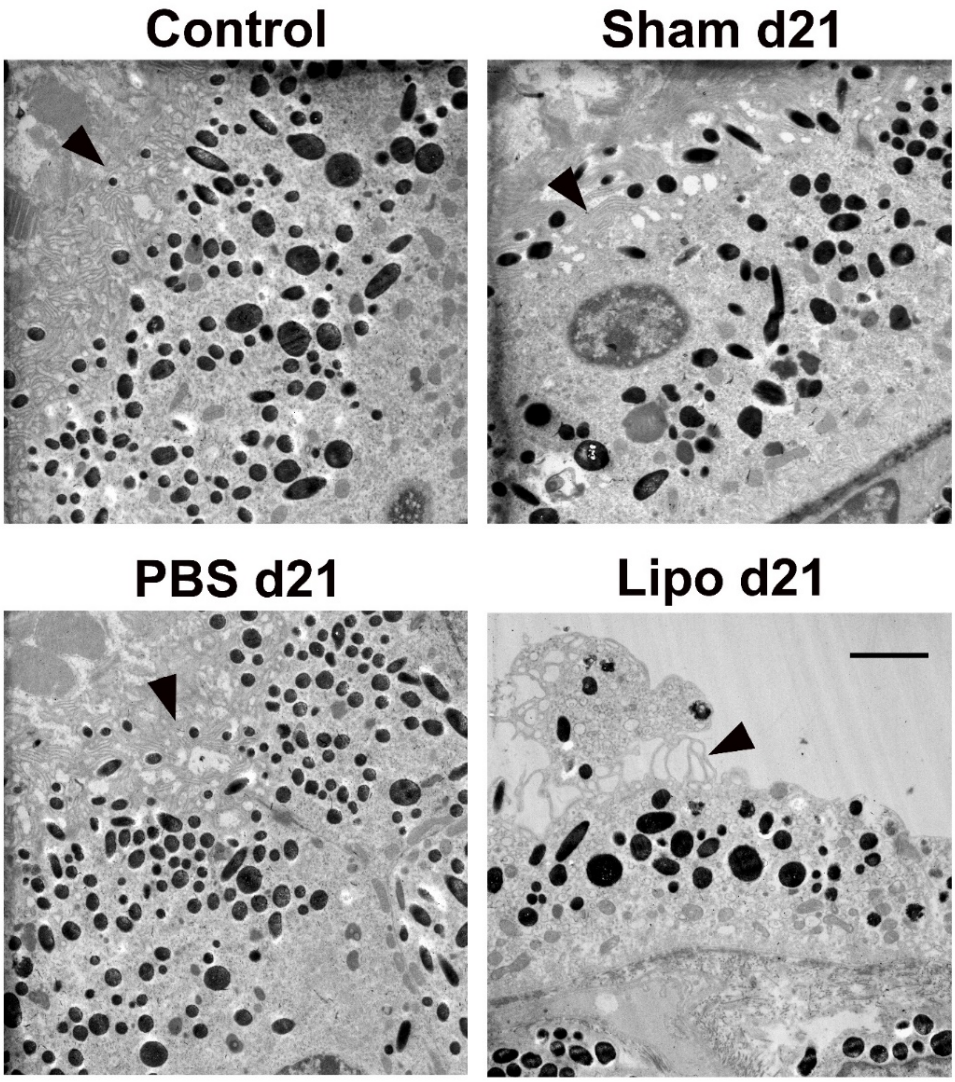

Fig. 3.50: The Microvilli of Control and 21 Days after Sham, PBS, and LF Injection
Arrowheads point to the microvilli which are on the top of the RPE cells. Scale bar: 600 nm.

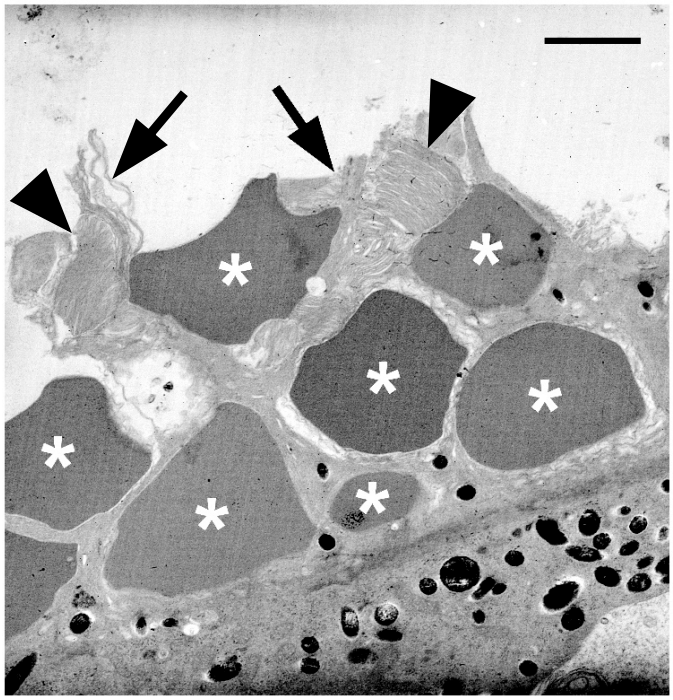

Fig. 3.51: EM Image 7 Days after Injection of Lipofuscin.
The arrows point to microvilli of the RPE cell. White asterisks show LF granules that were wrapped up in the microvilli.
A few fragments of photoreceptor outer segments (black arrowheads) can be seen on the top of the RPE cell and the microvilli. In addition, it is clearly seen that the microvilli are very short, and their number is reduced compared to a healthy retina.
Scale bar: 600 nm

Figure 3.52 clearly shows an RPE cell that lost almost all melanin and became thinner, tending to atrophy. The number of the microvilli became very small, and they became very short.

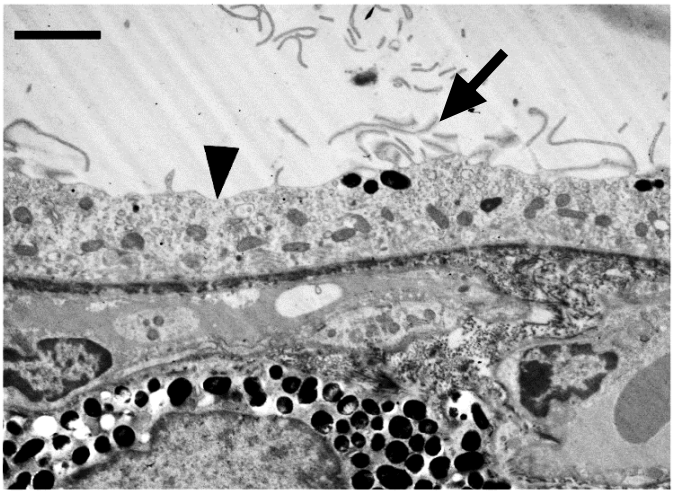

Fig. 3.52: RPE Cell and Its Microvilli
The black arrowhead points to an RPE cell. Only few microvilli are left (black arrow). 21 days after injection of lipofuscin.
Scale bar: 600 nm.

3.8.5 The Effect on Structure of the Photoreceptors

21 days after injection of LF in younger mice, almost all the photoreceptor outer segments were lost, only some remnants were found. In contrast, the structure, and the number of the photo-receptor outer segments are not very different between the sham and PBS injected eyes compared to the controls. We also noticed that the structure of the photoreceptor outer segments

is changed in old or elder mice without any injection and treatment compared to younger control mice. In addition, some RPE cells show clear signs of atrophy after injection of LF (see figure 3.53).

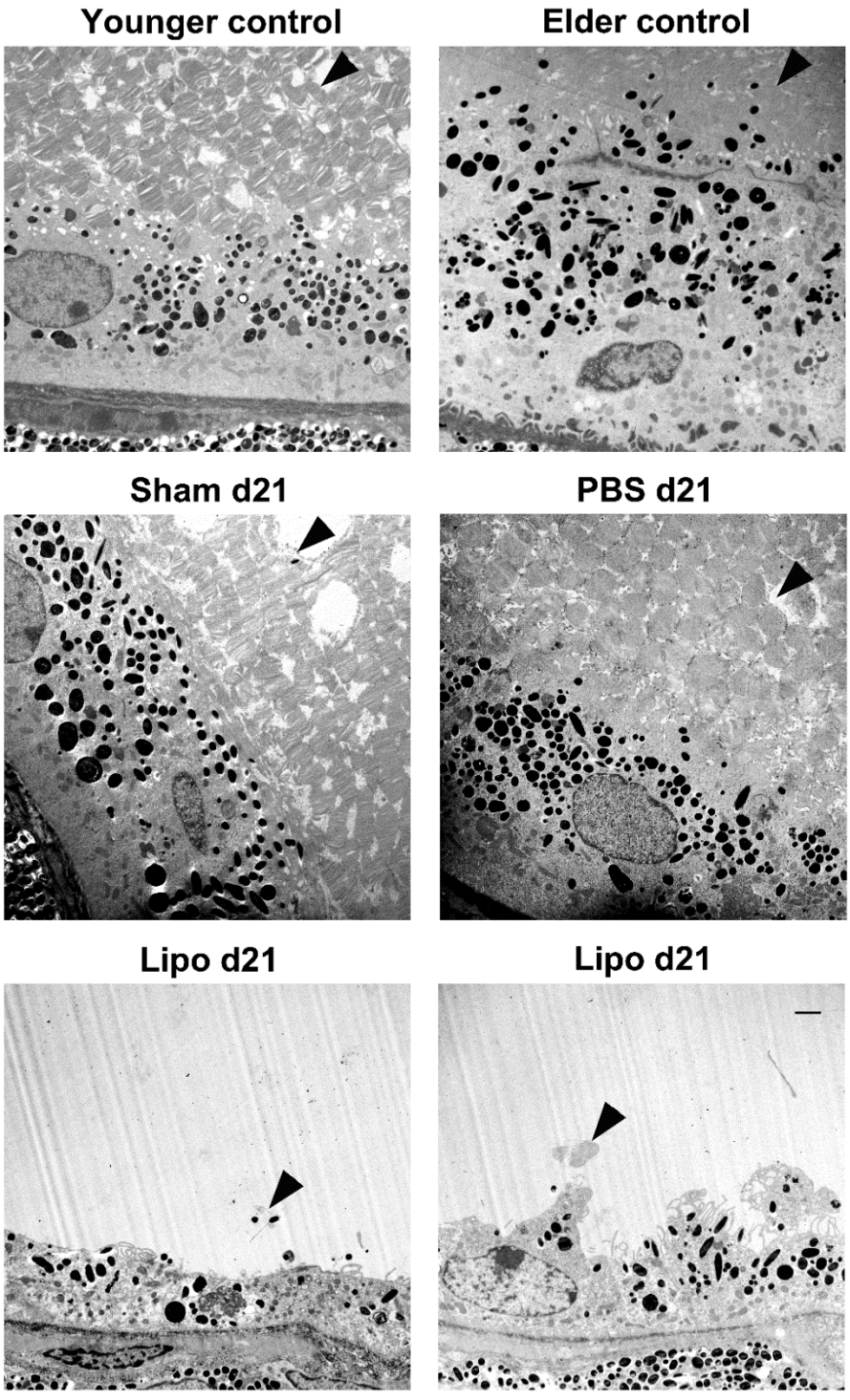

Fig. 3.53: The Photoreceptor Outer Segments in Younger and Elder Controls and Eyes 21 Days after Sham, PBS, and LF Injection.

Arrowheads point to the areas of photoreceptor outer segments. Scale bar in LF day 21: 600 nm.

4 Discussion

4.1 Synopsis

In this study, the effects of subretinally injected human LF on the murine retina were investigated *in vivo*.

The expression of the genes of several cytokines and growth factors was detected by PCR after subretinal injection of an LF suspension. It can be assumed that an injury to the eye by the injection needle alone may cause structural changes. Furthermore, the subretinal injection of fluid might also result in structural changes. It had been hypothesised that Iba1 positive cells (microglial cells or/and macrophages) take up lipofuscin, leading to an activation of the cells and to the release of pro-inflammatory cytokines and chemokines, which might contribute to retinal pathologies like age-related macular degeneration (AMD).

In the following paragraphs, the procedure is described of how subretinally injected LF from human RPE is phagocytosed by Iba1-positive cells. It is shown that the Iba1-positive cells contained LF granules 14 days after subretinal LF injection. In addition, the LF granules that were wrapped up in the RPE microvilli are also demonstrated. Furthermore, we discuss the indications for retinal degeneration after LF injection. The effects of the cell-derived inflammation are discussed with their relevance to retinal degeneration. One step further, the effects of microglial inhibitors (TKP and Minocycline) are also discussed. Moreover, the different effects of PBS and LF injection are also mentioned.

4.2 Feasibility of LF Isolation from Human RPE

In this study, LF was identified in histological sections by its autofluorescence using fluorescence microscopy with a GFP filter (excitation 470 nm, emission 525 nm) (see figures 1.2, 1.3). Since there is no specific antibody staining for lipofuscin, using its autofluorescence is the standard method for LF identification and detection (Leclaire, Nettels-Hackert *et al*. 2019). Besides its identification by autofluorescence, some classical histochemical techniques are also suitable for the observation of LF, such as Masson-Fontana and Schmorl staining (Chan, Ho *et*

al. 2003). However, because the identification of LF by autofluorescence is easy and reliable, we preferred this method to histochemical methods.

LF accumulates mainly in lysosomes. Therefore, dysfunction of the autophagolysosomal system is thought to play an important role in LF production (Terman, Dalen *et al*. 2004). In addition, many studies have shown that autophagy activity is reduced in aging animal and cell models, which seems to correspond to the accumulation of LF (Shirakabe, Ikeda *et al*. 2016) (Leon and Gustafsson 2016).

Age-related macular degeneration (AMD) is a degenerative disease of the central RPE and retina, and it is the most important cause of vision loss in the elderly population. AMD has a multifactorial aetiology. AMD is essentially characterised by the presence of lysosomal derived deposits, such as LF and melanolipofuscin. Generally, it is believed that LF can promote the incidence of AMD: because of its nature as a fluorochrome, the particles of LF in the RPE exposed to blue light produce pro-inflammatory effects and phototoxicity, which are mediated by reactive oxygen intermediates (ROI) and lead to an atrophy in AMD patients (Pollreisz, Messinger *et al*. 2018). Interestingly, A2E, the main fluorophore of LF, accumulates during AMD progression, and it appears to directly contribute to the photoinduced oxidative stress, resulting in the destruction of RPE membrane integrity.

4.3 LF and Microglial Cells

The accumulation of LF in cells is a hallmark of aging. RPE cells are regarded as LF-producing cells in the retina, and the LF in RPE is considered to be the main source of fundus autofluorescence (AF) (Delori, Goger *et al*. 2001).

There are at least three subsets of microglia in the retina: perivascular, parenchymal, and sub-retinal microglia (Dick, Ford *et al*. 1995) (Ng and Streilein 2001). In the study of Xu *et al*., it was demonstrated that in senescent mice, although LF particles were detected in RPE cells, more LF particles were found in Iba1-positive microglia, especially in the subretinal space and around blood vessels (perivascular). They also observed signs of AF in microglia. These phenomena indicate that subretinal microglia are involved in the removal of extensive

photoreceptor cell debris (Xu, Chen *et al*. 2008). In our study, we also found LF granules in many microglial cells, which were located in the subretinal space after LF injection (see figures 3.23 and 3.24).

At present, the origin of LF in retinal microglia is unknown. However, it is believed that in most post-mitotic cells, LF is derived from components of autophagocytosed cellular debris that is oxidised inside or outside the compartment of the lysosomes (Terman and Brunk 1998). The areas around the subretinal space and the blood vessels are important places to provide nutrition and oxygen to the retina and for clearing away metabolic waste. Choroidal macrophages and the microglia in the retina are vital cells in charge of removing retinal waste. Compared to microglia in other retinal areas, microglia in these regions may have higher phagocytic activity. Therefore, it is imaginable that retinal microglia are more likely to be affected by waste product overload. With aging, the ability of these cells to digest phagocytic waste may decrease, eventually becoming apparent as LF deposition increases. The results of Xu *et al*. indicate that microglia in these two locations (the subretinal space and nearby the blood vessels) are more active or more phagocytic than those in other retinal sites, and may play key roles in age-related retinal degeneration as in AMD. Xu *et al*. could demonstrate that in senescent mice, microglial cells are recruited to these locations, especially to the subretinal space, likely to phagocytose dysfunctional or apoptotic RPE cells. Additionally, their data show that at least in aging mouse retinae, microglial cells are an important source of fundus autofluorescence (Xu, Chen *et al*. 2008). These observations are consistent with our findings. Firstly, we found in the elder mice and in the Callithrix monkey that the LF in the RPE and the Bruch's member layer was much more abundant than it was in younger animals (see figures 1.2, 1.3). Moreover, the RPE and the Bruch's member layer in the elder mice was significantly thicker than it was in the younger mice (see figure 3.41). Secondly, we demonstrated in our study that Iba1-positive cells were present in the subretinal space after LF injection and most of them displayed a morphology suggestive of an activated state (see figures.3.23, 3.24 and 3.40).

It has been demonstrated in adult mice that retinal microglial cells migrate to the subretinal space under light stimulation (Ng and Streilein 2001). In a bone marrow chimera model, Xu *et al*. demonstrated that 6 months after bone marrow transplantation, retinal microglia migrated from the inner retina to the photoreceptor out segment (POS) layer in the peripheral area of the retina (Xu, Chen *et al*. 2007). Under pathological conditions, many studies have observed migration of retinal microglia into the subretinal space (Gupta, Brown *et al*. 2003) (Zeng, Zhu *et al*. 2005).

Microglia in the subretinal space were found to contain discs of POS (Ng and Streilein 2001) and melanosomes, which indicates a phagocytic activity. The possibility of microglia migrating to the subretinal space mainly to help RPE cells clear debris and even phagocytose the apoptotic RPE cells themselves. However, the ingested discs of POS and/or other debris may not be digested entirely, and this is hypothesised to be the mechanism of LF generation. LF changes the phenotype and function of microglia, such as after LF injection short time, even after 7 days, the microglial cells were detected in subretinal space and become an amoebic active pattern. It is believed that LF has a toxic effect on its host cells (Xu, Chen *et al*. 2008). LF also activates microglia and stimulates them to produce chemokines and inflammatory cytokines, which, in turn, may affect neural retina tissue (Leclaire, Nettels-Hackert *et al*. 2019). The report by Kunert *et al*. showed that with age, activated microglial cells accumulate in the photoreceptor layer (Kunert, Fitzgerald *et al*. 1999).

Xu *et al*. did not observe any apoptotic photoreceptor cells in the area where microglia accumulated in the sub-retinal space using electron microscopy. But they detected some adjacent degenerated RPE cells (Xu, Chen *et al*. 2007). However, in our study, we found that the number of photoreceptors was reduced after LF injection compared to control eyes after injection of PBS, sham treatment or without any treatment (see figure. 3.53).

Microglia are not normally present in the outer layer of the retina, however, with increasing age and in AMD, they migrate into the subretinal space and are activated, presumably to remove

age-related debris and support RPE. However, on the other hand, they can also cause oxidative stress and facilitate further degeneration (Ozaki, Campbell *et al*. 2014).

In our study, the microglial cells could clearly be identified in the subretinal space after PBS and LF injection in the subretinal space (see figures 3.22, 3.23 and 3.24). Without adding microglial inhibitory agents, the number of the MG in the subretinal space increased significantly (see figure.3.38).

4.4 Epiretinal Membrane Imaged by Multicolour Imaging

Imaging by the multi-colour mode consists of three independent lasers: blue, green, and infrared lasers, which simultaneously scan the shallow, middle, and deep layers of the retina, and then use superposition and pseudo-colour technology to clearly display all layers of the retina. Because the blue light wavelength is 488 nm, the penetration ability is weak, and it is mainly used to image the inner layers of the retina.

An epiretinal membrane on OCT is mainly manifested as a continuous highly reflective yellow-green light band of varying thicknesses on the surface of the nerve fibre layer and may be accompanied by retinal folds and tortuous changes in the surrounding small blood vessels.

The colour of an epiretinal membrane may vary in multi-colour imaging. A thicker membrane appears darker than a thinner one. Therefore, the colour depth can be used as an indicator to estimate the thickness of the epiretinal membrane (WANG Xiao 2018).

14 days and 28 days after LF injection, a reflection was visible in all three channels of multi-colour imaging at the injection site. In contrast, such reflections were visible only transiently 14 days after PBS injection. Each time point after sham injection or 7 or 28 days after PBS injection, reflections were seen only in the infrared channel. It may be suggested that the LF injection led to the formation of epiretinal membranes at day 14 and day 28 after injection (see figure.3.7).

4.5 ERG and AMD

Visual electrophysiology is an examination method that records the biological electrical activities of the visual system to diagnose diseases, identify the efficacy of the therapy and

evaluate the prognosis. It is a non-invasive objective visual function test method, mainly including electroretinography (ERG) and measurement of visual evoked potential (VEP). After the retina is stimulated by light flashes, a series of electrical responses can be observed, which originate from the photoreceptors and are transmitted to the post-receptoral neurones (horizontal cells, bipolar cells, amacrine cells and ganglion cells). The electroretinogram is the complex wave resulting of the responses of these different neurones, and it depends on their activity, the normal function of the RPE, the Müller cells, and retinal and choroidal blood circulation. In the electroretinogram, the a-wave and the b-wave can be distinguished, where the a-wave indicates the activity of the photoreceptors, and the b-wave indicates the activity of the inner retina, especially the ON bipolar cells, and the Müller cells. The 30 Hertz Flicker ERG is an orientation to estimate the post-receptor activity of the cones.

The oscillatory potentials are a measure of the extent of communication between the bipolar, amacrine, and ganglion cells. Usually, the amplitudes of the first four oscillations are added up to the so-called "oscillatory index".

Besides the amplitudes of a-waves and b-waves, pathological processes in the retina may also affect the speed of signal processing and transmission. This manifests itself then in altered times between the stimulating flash of light and the occurrence of the minimum of the a-wave and/or the maximum of the b-wave or of oscillations, the so-called latencies. Therefore, in this study, we also compare the latencies.

Evaluating the function of the photoreceptors in AMD, there is evidence that rods are firstly affected compared to cone in early AMD, resulting in a significant change in dark vision sensitivity. Rod-mediated mfERG responses are delayed in early AMD and elderly healthy individuals (Pedersen, Moller *et al*. 2010). Yavas *et al*. found that patients with early and late AMD had a lower mfERG response compared to the control group (old healthy individuals), but no significant difference was found between the early and late stages of the disease (Birch, Anderson *et al*. 1993).

In our ERG measurements, we found a decrease of amplitudes of a-waves and b-waves two weeks after the LF injection. The decrease was more pronounced at the highest light intensity than at the lower light intensity in the scotopic ERG. In the photopic ERG recorded in the LF injection group, the amplitudes of b-wave first decreased one week after the injection and did not recover fully two weeks after the injection. These changes are very different from those after sham and PBS injection. After LF injection, especially after two weeks in scotopic ERG, the changes described above are very similar to the early ERG performance in case of AMD. The difference between the sham, PBS and LF injection was more obvious in the scotopic ERG than in the photopic ERG (see figures 3.16, 3.17, 3.18). The one reason is that rods account for about 97% of all photoreceptors in mice. Another reason may be that the changes in the retina after LF injection could be similar to the changes observed in early AMD, as mentioned above: as also in early AMD, the rods are the first cells to be affected by changes.

4.6 Effects of Increased Pro-inflammatory Cytokines and Chemokines on Retinal and Neuronal Degeneration

The inflammatory response is widely regarded as one of the initiating and/or promoting factors of CNV in AMD (Bird 2010). Studies on the role of chemokines and their receptors in AMD (Olson, Courtney *et al*. 2007) (Xie, Kamei *et al*. 2011) indicate that chemokine targeting could be a potential therapeutic approach for AMD.

For the quantification of gene expression, we selected genes whose involvement in neovascular and inflammatory processes is already known from previous studies. VEGF-A (vascular endothelial growth factor) triggers neovascularisation. Angiogenic effects are also attributed to FGF-2 (fibroblast growth factor) and the pro-inflammatory cytokine interleukin-8 (IL-8). IL-8 does not exist in mice, so we examined CXCL1, which is also known as Gro-α or KC, and is a functional homologue of IL-8. Tumour necrosis factor (TNF-α), IL-1β, IL-6, and the chemokine CCL-2 were also investigated as typical pro-inflammatory cytokines. From previous studies, it is known that IL-6 and TNF-α are secreted by microglia in pathological situations. We therefore initially concentrated on these two cytokines.

Given the results of our experimental procedures, an inflammatory response towards LF in the retina is very likely. As part of this project, we also examined the effects of the microglia-inhibiting substances minocycline and the tripeptide TKP. It was of interest here whether these substances reduce a possible production of pro-inflammatory cytokines (see figure 3.26). For this purpose, the animals were treated with solutions of the substances over the test period after the injection of LF by placing daily a drop of these solutions on the eyes.

4.6.1 TNF- α

TNF-α is a pro-inflammatory cytokine, which is mostly released by macrophages, reactive astrocytes (Brenner, Yamin *et al*. 1993) and microglia (Meda, Cassatella *et al*. 1995). Glial cell activation at sites of CNS injury caused by a variety of diseases is involved in tissue injury by releasing TNF-α (Raivich, Bohatschek *et al*. 1999). In several retinal diseases, increased TNF-α production after glial cell activation is also associated with subsequent neuronal cell death. The localisation of TNF-α is most evident in the inner layers of the retina, consistent with the distribution of retinal glial cells. Cell bodies of the Müller cells span across almost the whole retina, and the astrocytes are mainly located in the nerve fibre layer and in the retinal ganglion cell layer. Furthermore, double immunofluorescence labelling further confirmed that TNF-α is mainly produced by retinal glial cells (Robinson and Dreher 1990) (Stone, Hollander *et al*. 1991). Madigan *et al*. demonstrated that TNF-α can cause axon degeneration in the rabbit optic nerve after intravitreal injection of TNF-α *in vivo* (Madigan, Sadun *et al*. 1996).

As a key mechanism for maintaining intracellular homeostasis, autophagy plays an important role in growth, adaptation, innate and acquired immunity, and aging (Karl and Reh 2010). Some studies have linked autophagy to the onset and development of many ocular diseases, including retinal diseases such as age-related macular degeneration (Saadat, Murakami *et al*. 2014), corneal dystrophy (Choi, Kim *et al*. 2011), and glaucoma (Piras, Gianetto *et al*. 2011). Xie *et al*. found that protective autophagy by using TNF-α inhibitors led to a decrease in photoreceptor cell death and an increase in cell survival (Xie, Zhu *et al*. 2017).

4.6.1.1 Clinical Implications of TNF-α

In healthy eyes, RPE cells are polarised, however, they lose their polarity in AMD. It is important to note that TNF-α alone can affect the barrier function of polarised RPE cells (Bhutto and Lutty 2012).

4.6.1.2 Paradoxical Effect of TNF-α

Mac Nair *et al*. found that TNF-α is not conducive to RGC and protects RGC, which seems to be contradictory. However, their data show that early TNF-α exposure before the optic nerve injury may be protective, whereas chronic TNF-α expression may finally lead to neuronal damage and loss (Mac Nair, Fernandes *et al*. 2014).

In our study, the expression of TNF-α increased one day after the injection of PBS and, to a higher extent, of LF, both in the retina and in the RPE/choroid complex. As demonstrated in this study by immunofluorescence staining, TNF-α is also present in the retina of healthy control mice. This could indicate that after injection, early TNF-α exposure may be protective. It is striking that the level of TNF-α expression in the RPE/choroid complex is higher than in the retina. This indicates the importance of RPE cells as suppliers of pro-inflammatory cytokines in inflammatory processes (see figure 3.42). The results of the immunostaining clearly show that immunoreactivity (IR) against TNF-α is stronger after LF injection than under the treatment with the microglial inhibitors minocycline and TKP (see figure 3.28)

Tezel *et al*. observed that there was IR for TNF-α in normal retinae even though it was weak and it was limited to a few glial cells and their processes as well as blood vessels (Tezel, Li *et al*. 2001). In our study, we also found that IR for TNF-α was present in normal retinae and showed some co-localisations with NeuN-positive cells (see fig.3.37).

4.6.2 IL-6

IL-6 is an interleukin that is not only a pro-inflammatory cytokine but also an anti-inflammatory myokine (Ferguson-Smith, Chen *et al*. 1988). Leibinger *et al*. found that IL-6 expression was significantly induced in the retina after mechanical stimulation of the retina and optic nerve injury. It was also postulated that IL-6 contributes to the beneficial effects of inflammatory

stimulation. Such as, binding of IL-6 to IL-6R initiates the dimerisation of gp130 and subsequent downstream signal transduction, which leads to the activation of selected cells like microglia. This microglial cell activation is involved in pathogen defence responses (Leibinger, Muller *et al*. 2013). Echevarria *et al*. suggested that although constitutive IL-6 deficiency appears to promote cell survival and to promote an anti-inflammatory environment, IL-6 deficiency overreacts to TNF-α and exposes the retina to stressors and it reduces the expression of anti-apoptotic factors in the retina (Echevarria, Rickman *et al*. 2016).

Chong *et al*. showed that the rate of photoreceptor apoptosis can be significantly increased by genetic ablation or inhibition of IL-6 by giving neutralizing antibodies to IL-6, therefore supporting the role of IL-6 as a controller of photoreceptor apoptosis after separation of the neuronal retina from the RPE (Chong, Boehlke *et al*. 2008).

IL-6 acts by two different pathways on cells. One activation pathway is through the formation of a complex with the soluble IL-6 receptor (sIL-6R), which is released by naïve T-cells during their differentiation. The complex stimulates cells that express gp130 but do not surface-bind to IL-6R and are therefore inherently insensitive to IL-6. gp130 is expressed in many cells, including glial cells and neurons, explaining the widespread effects of chronic IL-6 elevation. Formation and stimulation of the IL6-sIL6R complex are known as trans-signalling (Rose-John and Heinrich 1994). The second pathway is the classical anti-inflammatory pathway that works by stimulating the membrane-bound IL-6 receptor (IL-6R), which initiates dimerisation of gp130 and subsequent downstream signalling, leading to selective cell activation in these microglia, which is appropriate for pathogen defence responses (Taga, Hibi *et al*. 1989).

While the RPE is known to release IL-6, the presence of IL-6 immunoreactivity in the photoreceptor inner segments in our study (see figure 3.26) remains to be explained. To the best of our knowledge, no author has mentioned presence of IL-6 in the inner segments of the retina so far.

Expression of IL-6 increased one day after the injection of LF, both in the retina and in the RPE/choroid complex. The expression of IL-6 was usually higher after LF injection compared

to controls that did not receive any injection and compared to controls that received solely PBS injection. The level of expression in the RPE/choroid complex was much higher than in the retina (see figure 3.42). Immunohistochemistry shows this effect especially in the GCL and photoreceptor inner segments. TKP suppressed the immunoreactivity for IL-6 much stronger than minocycline (see figure 3.26).

4.6.3 TNF-α and IL-6

In summary, combined with our results, we found that there are some co-localisations of NeuN with IL6 and TNF-α IR. However, some studies showed that TNF-α is mainly produced by glial cells in the retina (Robinson and Dreher 1990) (Stone, Hollander *et al*. 1991).

In other studies, it was found that IL-6 is a multipotent cytokine that acts in inflammation, angiogenesis, haematopoiesis, neuronal survival, and in cell differentiation (Ebrahem, Minamoto *et al*. 2006). In the retina, IL-6 is synthesised by retinal pigment epithelium and Müller cells (Yoshida, Sotozono *et al*. 2001). Chong *et al*. found that IL-6 could play a photoprotective and neuroprotective role in retinal RPE separation performed by subretinal injection of 1% hyaluronic acid (Chong, Boehlke *et al*. 2008). In the central nervous system, IL-6 is synthesised by microglia, neurons, and astrocytes (Gadient and Otten 1997). Leclaire *et al*. found that very high levels of IL-6 are produced by microglial cells after incubation with LF (Leclaire, Nettels-Hackert *et al*. 2019).

According to our results, it can be hypothesised that ganglion cells also produce IL-6 and TNF-α**,** or/and Il6 as well as TNF-α might bind ganglion cells going to GCL. In addition, IL-6 is not only an inflammatory factor, but also a growth factor for nerve cells. However, we also found IL-6 to be present in photoreceptors (see figure 3.26) It could be hypothesised that IL-6, after being secreted from RPE, enters the photoreceptor cell layer to protect the photoreceptors, or act as a growth factor for photoreceptors.

4.6.4 The Effect of HIF-1α and Its Target Genes in AMD

Hypoxia-inducible factor (HIF)-1α is a major hypoxia signalling protein that responds to low oxygen concentrations and regulates various target genes (Semenza 2004). It consists of an α-

subunit that is oxygen-sensitive and α, β subunit. In the presence of oxygen, HIF-1α is hydroxylated at two prolyl residues (Pro^{402} and Pro^{564}) by HIF prolyl-4-hydroxylase. Hydroxylation makes HIF-1α susceptible for ubiquitination and degradation (Ivan, Kondo *et al*. 2001). In case of hypoxia, prolyl hydroxylation is inhibited, HIF-1α migrates to the nucleus, dimerises with HIF-1β, and activates gene transcription. HIF-1α stimulation involves gene expression of multiple cellular processes, including vasodilation and neovascularisation proteins, erythropoietin or VEGF (Ke and Costa 2006). VEGF-A is the most important factor in pathological neovascularisation in the eye (Homayouni 2009).

HIF-1α is heavily expressed in the retina (Hughes, Groot *et al*. 2010). Several of the target genes of HIF-1α have been identified. Under normoxia, the level of production of these targets is relatively low. Target genes play a very important role in the regulation of several key cellular processes such as angiogenesis, cell differentiation, apoptosis, and erythropoiesis (Vadlapatla, Vadlapudi *et al*. 2013).

There is growing evidence that HIF-1α and its target genes contribute to retinal neuroprotection in certain retinal degenerative diseases, including age-related macular degeneration, diabetic retinopathy, and glaucoma (Cheng, Yu *et al*. 2017). Several drugs, such as dimethyloxaloglycine (DMOG), deferoxamine, Roxadustat can lead to a stabilisation or activation of HIF-1α, thereby conferring retinal neuroprotective effects in animal models of retinal degeneration, such as oxygen-induced retinopathy (OIR), retinopathy of prematurity, and light-induced retinal degeneration (Hoppe, Lee *et al*. 2014).

Oxidative stress is associated with the senescence of RPE cells and the pathogenesis of AMD. The development of choroidal neovascularisation (CNV), mainly mediated by HIF-1α and VEGF, is the most important complication in AMD. Thus, inhibition of HIF-1α and VEGF is commonly used to treat AMD; however, focused activation of HIF transcription factors in normoxic photoreceptors has been found to result in transient rod protection against light damage (Lange, Heynen *et al*. 2011). In our study, only minor effects on IR for HIF-α were seen after treatment with minocycline or TKP (see figure 3.30).

Inhibition of VEGF mentioned above by anti-VEGF agents is widely used in the treatment of CNV in AMD. However, given the well-documented role of VEGF in the normal development of the retinal vascular system, long-term inhibition of VEGF may have deleterious effects on the remaining healthy retina (Hernandez and Simo 2012). Non-isoform-specific inhibition of VEGF can limit the neuroprotective effects of some VEGF isoforms and damage retinal and sensory neurons. Inhibition of VEGF after photodynamic therapy resulted in elevated VEGF levels, leading to photoreceptor apoptosis, suggesting a neuroprotective effect of VEGF after photodynamic therapy (Suzuki *et al*., 2011). The depletion of VEGF-A specifically in neural progenitor cells leads to retinal thinning and abnormal cortical development (Haigh, Morelli *et al*. 2003).

In our results of qPCR, VEGF-A is expressed in a relatively high degree in the untreated eye, both in the retina and in the RPE/choroid complex. In the retina, VEGF-A mRNA levels decrease slightly two weeks after injections. Expression increases transiently in the RPE/choroid complex after injection of PBS and is not affected after injection of LF (see figure 3.44).

In the immunostaining, IR for VEGF was found in the GCL and IPL of the retina in the treatment with PBS and minocycline 7 days and 14 days after injection. 28 days after injection, it was not present in the PBS group, and in the minocycline group only in the GCL. There was almost no IR for VEGF present in the TKP group after 7 days, and it appeared gradually in the GCL and IPL 14 days and 28 days after LF injection (see figure 3.36).

These data might be supporting the hypothesis that after injury, the retina, RPE and other tissues try to protect the neurones by increasing the level of VEGF-A. TKP is not only a microglia inhibitor but also may play an important role in regulating the expression level of VEGF-A.

4.6.5 Pro-inflammation and AMD

It is known that inflammation contributes to the pathogenesis of AMD (Kauppinen, Paterno *et al*. 2016). Macrophages and infiltrating lymphocytes may promote AMD-related RPE dysfunction during ocular inflammation (Cousins, Espinosa-Heidmann *et al*. 2004).

Kutty *et al*. found that TNF-α, IL-1β, and IFN-γ can reduce the expression of the essential genes involved in the visual cycle. Therefore, the downregulation of key functional gene expression due to the secretion of TNF-α, IL-1β, and IFN-γ by inflammatory cells targeting RPE cells may potentially lead to RPE dysfunction related to AMD pathology (Kutty, Samuel *et al*. 2016).

Lechner *et al*. found that PBMC (peripheral blood mononuclear cells), especially monocytes, may promote the development of CNV in nAMD by recruiting them to the macula to secrete elevated levels of IL-8, CCL2, and VEGF (Lechner, Chen *et al*. 2017).

In an inflammatory response, cytokines are conducive to the inflammatory cascade response at local and systemic levels. Monocytes differentiate into macrophages through the combined action of CCL2 (monocyte chemoattractant protein-1, MCP-1), which is a chemokine for monocytes and other immune cells. In AMD, activated macrophages (Forrester 2003) and microglia secrete and respond to cytokines, and then migrate to injury sites. According to the activation state of the microglia and macrophages, they may clear subretinal deposits or aggravate inflammation and cause CNV (Sakurai, Anand *et al*. 2003).

Interleukin-6 (IL-6) is commonly used as a marker of systemic inflammation and is a pro-inflammatory cytokine produced at the sites of both acute and chronic inflammation by some cells, such as macrophages. IL-6 can cause RPE degeneration (Leung, Barnstable *et al*. 2009)**.** Newman *et al*. performed RPE choroidal transcription profile analysis from eyes with geographic atrophy, which is an advanced form of dry AMD, and found that IL-6 transcription levels were higher than in the control group (Newman, Gallo *et al*. 2012). Jonas *et al*. suggested that wet AMD showed elevated IL-6 levels in the aqueous humour (Jonas, Tao *et al*. 2010). Although IL-6 seems to have been elevated at the local level of AMD, the association at the systemic level is unclear (Seddon, George *et al*. 2005).

All of the cytokines CXCL1, CXCL2, CXCL9, CXCL10, CXCL11, CCL2, and CCL8 were detected in the RPE and in the choroid of all AMD subtypes studied, and the expression of some or all cytokines was increased (Newman, Gallo *et al*. 2012). These chemokines are involved in the recruitment of leukocyte and several chemokines. The intraocular CCL2 concentrations are increased in wet AMD eyes (Jonas, Tao *et al*. 2010).

In AMD, several PRRs (pattern-recognition receptors) are activated by endogenous intra-cellular and extracellular danger signals, which cause an inflammatory response that goes beyond para-inflammation. Para-inflammation reactions are the responses to dysfunction or harmful pressure, which have features between the basal and the inflammatory states ((Xu, Chen *et al*. 2009). Age-related changes in the immune system contribute to this devastating process by changing the function of immune cells. Degeneration of RPE cells triggers a vicious cycle that promotes the development of chronic inflammation in the choroid and retina (Kauppinen, Paterno *et al*. 2016).

The activation PRRs of inflammation causes the cells to secrete chemokines and cytokines, such as TNF-α, IL-12, IL-1β, IL-6, and IL-8 (CXCL8). The local effects of TNF-α and IL-1β include the activation of endothelial cells, which is one of the most prominent processes at the start of inflammation (Lentsch and Ward 2000). Other chemokines of the CXC family, *e.g*. CXCL1 (keratinocyte-derived chemokine; KC) and CXCL2 (MIP-2) are also involved in the recruitment of neutrophils (Kobayashi 2008).

In our results of qPCR, CXCL1 was expressed much more in the RPE than in the retina (see figure 3.43), which again emphasises the role of the RPE in cytokine expression.

4.6.6 FGF-2 and Ocular Angiogenesis

FGF-2, also known as basic FGF, is a heparin-binding growth factor that appears in a variety of isoforms. FGF-2 signals through four receptors, *i.e.*, tyrosine kinases (FGF receptor 1 to FGF receptor 4) and plays a role in various developmental processes including angiogenesis.

Increased expression of FGF-2 has been detected in the CNV membrane of patients with AMD and in epiretinal membranes of patients with proliferative diabetic retinopathy. However, in an

experimental model of CNV, exogenous administration of FGF-2 only caused new blood vessel formation in the subretinal space without penetrating Bruch's membrane (Rubio and Adamis 2016).

Some studies have found that transgenic mice with an increased expression of FGF-2 in the retina produce CNV after treatment with a low-intensity laser (enough to damage the photo-receptors, but not the Bruch's membrane), while wild-type mice do not. Along with studies demonstrating that genetic ablation of the FGF-2 gene did not hold back the formation of laser-induced CNV, the results of these studies indicate that FGF-2 itself is not sufficient to provoke CNV in the absence of additional stimulation and that FGF-2 does not necessarily lead to CNV induction (Rubio and Adamis 2016).

Di Pierdomenico *et al*. found that degenerating photoreceptors in P23H-1 and RCS rats could be morphologically rescued by an intravitreal injection of neurotrophic factors (FGF-2, CNTF, or PEDF), which suggests that neurotrophic factors have neuroprotective effects. It has nothing to do with the cause of degeneration (RPE malfunction or rhodopsin mutation). However, only FGF-2 treatment can significantly save the average number of nuclear rows in ONL (Di Pierdomenico, Scholz *et al*. 2018). In addition, some other results suggest that FGF-2 not only rescues the morphology of photoreceptor, but also raise the survival of the photoreceptor, reduces apoptosis of the photoreceptor cells, and improves the responses of ERG(Sakai, Kuno et al. 2007).

We found that FGF-2 is mainly expressed in the retina (see figure 3.44). The expression of FGF-2 after LF injection was higher than after PBS injection 3 and 7 days after injection (see figure 3.44). Probably, increased expression of FGF-2 is an attempt of the retina to protect itself from deleterious effects of LF injection.

4.7 Microglial Inhibitors

In the following, the results of microglia inhibitors and anti-inflammatory agents, the tripeptide TKP and minocycline, are discussed.

4.7.1 The Effect of TKP

TKP is a tripeptide, composed of threonine, lysine and proline. It is an inhibitor of microglial cells and macrophages. TKP can delay neuronal death and enhance axonal regeneration. TKP is an effective inhibitor of microglia activation (Bhasin, Wu *et al*. 2007). Thanos *et al*. reported that TKP significantly decreased the proliferation of MG and afterwards reduced the ganglion cell degradation after single or multiple injections of TKP into the vitreous of the rats (Thanos, Mey *et al*. 1993).

The results of our study demonstrate that the beneficial effects of TKP are not only anti-inflammatory, but TKP also inhibits migration of retinal microglial cells into the subretinal space after injection (see figure 3.38). Furthermore, the results of our study indicate that TKP inhibits production of inflammatory cytokines. Thus, action of TKP could modulate processes leading to late forms of AMD.

4.7.2 The Effect of Minocycline

Minocycline is a microglia inhibitor that is widely used to perform neuroprotection studies in CNS diseases (Hashemi-Monfared, Firouzi *et al*. 2018).

Studies have indicated that minocycline has antibacterial, anti-apoptotic, anti-inflammatory and neuroprotective properties (Arroba, Alvarez-Lindo *et al*. 2011) (Scholz, Sobotka *et al*. 2015). Direct anti-apoptotic effects on photoreceptors have also been described, and an effect by its anti-inflammatory properties (Scholz, Sobotka *et al*. 2015). The results of Di Pierdomenico *et al*. suggest that the application of minocycline significantly reduces the activation and migration of microglia, maintain the retinal structure by preserving the morphology of the outer segments of the photoreceptor cells, thereby, protect these neurons (Di Pierdomenico, Scholz *et al*. 2018).

Minocycline has some neuroprotective effects in a mouse model of Huntington's dance syndrome (Lacassin, Schaffo *et al*. 1995).

A study reported the effects of minocycline on clinical and magnetic resonance imaging (MRI) results and serum immune molecules in 40 patients with multiple sclerosis (MS) during 24 months of open-label minocycline treatment. The clinical and MRI results of this study are

supported by systemic immunological alterations and call for further studies of minocycline in MS (Maier, Merkler *et al*. 2007).

In a meta-analysis, the overall antidepressant effect size of minocycline compared to placebo was 0.78, indicating a potential antidepressant effect (Popovic, Schubart *et al*. 2002).

The activation of microglial cells is an early event in retinal degeneration (Arroba, Alvarez-Lindo *et al*. 2011), so modulating these cells may be a potential treatment to provide photoreceptor neuroprotection. In contrast, some studies have shown that microglia are needed to promote the survival of photoreceptor cells (Arroba, Alvarez-Lindo *et al*. 2011) (Guadagni, Novelli *et al*. 2015). In fact, different functions such as neuroprotection but also neurodestructive effects have been proposed for resident, activated, and for migrating microglial cells (Narayan, Wood *et al*. 2016). Nevertheless, Di Pierdomenico *et al*. believe that the neuroinflammation caused by the main loss of the rods plays an important role in the secondary loss of the cones, the most serious consequence of retinitis pigmentosa (RP) (Guadagni, Novelli *et al*. 2015) (Narayan, Wood *et al*. 2016) (Di Pierdomenico, Garcia-Ayuso *et al*. 2019).

In our study, we found that minocycline and TKP have very similar effects in slowing down the entry of retinal microglia into the subretinal space and their return into the retina (see figure 3.38). Therefore, much less microglial cells were present in the subretinal space one and two weeks after the injection of LF under the influence of minocycline and TKP, whereas slightly more microglial cells were in the subretinal space after four weeks. Nevertheless, the suppressive effect of minocycline on the inflammatory reaction was weaker than the effect of TKP in most cases (see figures 3.26, 3.27, 3.29, 3.31 and 3.34). The results of our study indicate that the inflammatory reaction of the microglia and the RPE during the phagocytosis of LF may be involved in the pathogenesis of AMD, and inhibition of this inflammatory reaction could potentially be a therapeutic approach.

4.8 The Effects of Injected LF Studied by Electron Microscopy

In normal aged mice, retinal degeneration becomes more and more obvious, as in these mice slight signs of disorder and of shortening of the photoreceptor layer, and even complete photoreceptors loss occur. Similar to our result of 21days after LF injection (see figure 3.53).

In our study, we detected the drusen-like deposits or undigested POS phagosomes in the sub-retinal space three weeks after subretinal LF injection in younger mice (see figure 3.47). Moreover, cystic membranous degradation of RPE could be observed in RPE cells. In contrast, after sham and PBS injection, these degenerative features could not be found (see figures 3.46 and 3.47). These degenerative features are consistent with those befall in human atrophic AMD (see figure.1.9).

Similarly, Bruch's membrane thickening with extensive alteration in RPE basal labyrinth, large sub-RPE drusenoid (*i.e.*, drusen-like) deposits, cystic membranous degradation of RPE, and undigested POS phagosomes were detected in sTg-IRBP:HEL mice, which could serve as a model for drusen formation in dry AMD. (Liu, Molzer *et al*. 2019).

We observed RPE cell atrophy and shortening and a disorganisation of the photoreceptor layer and even a complete photoreceptor loss in some positions after LF injection. These features of degeneration are consistent with those found in human atrophic AMD *i.e.*, in geographic atrophy. These signs of retinal degeneration did not occur in the animals treated with PBS and with sham injection (see figure.3.50).

In our study, we observed a thinning and a disorganisation of Bruch's membrane. This is different from the findings by Liu *et al*., who observed Bruch's membrane thickening in a transgenic mouse model of drusen formation (Liu, Molzer *et al*. 2019) (see figures 3.46 and 3.47).

4.8.1 The Effects in RPE Basal Labyrinth

The basal surface of the RPE is highly folded and is called a labyrinth. It interacts with the Bruch's membrane, and it is believed to promote transport of water and soluble substances. The

labyrinth has a complex but ordered structure that is lost with age and in case of choroidal diseases. Hayes *et al*. suggested that the geometry of these elements and the areas that have contact with the mitochondria and endoplasmic reticulum may promote ion migration, which in turn promotes water migration through the RPE base surface (Hayes, Burgoyne *et al*. 2019).

In our study, we found that the labyrinth lost its structural order in young mice after LF injection especially at day 21. Similar findings were observed in senescent control mice. Our results therefore support the thesis that with RPE impairment and with increasing age, the structure of the labyrinth is destroyed, and the labyrinth loses its function, which might be one of the reasons for the RPE cells atrophy (see figure 3.49).

4.8.2 The Effects in RPE Cells and Its Microvilli

The RPE is a one-cell layered epithelium containing very long lamellar apical microvilli that extend into the interphotoreceptor matrix. The microvilli interact with the photoreceptor outer segments (POS) extending from the outer part of the retina. The individual POS of a cone can be associated with 30-40 microvilli. They vary in length, with only a few reaching the POS. The apical microvilli of the RPE wrap around the POS, extending halfway to them. Multiple microvilli may surround each other and simultaneously surround the POS, whereas a single RPE microvillus may completely surround the outer segment. (Bonilha, Rayborn *et al*. 2006).

RPE performs highly unique and specialised functions, which are essential for the dynamic balance of the neural retina. All the functions of RPE involve the microvilli which are the top of RPE cells (Lamb and Pugh 2004).

With increasing age, the RPE undergoes many well-characterised structural changes, including the loss of melanin particles, an increase in residual microsomal density, an accumulation of LF and of basal deposits on or within Bruch's membrane and the formation of drusen (between the basal layer of the RPE and the inner collagen layer of Bruch's membrane). Furthermore, Bruch's membrane thickens, and a microvilli atrophy and a disorganisation of the labyrinth can be observed (Gu, Neric *et al*. 2012). The characteristics of these age-related changes of the RPE have some features in common with changes observed in AMD (Bonilha 2008).

In our study, we observed that the microvilli of the RPE cells lost their orderly structure and became shorter after LF injection than in control animals (see figures 3.50**)**. Moreover, the number of microvilli decreased heavily, compared to the group that was treated with sham and to the group with PBS injection and also to the younger negative control mice. As we described above, all the functions of RPE involve the microvilli. This atrophy of microvilli (see figures 3.51 and 3.52) and the resulting loss of function of the RPE could be one reason why a reduced number of photoreceptors was observed. We also noticed that the RPE cells lost melanin on day 21 after LF injection. Moreover, we observed an RPE cell atrophy, a formation of drusen-like granular deposits, and an accumulation of LF granular in microvilli. This underlines the possible influence of subretinally injected LF on RPE cells (see figures 3.46, 3.47 and 3.50).

4.9 The Features of AMD in OCTA

OCT angiography (OCTA) is a novel technique that allows a precise visualisation of blood flow in retinal and choroidal blood vessels.

OCTA utilises the advancement of image resolution and acquisition speed in order to generate detailed three-dimensional vascular maps of the retina. By acquiring images in rapid succession and evaluating their differences, the software in the OCTA devices can identify blood flow in blood vessels. These images are depth coded to form a three-dimensional volume. This image can be scanned and checked for all vascular abnormalities at the retinal level (Spaide, Klancnik *et al*. 2015).

OCTA is not affected by bottom layer leakage, so it can directly image neovascular lesions (Bonini Filho, de Carlo *et al*. 2015). While blood vessels in fluorescence angiography may be hidden by a leakage, they can be readily visualised 易于可视化using OCTA.

The three-dimensional 维aspect of the OCTA images helps distinguish between type 1 and type 2 CNV membranes (CNVMs) (Spaide, Klancnik *et al*. 2015). Depending on their presence below or above RPE, this depth information can not only be used to identify type 3 neo-vascularisations but also to visualise retinal angiomatous [ˌændʒi'oʊmətəs] proliferation (RAP) lesions.

OCTA has made significant progress in the management of AMD patients, but there are still some limitations and disadvantages, such as motion artefacts 运动假象 and projection 投影 artefacts. Moreover, in contrast to fluorescein angiography (FA), leakages cannot be visualised by OCTA (de Carlo, Romano *et al*. 2015).

In our study, we noticed that avascular layers, *i.e.*, the outer retina, have a normal appearance at the injection site after sham treatment. However, after PBS and LF injection, a blood flow is visible in the outer retina (see figure 3.12). This indicates that some blood vessels may have grown into the outer retina as part of a kind of wound healing.

4.10 About Immunostaining

We subsequently performed many immunohistochemical staining of the microglial cells against Iba1 or CD11b with a Texas Red-conjugated second antibody. This had the advantage that, in addition to the Texas Red fluorescence, the auto-fluorescence of any present LF can be detected. This way, we were able to find autofluorescent cells and microglial cells positive for Iba-1 or CD11b that contained LF in the subretinal area of the eyes of older mice 5, 7 and 14 days after the injection of LF (see figures 3.22, 3.23 and 3.24).

And we also performed some immunohistochemical double staining of the microglia cells with AF 488-conjugated (green colour) second antibody and several other proteins with a Texas Red-conjugated second antibody (see figures.3.26, 3.27, 3.28, 3.29 3.30, 3.31, 3.32, and 3.36). Results of staining for the different cytokines were in line with the results of qPCR analysis.

5. Conclusions

In this study, it is shown for the first time that microglial cells are activated after a subretinal injection of LF. The interaction between the microglia and LF is clearly shown in this study.

After subretinal injection of LF, microglial cells migrated into the subretinal space, where their morphology changed towards an activated state, *i.e.*, with shorter or completely missing processes and an amoeboid shape. Moreover, there was a sharp transient increase in pro-inflammatory cytokines after LF injection, which was more pronounced and longer lasting in the RPE/choroid complex than in the retina. Pro-angiogenic factors did not show such a clear increase. Treatment with microglial inhibitors resulted in a decreased number of microglial cells in the subretinal space after LF injection after one and two weeks, and a reduced expression of pro-inflammatory cytokines.

Inspection of the back of the eye on the ultrastructural level revealed changes in the Bruch's membrane and the structural integrity of RPE cells and photoreceptor outer segments.

We can conclude that injecting human LF into the subretinal space of mice imitates pathological processes seen in AMD, in particular geographic atrophy.

As a further step, investigation of the effects of microglial inhibitors on gene expression and morphological integrity of the RPE may be of interest in future studies.

Reference

Alliot, F., E. Lecain, B. Grima and B. Pessac (1991). "Microglial progenitors with a high proliferative potential in the embryonic and adult mouse brain." Proc Natl Acad Sci U S A **88**(4): 1541-1545.

Ambati, J., A. Anand, S. Fernandez, E. Sakurai, B. C. Lynn, W. A. Kuziel, B. J. Rollins and B. K. Ambati (2003). "An animal model of age-related macular degeneration in senescent Ccl-2- or Ccr-2-deficient mice." Nat Med **9**(11): 1390-1397.

Arroba, A. I., N. Alvarez-Lindo, N. van Rooijen and E. J. de la Rosa (2011). "Microglia-mediated IGF-I neuroprotection in the rd10 mouse model of retinitis pigmentosa." Invest Ophthalmol Vis Sci **52**(12): 9124-9130.

Bennett, M. L., F. C. Bennett, S. A. Liddelow, B. Ajami, J. L. Zamanian, N. B. Fernhoff, S. B. Mulinyawe, C. J. Bohlen, A. Adil, A. Tucker, I. L. Weissman, E. F. Chang, G. Li, G. A. Grant, M. G. Hayden Gephart and B. A. Barres (2016). "New tools for studying microglia in the mouse and human CNS." Proc Natl Acad Sci U S A **113**(12): E1738-1746.

Bhasin, M., M. Wu and S. E. Tsirka (2007). "Modulation of microglial/macrophage activation by macrophage inhibitory factor (TKP) or tuftsin (TKPR) attenuates the disease course of experimental autoimmune encephalomyelitis." BMC Immunol **8**: 10.

Bhutto, I. and G. Lutty (2012). "Understanding age-related macular degeneration (AMD): relationships between the photoreceptor/retinal pigment epithelium/Bruch's membrane/choriocapillaris complex." Mol Aspects Med **33**(4): 295-317.

Birch, D. G., J. L. Anderson, G. E. Fish and B. F. Jost (1993). "Pattern-reversal electro-retinographic follow-up of laser photocoagulation for subfoveal neovascular lesions in age-related macular degeneration." Am J Ophthalmol **116**(2): 148-155.

Bird, A. C. (2010). "Therapeutic targets in age-related macular disease." J Clin Invest **120**(9): 3033-3041.

Bodeutsch, N. and S. Thanos (2000). "Migration of phagocytotic cells and development of the murine intraretinal microglial network: an in vivo study using fluorescent dyes." Glia **32**(1): 91-101.

Bonilha, V. L. (2008). "Age and disease-related structural changes in the retinal pigment epithelium." Clin Ophthalmol **2**(2): 413-424.

Bonilha, V. L., M. E. Rayborn, S. K. Bhattacharya, X. Gu, J. S. Crabb, J. W. Crabb and J. G. Hollyfield (2006). "The retinal pigment epithelium apical microvilli and retinal function." Adv Exp Med Biol **572**: 519-524.

Bonini Filho, M. A., T. E. de Carlo, D. Ferrara, M. Adhi, C. R. Baumal, A. J. Witkin, E. Reichel, J. S. Duker and N. K. Waheed (2015). "Association of Choroidal Neovascularization and Central Serous Chorioretinopathy With Optical Coherence Tomography Angiography." JAMA Ophthalmol **133**(8): 899-906.

Booij, J. C., D. C. Baas, J. Beisekeeva, T. G. Gorgels and A. A. Bergen (2010). "The dynamic nature of Bruch's membrane." Prog Retin Eye Res **29**(1): 1-18.

Brenner, T., A. Yamin, O. Abramsky and R. Gallily (1993). "Stimulation of tumor necrosis factor-alpha production by mycoplasmas and inhibition by dexamethasone in cultured astrocytes." Brain Res **608**(2): 273-279.

Buschini, E., A. Piras, R. Nuzzi and A. Vercelli (2011). "Age related macular degeneration and drusen: neuroinflammation in the retina." Prog Neurobiol **95**(1): 14-25.

Chan, A. C., L. C. Ho, W. W. Yip and F. C. Cheung (2003). "Pigmented ependymoma with lipofuscin and neuromelanin production." Arch Pathol Lab Med **127**(7): 872-875.

Cheng, L., H. Yu, N. Yan, K. Lai and M. Xiang (2017). "Hypoxia-Inducible Factor-1alpha Target Genes Contribute to Retinal Neuroprotection." Front Cell Neurosci **11**: 20.

Choi, S. I., B. Y. Kim, S. Dadakhujaev, J. V. Jester, H. Ryu, T. I. Kim and E. K. Kim (2011). "Inhibition of TGFBIp expression by lithium: implications for TGFBI-linked corneal dystrophy therapy." Invest Ophthalmol Vis Sci **52**(6): 3293-3300.

Chong, D. Y., C. S. Boehlke, Q. D. Zheng, L. Zhang, Y. Han and D. N. Zacks (2008). "Interleukin-6 as a photoreceptor neuroprotectant in an experimental model of retinal detachment." Invest Ophthalmol Vis Sci **49**(7): 3193-3200.

Claudepierre, T., M. Paques, M. Simonutti, I. Buard, J. Sahel, R. A. Maue, S. Picaud and F. W. Pfrieger (2010). "Lack of Niemann-Pick type C1 induces age-related degeneration in the mouse retina." Mol Cell Neurosci **43**(1): 164-176.

Cousins, S. W., D. G. Espinosa-Heidmann and K. G. Csaky (2004). "Monocyte activation in patients with age-related macular degeneration: a biomarker of risk for choroidal neovascularization?" Arch Ophthalmol **122**(7): 1013-1018.

Curcio, C. A., E. C. Zanzottera, T. Ach, C. Balaratnasingam and K. B. Freund (2017). "Activated Retinal Pigment Epithelium, an Optical Coherence Tomography Biomarker for Progression in Age-Related Macular Degeneration." Invest Ophthalmol Vis Sci **58**(6): BIO211-BIO226.

Daruich, A., A. Matet, A. Dirani, E. Bousquet, M. Zhao, N. Farman, F. Jaisser and F. Behar-Cohen (2015). "Central serous chorioretinopathy: Recent findings and new physiopathology hypothesis." Prog Retin Eye Res **48**: 82-118.

de Carlo, T. E., A. Romano, N. K. Waheed and J. S. Duker (2015). "A review of optical coherence tomography angiography (OCTA)." Int J Retina Vitreous **1**: 5.

de Jong, P. T. (2006). "Age-related macular degeneration." N Engl J Med **355**(14): 1474-1485.

Deierborg, T., L. Roybon, A. R. Inacio, J. Pesic and P. Brundin (2010). "Brain injury activates microglia that induce neural stem cell proliferation ex vivo and promote differentiation of neurosphere-derived cells into neurons and oligodendrocytes." Neuroscience **171**(4): 1386-1396.

Delori, F. C., D. G. Goger and C. K. Dorey (2001). "Age-related accumulation and spatial distribution of lipofuscin in RPE of normal subjects." Invest Ophthalmol Vis Sci **42**(8): 1855-1866.

Di Pierdomenico, J., D. Garcia-Ayuso, M. Agudo-Barriuso, M. Vidal-Sanz and M. P. Villegas-Perez (2019). "Role of microglial cells in photoreceptor degeneration." Neural Regen Res **14**(7): 1186-1190.

Di Pierdomenico, J., R. Scholz, F. J. Valiente-Soriano, M. C. Sanchez-Migallon, M. Vidal-Sanz, T. Langmann, M. Agudo-Barriuso, D. Garcia-Ayuso and M. P. Villegas-Perez (2018). "Neuroprotective Effects of FGF2 and Minocycline in Two Animal Models of Inherited Retinal Degeneration." Invest Ophthalmol Vis Sci **59**(11): 4392-4403.

Dick, A. D., A. L. Ford, J. V. Forrester and J. D. Sedgwick (1995). "Flow cytometric identification of a minority population of MHC class II positive cells in the normal rat retina distinct from CD45lowCD11b/c+CD4low parenchymal microglia." Br J Ophthalmol **79**(9): 834-840.

Double, K. L., V. N. Dedov, H. Fedorow, E. Kettle, G. M. Halliday, B. Garner and U. T. Brunk (2008). "The comparative biology of neuromelanin and lipofuscin in the human brain." Cell Mol Life Sci **65**(11): 1669-1682.

Ebrahem, Q., A. Minamoto, G. Hoppe, B. Anand-Apte and J. E. Sears (2006). "Triamcinolone acetonide inhibits IL-6- and VEGF-induced angiogenesis downstream of the IL-6 and VEGF receptors." Invest Ophthalmol Vis Sci **47**(11): 4935-4941.

Echevarria, F. D., A. E. Rickman and R. M. Sappington (2016). "Interleukin-6: A Constitutive Modulator of Glycoprotein 130, Neuroinflammatory and Cell Survival Signaling in Retina." J Clin Cell Immunol **7**(4).

Ferguson-Smith, A. C., Y. F. Chen, M. S. Newman, L. T. May, P. B. Sehgal and F. H. Ruddle (1988). "Regional localization of the interferon-beta 2/B-cell stimulatory factor 2/hepatocyte stimulating factor gene to human chromosome 7p15-p21." Genomics **2**(3): 203-208.

Ferrington, D. A., D. Sinha and K. Kaarniranta (2016). "Defects in retinal pigment epithelial cell proteolysis and the pathology associated with age-related macular degeneration." Prog Retin Eye Res **51**: 69-89.

Fields, M. A., L. V. Del Priore, R. A. Adelman and L. J. Rizzolo (2019). "Interactions of the choroid, Bruch's membrane, retinal pigment epithelium, and neurosensory retina collaborate to form the outer blood-retinal-barrier." Prog Retin Eye Res: 100803.

Forrester, J. V. (2003). "Macrophages eyed in macular degeneration." Nat Med **9**(11): 1350-1351.

Gadient, R. A. and U. H. Otten (1997). "Interleukin-6 (IL-6)--a molecule with both beneficial and destructive potentials." Prog Neurobiol **52**(5): 379-390.

Garcia-Layana, A., F. Cabrera-Lopez, J. Garcia-Arumi, L. Arias-Barquet and J. M. Ruiz-Moreno (2017). "Early and intermediate age-related macular degeneration: update and clinical review." Clin Interv Aging **12**: 1579-1587.

Graeber, M. B. and W. J. Streit (2010). "Microglia: biology and pathology." Acta Neuropathol **119**(1): 89-105.

Gramage, E., J. Li and P. Hitchcock (2014). "The expression and function of midkine in the vertebrate retina." Br J Pharmacol **171**(4): 913-923.

Gu, X., N. J. Neric, J. S. Crabb, J. W. Crabb, S. K. Bhattacharya, M. E. Rayborn, J. G. Hollyfield and V. L. Bonilha (2012). "Age-related changes in the retinal pigment epithelium (RPE)." PLoS One **7**(6): e38673.

Guadagni, V., E. Novelli, I. Piano, C. Gargini and E. Strettoi (2015). "Pharmacological approaches to retinitis pigmentosa: A laboratory perspective." Prog Retin Eye Res **48**: 62-81.

Gupta, N., K. E. Brown and A. H. Milam (2003). "Activated microglia in human retinitis pigmentosa, late-onset retinal degeneration, and age-related macular degeneration." Exp Eye Res **76**(4): 463-471.

Haigh, J. J., P. I. Morelli, H. Gerhardt, K. Haigh, J. Tsien, A. Damert, L. Miquerol, U. Muhlner, R. Klein, N. Ferrara, E. F. Wagner, C. Betsholtz and A. Nagy (2003). "Cortical and retinal defects caused by dosage-dependent reductions in VEGF-A paracrine signaling." Dev Biol **262**(2): 225-241.

Harry, G. J. and A. D. Kraft (2008). "Neuroinflammation and microglia: considerations and approaches for neurotoxicity assessment." Expert Opin Drug Metab Toxicol **4**(10): 1265-1277.

Hashemi-Monfared, A., M. Firouzi, Z. Bahrami, H. Zahednasab and M. H. Harirchian (2018). "Minocycline decreases CD36 and increases CD44 in LPS-induced microglia." J Neuroimmunol **317**: 95-99.

Hayes, M. J., T. Burgoyne, S. T. Wavre-Shapton, T. Tolmachova, M. C. Seabra and C. E. Futter (2019). "Remodeling of the Basal Labyrinth of Retinal Pigment Epithelial Cells With Osmotic Challenge, Age, and Disease." Invest Ophthalmol Vis Sci **60**(7): 2515-2524.

Hebbar, S., A. Khandelwal, R. Jayashree, S. J. Hindle, Y. N. Chiang, J. Y. Yew, S. T. Sweeney and D. Schwudke (2017). "Lipid metabolic perturbation is an early-onset phenotype in adult spinster mutants: a Drosophila model for lysosomal storage disorders." Mol Biol Cell **28**(26): 3728-3740.

Heiduschka, P. and S. Thanos (2006). "Cortisol promotes survival and regeneration of axotomised retinal ganglion cells and enhances effects of aurintricarboxylic acid." Graefes Arch Clin Exp Ophthalmol **244**(11): 1512-1521.

Hernandez, C. and R. Simo (2012). "Neuroprotection in diabetic retinopathy." Curr Diab Rep **12**(4): 329-337.

Hirabayashi, Y., O. Fujimori and S. Shimizu (2003). "Bruch's membrane of the brachymorphic mouse." Med Electron Microsc **36**(3): 139-146.

Hohn, A. and T. Grune (2013). "Lipofuscin: formation, effects and role of macroautophagy." Redox Biol **1**: 140-144.

Homayouni, M. (2009). "Vascular endothelial growth factors and their inhibitors in ocular neovascular disorders." J Ophthalmic Vis Res **4**(2): 105-114.

Hoppe, G., T. J. Lee, S. Yoon, M. Yu, N. S. Peachey, M. Rayborn, M. J. Zutel, G. Trichonas, J. Au and J. E. Sears (2014). "Inducing a visceral organ to protect a peripheral capillary bed: stabilizing hepatic HIF-1alpha prevents oxygen-induced retinopathy." Am J Pathol **184**(6): 1890-1899.

Huang, Y., Z. Xu, S. Xiong, G. Qin, F. Sun, J. Yang, T. F. Yuan, L. Zhao, K. Wang, Y. X. Liang, L. Fu, T. Wu, K. F. So, Y. Rao and B. Peng (2018). "Dual extra-retinal origins of microglia in the model of retinal microglia repopulation." Cell Discov **4**: 9.

Hughes, J. M., A. J. Groot, P. van der Groep, R. Sersansie, M. Vooijs, P. J. van Diest, C. J. Van Noorden, R. O. Schlingemann and I. Klaassen (2010). "Active HIF-1 in the normal human retina." J Histochem Cytochem **58**(3): 247-254.

Ivan, M., K. Kondo, H. Yang, W. Kim, J. Valiando, M. Ohh, A. Salic, J. M. Asara, W. S. Lane and W. G. Kaelin, Jr. (2001). "HIFalpha targeted for VHL-mediated destruction by proline hydroxylation: implications for O2 sensing." Science **292**(5516): 464-468.

J， Hogan, M. and A. J. E. W. J (1971). Histology of the Human Eye, Sauders**:** 320.

Jonas, J. B., Y. Tao, M. Neumaier and P. Findeisen (2010). "Monocyte chemoattractant protein 1, intercellular adhesion molecule 1, and vascular cell adhesion molecule 1 in exudative age-related macular degeneration." Arch Ophthalmol **128**(10): 1281-1286.

Kaarniranta, K., A. Salminen, E. L. Eskelinen and J. Kopitz (2009). "Heat shock proteins as gatekeepers of proteolytic pathways-Implications for age-related macular degeneration (AMD)." Ageing Res Rev **8**(2): 128-139.

Kaemmerer, E., F. Schutt, T. U. Krohne, F. G. Holz and J. Kopitz (2007). "Effects of lipid peroxidation-related protein modifications on RPE lysosomal functions and POS phagocytosis." Invest Ophthalmol Vis Sci **48**(3): 1342-1347.

Kamran, P., K. I. Sereti, P. Zhao, S. R. Ali, I. L. Weissman and R. Ardehali (2013). "Parabiosis in mice: a detailed protocol." J Vis Exp(80).

Karl, M. O. and T. A. Reh (2010). "Regenerative medicine for retinal diseases: activating endogenous repair mechanisms." Trends Mol Med **16**(4): 193-202.

Karlstetter, M., R. Scholz, M. Rutar, W. T. Wong, J. M. Provis and T. Langmann (2015). "Retinal microglia: just bystander or target for therapy?" Prog Retin Eye Res **45**: 30-57.

Kauppinen, A., J. J. Paterno, J. Blasiak, A. Salminen and K. Kaarniranta (2016). "Inflammation and its role in age-related macular degeneration." Cell Mol Life Sci **73**(9): 1765-1786.

Ke, Q. and M. Costa (2006). "Hypoxia-inducible factor-1 (HIF-1)." Mol Pharmacol **70**(5): 1469-1480.

Kobayashi, Y. (2008). "The role of chemokines in neutrophil biology." Front Biosci **13**: 2400-2407.

Konig, J., C. Ott, M. Hugo, T. Jung, A. L. Bulteau, T. Grune and A. Hohn (2017). "Mitochondrial contribution to lipofuscin formation." Redox Biol **11**: 673-681.

Korte, G. E., T. Gerszberg, F. Pua and P. Henkind (1986). "Choriocapillaris atrophy after experimental destruction of the retinal pigment epithelium in the rat. A study in thin sections and vascular casts." Acta Anat (Basel) **127**(3): 171-175.

Krause, T. A., A. F. Alex, D. R. Engel, C. Kurts and N. Eter (2014). "VEGF-production by CCR2-dependent macrophages contributes to laser-induced choroidal neovascularization." PLoS One **9**(4): e94313.

Kunert, K. S., M. E. Fitzgerald, L. Thomson and C. K. Dorey (1999). "Microglia increase as photoreceptors decrease in the aging avian retina." Curr Eye Res **18**(6): 440-447.

Kutty, R. K., W. Samuel, K. Boyce, A. Cherukuri, T. Duncan, C. Jaworski, C. N. Nagineni and T. M. Redmond (2016). "Proinflammatory cytokines decrease the expression of genes critical for RPE function." Mol Vis **22**: 1156-1168.

Lacassin, F., D. Schaffo, C. Perronne, P. Longuet, C. Leport and J. L. Vilde (1995). "Clarithromycin-minocycline combination as salvage therapy for toxoplasmosis in patients infected with human immunodeficiency virus." Antimicrob Agents Chemother **39**(1): 276-277.

Lamb, L. E. and J. D. Simon (2004). "A2E: a component of ocular lipofuscin." Photochem Photobiol **79**(2): 127-136.

Lamb, T. D. and E. N. Pugh, Jr. (2004). "Dark adaptation and the retinoid cycle of vision." Prog Retin Eye Res **23**(3): 307-380.

Lange, C., S. R. Heynen, N. Tanimoto, M. Thiersch, Y. Z. Le, I. Meneau, M. W. Seeliger, M. Samardzija, C. Caprara and C. Grimm (2011). "Normoxic activation of hypoxia-inducible factors in photoreceptors provides transient protection against light-induced retinal degeneration." Invest Ophthalmol Vis Sci **52**(8): 5872-5880.

Langenhan, T., G. Aust and J. Hamann (2013). "Sticky signaling--adhesion class G protein-coupled receptors take the stage." Sci Signal **6**(276): re3.

Lechner, J., M. Chen, R. E. Hogg, L. Toth, G. Silvestri, U. Chakravarthy and H. Xu (2017). "Peripheral blood mononuclear cells from neovascular age-related macular degeneration patients produce higher levels of chemokines CCL2 (MCP-1) and CXCL8 (IL-8)." J Neuroinflammation **14**(1): 42.

Leclaire, M. D., G. Nettels-Hackert, J. Konig, A. Hohn, T. Grune, C. E. Uhlig, U. Hansen, N. Eter and P. Heiduschka (2019). "Lipofuscin-dependent stimulation of microglial cells." Graefes Arch Clin Exp Ophthalmol **257**(5): 931-952.

Lee, C. J., J. A. Vroom, H. A. Fishman and S. F. Bent (2006). "Determination of human lens capsule permeability and its feasibility as a replacement for Bruch's membrane." Biomaterials **27**(8): 1670-1678.

Leibinger, M., A. Muller, P. Gobrecht, H. Diekmann, A. Andreadaki and D. Fischer (2013). "Interleukin-6 contributes to CNS axon regeneration upon inflammatory stimulation." Cell Death Dis **4**: e609.

Lentsch, A. B. and P. A. Ward (2000). "Regulation of inflammatory vascular damage." J Pathol **190**(3): 343-348.

Leon, L. J. and A. B. Gustafsson (2016). "Staying young at heart: autophagy and adaptation to cardiac aging." J Mol Cell Cardiol **95**: 78-85.

Leung, K. W., C. J. Barnstable and J. Tombran-Tink (2009). "Bacterial endotoxin activates retinal pigment epithelial cells and induces their degeneration through IL-6 and IL-8 autocrine signaling." Mol Immunol **46**(7): 1374-1386.

Li, L., N. Eter and P. Heiduschka (2015). "The microglia in healthy and diseased retina." Exp Eye Res **136**: 116-130.

Li, Y., X. F. Du, C. S. Liu, Z. L. Wen and J. L. Du (2012). "Reciprocal regulation between resting microglial dynamics and neuronal activity in vivo." Dev Cell **23**(6): 1189-1202.

Liu, Y. H., C. Molzer, G. C. Milne, L. Kuffova and J. V. Forrester (2019). "Transmission Electron Microscopy Data on drusen-like deposits in the retinal degeneration sTg-IRBP: HEL mouse model." Data Brief **22**: 140-144.

Lopez-Otin, C., M. A. Blasco, L. Partridge, M. Serrano and G. Kroemer (2013). "The hallmarks of aging." Cell **153**(6): 1194-1217.

Ma, W., S. Coon, L. Zhao, R. N. Fariss and W. T. Wong (2013). "A2E accumulation influences retinal microglial activation and complement regulation." Neurobiol Aging **34**(3): 943-960.

Ma, W., L. Zhao, A. M. Fontainhas, R. N. Fariss and W. T. Wong (2009). "Microglia in the mouse retina alter the structure and function of retinal pigmented epithelial cells: a potential cellular interaction relevant to AMD." PLoS One **4**(11): e7945.

Mac Nair, C. E., K. A. Fernandes, C. L. Schlamp, R. T. Libby and R. W. Nickells (2014). "Tumor necrosis factor alpha has an early protective effect on retinal ganglion cells after optic nerve crush." J Neuroinflammation **11**: 194.

Madeira, M. H., R. Boia, P. F. Santos, A. F. Ambrosio and A. R. Santiago (2015). "Contribution of microglia-mediated neuroinflammation to retinal degenerative diseases." Mediators Inflamm **2015**: 673090.

Madigan, M. C., A. A. Sadun, N. S. Rao, P. U. Dugel, W. N. Tenhula and P. S. Gill (1996). "Tumor necrosis factor-alpha (TNF-alpha)-induced optic neuropathy in rabbits." Neurol Res **18**(2): 176-184.

Maier, K., D. Merkler, J. Gerber, N. Taheri, A. V. Kuhnert, S. K. Williams, C. Neusch, M. Bahr and R. Diem (2007). "Multiple neuroprotective mechanisms of minocycline in autoimmune CNS inflammation." Neurobiol Dis **25**(3): 514-525.

Margolis, R. and R. F. Spaide (2009). "A pilot study of enhanced depth imaging optical coherence tomography of the choroid in normal eyes." Am J Ophthalmol **147**(5): 811-815.

Meda, L., M. A. Cassatella, G. I. Szendrei, L. Otvos, Jr., P. Baron, M. Villalba, D. Ferrari and F. Rossi (1995). "Activation of microglial cells by beta-amyloid protein and interferon-gamma." Nature **374**(6523): 647-650.

Medzhitov, R. (2008). "Origin and physiological roles of inflammation." Nature **454**(7203): 428-435.

Moreno-Garcia, A., A. Kun, O. Calero, M. Medina and M. Calero (2018). "An Overview of the Role of Lipofuscin in Age-Related Neurodegeneration." Front Neurosci **12**: 464.

Mustafi, D., B. M. Kevany, C. Genoud, K. Okano, A. V. Cideciyan, A. Sumaroka, A. J. Roman, S. G. Jacobson, A. Engel, M. D. Adams and K. Palczewski (2011). "Defective photoreceptor phagocytosis in a mouse model of enhanced S-cone syndrome causes progressive retinal degeneration." FASEB J **25**(9): 3157-3176.

Nandrot, E. F. (2014). "Animal Models, in "The Quest to Decipher RPE Phagocytosis"." Adv Exp Med Biol **801**: 77-83.

Narayan, D. S., J. P. Wood, G. Chidlow and R. J. Casson (2016). "A review of the mechanisms of cone degeneration in retinitis pigmentosa." Acta Ophthalmol **94**(8): 748-754.

Naskar, R., M. Wissing and S. Thanos (2002). "Detection of early neuron degeneration and accompanying microglial responses in the retina of a rat model of glaucoma." Invest Ophthalmol Vis Sci **43**(9): 2962-2968.

Newman, A. M., N. B. Gallo, L. S. Hancox, N. J. Miller, C. M. Radeke, M. A. Maloney, J. B. Cooper, G. S. Hageman, D. H. Anderson, L. V. Johnson and M. J. Radeke (2012). "Systems-level analysis of age-related macular degeneration reveals global biomarkers and phenotype-specific functional networks." Genome Med **4**(2): 16.

Ng, T. F. and J. W. Streilein (2001). "Light-induced migration of retinal microglia into the subretinal space." Invest Ophthalmol Vis Sci **42**(13): 3301-3310.

Nimmerjahn, A., F. Kirchhoff and F. Helmchen (2005). "Resting microglial cells are highly dynamic surveillants of brain parenchyma in vivo." Science **308**(5726): 1314-1318.

Ohsawa, K., Y. Imai, H. Kanazawa, Y. Sasaki and S. Kohsaka (2000). "Involvement of Iba1 in membrane ruffling and phagocytosis of macrophages/microglia." J Cell Sci **113 (Pt 17)**: 3073-3084.

Olson, J. L., R. J. Courtney and N. Mandava (2007). "Intravitreal infliximab and choroidal neovascularization in an animal model." Arch Ophthalmol **125**(9): 1221-1224.

Ozaki, E., M. Campbell, A. S. Kiang, M. Humphries, S. L. Doyle and P. Humphries (2014). "Inflammation in age-related macular degeneration." Adv Exp Med Biol **801**: 229-235.

Pan, X., C. B. P. De Aragao, J. P. Velasco-Martin, D. A. Priestman, H. Y. Wu, K. Takahashi, K. Yamaguchi, L. Sturiale, D. Garozzo, F. M. Platt, N. Lamarche-Vane, C. R. Morales, T. Miyagi and A. V. Pshezhetsky (2017). "Neuraminidases 3 and 4 regulate neuronal function by catabolizing brain gangliosides." FASEB J **31**(8): 3467-3483.

Pedersen, K. B., F. Moller, A. K. Sjolie and S. Andreasson (2010). "Electrophysiological assessment of retinal function during 6 months of bevacizumab treatment in neovascular age-related macular degeneration." Retina **30**(7): 1025-1033.

Piras, A., D. Gianetto, D. Conte, A. Bosone and A. Vercelli (2011). "Activation of autophagy in a rat model of retinal ischemia following high intraocular pressure." PLoS One **6**(7): e22514.

Pollreisz, A., J. D. Messinger, K. R. Sloan, T. J. Mittermueller, A. S. Weinhandl, E. K. Benson, G. J. Kidd, U. Schmidt-Erfurth and C. A. Curcio (2018). "Visualizing melanosomes, lipofuscin, and melanolipofuscin in human retinal pigment epithelium using serial block face scanning electron microscopy." Exp Eye Res **166**: 131-139.

Popovic, N., A. Schubart, B. D. Goetz, S. C. Zhang, C. Linington and I. D. Duncan (2002). "Inhibition of autoimmune encephalomyelitis by a tetracycline." Ann Neurol **51**(2): 215-223.

Raivich, G., M. Bohatschek, C. U. Kloss, A. Werner, L. L. Jones and G. W. Kreutzberg (1999). "Neuroglial activation repertoire in the injured brain: graded response, molecular mechanisms and cues to physiological function." Brain Res Brain Res Rev **30**(1): 77-105.

Ramrattan, R. S., T. L. van der Schaft, C. M. Mooy, W. C. de Bruijn, P. G. Mulder and P. T. de Jong (1994). "Morphometric analysis of Bruch's membrane, the choriocapillaris, and the choroid in aging." Invest Ophthalmol Vis Sci **35**(6): 2857-2864.

Ransohoff, R. M. (2007). "Microgliosis: the questions shape the answers." Nat Neurosci **10**(12): 1507-1509.

Rashid, K., I. Akhtar-Schaefer and T. Langmann (2019). "Microglia in Retinal Degeneration." Front Immunol **10**: 1975.

Reeg, S. and T. Grune (2015). "Protein Oxidation in Aging: Does It Play a Role in Aging Progression?" Antioxid Redox Signal **23**(3): 239-255.

Rivest, S. (2009). "Regulation of innate immune responses in the brain." Nat Rev Immunol **9**(6): 429-439.

Robinson, S. R. and Z. Dreher (1990). "Muller cells in adult rabbit retinae: morphology, distribution and implications for function and development." J Comp Neurol **292**(2): 178-192.

Rodolfo, C., S. Campello and F. Cecconi (2018). "Mitophagy in neurodegenerative diseases." Neurochem Int **117**: 156-166.

Rose-John, S. and P. C. Heinrich (1994). "Soluble receptors for cytokines and growth factors: generation and biological function." Biochem J **300 (Pt 2)**: 281-290.

Rubio, R. G. and A. P. Adamis (2016). "Ocular Angiogenesis: Vascular Endothelial Growth Factor and Other Factors." Dev Ophthalmol **55**: 28-37.

Runkle, E. A. and D. A. Antonetti (2011). "The blood-retinal barrier: structure and functional significance." Methods Mol Biol **686**: 133-148.

Saadat, K. A., Y. Murakami, X. Tan, Y. Nomura, T. Yasukawa, E. Okada, Y. Ikeda and Y. Yanagi (2014). "Inhibition of autophagy induces retinal pigment epithelial cell damage by the lipofuscin fluorophore A2E." FEBS Open Bio **4**: 1007-1014.

Sakai, T., N. Kuno, F. Takamatsu, E. Kimura, H. Kohno, K. Okano and K. Kitahara (2007). "Prolonged protective effect of basic fibroblast growth factor-impregnated nanoparticles in royal college of surgeons rats." Invest Ophthalmol Vis Sci **48**(7): 3381-3387.

Sakurai, E., A. Anand, B. K. Ambati, N. van Rooijen and J. Ambati (2003). "Macrophage depletion inhibits experimental choroidal neovascularization." Invest Ophthalmol Vis Sci **44**(8): 3578-3585.

Salter, M. W. and S. Beggs (2014). "Sublime microglia: expanding roles for the guardians of the CNS." Cell **158**(1): 15-24.

Sant'Anna, R., S. Navarro, S. Ventura, L. Paraoan and D. Foguel (2016). "Amyloid properties of the leader peptide of variant B cystatin C: implications for Alzheimer and macular degeneration." FEBS Lett **590**(5): 644-654.

Schafer, D. P., E. K. Lehrman, A. G. Kautzman, R. Koyama, A. R. Mardinly, R. Yamasaki, R. M. Ransohoff, M. E. Greenberg, B. A. Barres and B. Stevens (2012). "Microglia sculpt postnatal neural circuits in an activity and complement-dependent manner." Neuron **74**(4): 691-705.

Scholz, R., M. Sobotka, A. Caramoy, T. Stempfl, C. Moehle and T. Langmann (2015). "Minocycline counter-regulates pro-inflammatory microglia responses in the retina and protects from degeneration." J Neuroinflammation **12**: 209.

Schulz, C., E. Gomez Perdiguero, L. Chorro, H. Szabo-Rogers, N. Cagnard, K. Kierdorf, M. Prinz, B. Wu, S. E. Jacobsen, J. W. Pollard, J. Frampton, K. J. Liu and F. Geissmann (2012). "A lineage of myeloid cells independent of Myb and hematopoietic stem cells." Science **336**(6077): 86-90.

Schwartsburd, P. M. (1995). "On the origin of heterogeneity of lipofuscin fluorophores and their possible interrelations." Gerontology **41 Suppl 2**: 29-37.

Seddon, J. M., S. George, B. Rosner and N. Rifai (2005). "Progression of age-related macular degeneration: prospective assessment of C-reactive protein, interleukin 6, and other cardiovascular biomarkers." Arch Ophthalmol **123**(6): 774-782.

Seiberlich, V., J. Borchert, V. Zhukareva and C. Richter-Landsberg (2013). "Inhibition of protein deubiquitination by PR-619 activates the autophagic pathway in OLN-t40 oligodendroglial cells." Cell Biochem Biophys **67**(1): 149-160.

Semenza, G. L. (2004). "Hydroxylation of HIF-1: oxygen sensing at the molecular level." Physiology (Bethesda) **19**: 176-182.

Shirakabe, A., Y. Ikeda, S. Sciarretta, D. K. Zablocki and J. Sadoshima (2016). "Aging and Autophagy in the Heart." Circ Res **118**(10): 1563-1576.

Smith, W., J. Assink, R. Klein, P. Mitchell, C. C. Klaver, B. E. Klein, A. Hofman, S. Jensen, J. J. Wang and P. T. de Jong (2001). "Risk factors for age-related macular degeneration: Pooled findings from three continents." Ophthalmology **108**(4): 697-704.

Spaide, R. F., J. M. Klancnik, Jr. and M. J. Cooney (2015). "Retinal vascular layers imaged by fluorescein angiography and optical coherence tomography angiography." JAMA Ophthalmol **133**(1): 45-50.

Stone, J., H. Hollander and Z. Dreher (1991). ""Sunbursts" in the inner plexiform layer: a spectacular feature of Muller cells in the retina of the cat." J Comp Neurol **303**(3): 400-411.

Strauss, O. (2005). "The retinal pigment epithelium in visual function." Physiol Rev **85**(3): 845-881.

Su, N., S. Marz, T. Plagemann, J. Cao, H. J. Schnittler, N. Eter and P. Heiduschka (2019). "Occurrence of Transmembrane Protein 119 in the Retina is Not Restricted to the Microglia: An Immunohistochemical Study." Transl Vis Sci Technol **8**(6): 29.

Taga, T., M. Hibi, Y. Hirata, K. Yamasaki, K. Yasukawa, T. Matsuda, T. Hirano and T. Kishimoto (1989). "Interleukin-6 triggers the association of its receptor with a possible signal transducer, gp130." Cell **58**(3): 573-581.

Tarau, I. S., A. Berlin, C. A. Curcio and T. Ach (2019). "The Cytoskeleton of the Retinal Pigment Epithelium: from Normal Aging to Age-Related Macular Degeneration." Int J Mol Sci **20**(14).

Terman, A. (2001). "Garbage catastrophe theory of aging: imperfect removal of oxidative damage?" Redox Rep **6**(1): 15-26.

Terman, A. and U. T. Brunk (1998). "Lipofuscin: mechanisms of formation and increase with age." APMIS **106**(2): 265-276.

Terman, A. and U. T. Brunk (2005). "The aging myocardium: roles of mitochondrial damage and lysosomal degradation." Heart Lung Circ **14**(2): 107-114.

Terman, A., H. Dalen, J. W. Eaton, J. Neuzil and U. T. Brunk (2004). "Aging of cardiac myocytes in culture: oxidative stress, lipofuscin accumulation, and mitochondrial turnover." Ann N Y Acad Sci **1019**: 70-77.

Terman, A., T. Kurz, M. Navratil, E. A. Arriaga and U. T. Brunk (2010). "Mitochondrial turnover and aging of long-lived postmitotic cells: the mitochondrial-lysosomal axis theory of aging." Antioxid Redox Signal **12**(4): 503-535.

Tezel, G., L. Y. Li, R. V. Patil and M. B. Wax (2001). "TNF-alpha and TNF-alpha receptor-1 in the retina of normal and glaucomatous eyes." Invest Ophthalmol Vis Sci **42**(8): 1787-1794.

Thanos, S., J. Mey and M. Wild (1993). "Treatment of the adult retina with microglia-suppressing factors retards axotomy-induced neuronal degradation and enhances axonal regeneration in vivo and in vitro." J Neurosci **13**(2): 455-466.

Usui, S., Y. Ikuno, M. Akiba, I. Maruko, T. Sekiryu, K. Nishida and T. Iida (2012). "Circadian changes in subfoveal choroidal thickness and the relationship with circulatory factors in healthy subjects." Invest Ophthalmol Vis Sci **53**(4): 2300-2307.

Vadlapatla, R. K., A. D. Vadlapudi and A. K. Mitra (2013). "Hypoxia-inducible factor-1 (HIF-1): a potential target for intervention in ocular neovascular diseases." Curr Drug Targets **14**(8): 919-935.

van der Schaft, T. L., C. M. Mooy, W. C. de Bruijn, F. G. Oron, P. G. Mulder and P. T. de Jong (1992). "Histologic features of the early stages of age-related macular degeneration. A statistical analysis." Ophthalmology **99**(2): 278-286.

van Dijk, H. W., F. D. Verbraak, P. H. Kok, M. K. Garvin, M. Sonka, K. Lee, J. H. Devries, R. P. Michels, M. E. van Velthoven, R. O. Schlingemann and M. D. Abramoff (2010). "Decreased retinal ganglion cell layer thickness in patients with type 1 diabetes." Invest Ophthalmol Vis Sci **51**(7): 3660-3665.

Vecino, E., F. D. Rodriguez, N. Ruzafa, X. Pereiro and S. C. Sharma (2016). "Glia-neuron interactions in the mammalian retina." Prog Retin Eye Res **51**: 1-40.

Wang, A. L., T. J. Lukas, M. Yuan, N. Du, M. O. Tso and A. H. Neufeld (2009). "Autophagy and exosomes in the aged retinal pigment epithelium: possible relevance to drusen formation and age-related macular degeneration." PLoS One **4**(1): e4160.

Wang, W. Y., M. S. Tan, J. T. Yu and L. Tan (2015). "Role of pro-inflammatory cytokines released from microglia in Alzheimer's disease." Ann Transl Med **3**(10): 136.

WANG Xiao, L. S.-f., LU Jing, WANG Yi-shen, LÜ Lin, LUO Yan (2018). "Characteristics Analysis of Idiopathic Epiretinal Membrane by Multi-color Image and OCT." MEDICAL SCIENCES **39** 5.

Warburton, S., W. E. Davis, K. Southwick, H. Xin, A. T. Woolley, G. F. Burton and C. D. Thulin (2007). "Proteomic and phototoxic characterization of melanolipofuscin: correlation to disease and model for its origin." Mol Vis **13**: 318-329.

Wing, G. L., G. C. Blanchard and J. J. Weiter (1978). "The topography and age relationship of lipofuscin concentration in the retinal pigment epithelium." Invest Ophthalmol Vis Sci **17**(7): 601-607.

Xie, J., R. Zhu, Y. Peng, W. Gao, J. Du, L. Zhao, Y. Chi and L. Yang (2017). "Tumor necrosis factor-alpha regulates photoreceptor cell autophagy after retinal detachment." Sci Rep **7**(1): 17108.

Xie, P., M. Kamei, M. Suzuki, N. Matsumura, K. Nishida, S. Sakimoto, H. Sakaguchi and K. Nishida (2011). "Suppression and regression of choroidal neovascularization in mice by a novel CCR2 antagonist, INCB3344." PLoS One **6**(12): e28933.

Xu, H., M. Chen and J. V. Forrester (2009). "Para-inflammation in the aging retina." Prog Retin Eye Res **28**(5): 348-368.

Xu, H., M. Chen, A. Manivannan, N. Lois and J. V. Forrester (2008). "Age-dependent accumulation of lipofuscin in perivascular and subretinal microglia in experimental mice." Aging Cell **7**(1): 58-68.

Xu, H., M. Chen, E. J. Mayer, J. V. Forrester and A. D. Dick (2007). "Turnover of resident retinal microglia in the normal adult mouse." Glia **55**(11): 1189-1198.

Xu, H. Z. and Y. Z. Le (2011). "Significance of outer blood-retina barrier breakdown in diabetes and ischemia." Invest Ophthalmol Vis Sci **52**(5): 2160-2164.

Yona, S. and M. Stacey (2010). "Adhesion-GPCRs: structure to function. Preface." Adv Exp Med Biol **706**: v-vii.

Yoshida, S., C. Sotozono, T. Ikeda and S. Kinoshita (2001). "Interleukin-6 (IL-6) production by cytokine-stimulated human Muller cells." Curr Eye Res **22**(5): 341-347.

Young, R. W. (1971). "Shedding of discs from rod outer segments in the rhesus monkey." J Ultrastruct Res **34**(1): 190-203.

Zeng, H. Y., W. R. Green and M. O. Tso (2008). "Microglial activation in human diabetic retinopathy." Arch Ophthalmol **126**(2): 227-232.

Zeng, H. Y., X. A. Zhu, C. Zhang, L. P. Yang, L. M. Wu and M. O. Tso (2005). "Identification of sequential events and factors associated with microglial activation, migration, and cytotoxicity in retinal degeneration in rd mice." Invest Ophthalmol Vis Sci **46**(8): 2992-2999.

Zhang, Y., L. Zhao, X. Wang, W. Ma, A. Lazere, H. H. Qian, J. Zhang, M. Abu-Asab, R. N. Fariss, J. E. Roger and W. T. Wong (2018). "Repopulating retinal microglia restore endogenous organization and function under CX3CL1-CX3CR1 regulation." Sci Adv **4**(3): eaap8492.

Zhao, L., S. D. Spassieva, T. J. Jucius, L. D. Shultz, H. E. Shick, W. B. Macklin, Y. A. Hannun, L. M. Obeid and S. L. Ackerman (2011). "A deficiency of ceramide biosynthesis causes cerebellar purkinje cell neurodegeneration and lipofuscin accumulation." PLoS Genet **7**(5): e1002063.

Zhou, T., Z. Huang, X. Sun, X. Zhu, L. Zhou, M. Li, B. Cheng, X. Liu and C. He (2017). "Microglia Polarization with M1/M2 Phenotype Changes in rd1 Mouse Model of Retinal Degeneration." Front Neuroanat **11**: 77.

List of Animals Used in this Study

Cage and mice number (M)	Age (months)	Name of subretinal injection	Treatment	Period
Cage 438 M1	5	Lipofuscin	No eye drops	0 day
Cage 438 M2	5	Lipofuscin	No eye drops	1 day
Cage 441 M1	5	Lipofuscin	No eye drops	1 day
Cage 544 M3	18	Lipofuscin	No eye drops	1 day
Cage 436 M1	5	Lipofuscin	No eye drops	3 days
Cage 544 M1	18	Lipofuscin	No eye drops	3 days
Cage 438 M3	5	Lipofuscin	No eye drops	5 days
Cage 544 M2	18	Lipofuscin	No eye drops	5 days
Cage 547 M2	22	Lipofuscin	No eye drops	7 days
Cage 438 M4	5	Lipofuscin	No eye drops	7 days
Cage 548 M1	16	Lipofuscin	No eye drops	7 days
Cage 641 M1	5	Lipofuscin	No eye drops	7 days
Cage 394 M1	16	Lipofuscin	No eye drops	9 days
Cage 394 M2	16	Lipofuscin	No eye drops	9 days
Cage 394 M3	16	Lipofuscin	No eye drops	9 days
Cage 651 M3	4	Lipofuscin	No eye drops	12 days
Cage 546 M1	22	Lipofuscin	No eye drops	14 days
Cage 464 M2	24	Lipofuscin	No eye drops	14 days
Cage 558 M1	17	Lipofuscin	No eye drops	14 days
Cage 549 M2	21	Lipofuscin	No eye drops	15 days
Cage 641 M2	5	Lipofuscin	No eye drops	20 days
Cage 682 M1	6	Lipofuscin	No eye drops	21 days
Cage 677 M3	4	Lipofuscin	No eye drops	35 days
Cage 654 M2	5	Lipofuscin	No eye drops	3 months
Cage 621 M3	5	Lipofuscin	No eye drops	4 months
Cage 632 M3	5	Lipofuscin	No eye drops	4 months
Cage 675 M3	3	Lipofuscin	No eye drops	6 months
Cage 678 M3	3	Lipofuscin	No eye drops	6 months
Cage 440 M1	3	Lipofuscin	PBS eye drops	7 days
Cage 392 M1	16	Lipofuscin	PBS eye drops	7 days
Cage 392 M3	22	Lipofuscin	PBS eye drops	7 days
Cage 371 M1	20	Lipofuscin	PBS eye drops	14 days
Cage 370 M1	20	Lipofuscin	PBS eye drops	28 days
Cage 442 M1	14	Lipofuscin	PBS eye drops	28 days
Cage 430 M2	4	Lipofuscin	Mino eye drops	7 days
Cage 440 M3	3	Lipofuscin	Mino eye drops	7 days
Cage 422 M3	16	Lipofuscin	Mino eye drops	7 days
Cage 371 M2	20	Lipofuscin	Mino eye drops	14 days
Cage 372 M1	20	Lipofuscin	Mino eye drops	14 days
Cage 370 M2	20	Lipofuscin	Mino eye drops	28 days
Cage 442 M2	14	Lipofuscin	Mino eye drops	28 days
Cage 440 M2	3	Lipofuscin	TKP eye drops	7 days
Cage 430 M1	4	Lipofuscin	TKP eye drops	7 days
Cage 422 M2	16	Lipofuscin	TKP eye drops	7 days
Cage 371 M3	20	Lipofuscin	TKP eye drops	14 days

Cage 396 M1	14	Lipofuscin	TKP eye drops	14 days
Cage 370 M3	20	Lipofuscin	TKP eye drops	28 days
Cage 442 M3	14	Lipofuscin	TKP eye drops	28 days
Cage 545 M2	17	PBS	No eye drops	1 day
Cage 436 M2	5	PBS	No eye drops	3 days
Cage 545 M1	22	PBS	No eye drops	3 days
Cage 545 M3	17	PBS	No eye drops	5 days
Cage 547 M1	22	PBS	No eye drops	7 days
Cage 548 M3	15	PBS	No eye drops	7 days
Cage 645 M3	5	PBS	No eye drops	7 days
Cage 651 M2	4	PBS	No eye drops	12 days
Cage 621 M2	6	PBS	No eye drops	12 days
Cage 632 M2	6	PBS	No eye drops	12 days
Cage 556 M1	17	PBS	No eye drops	14 days
Cage 546 M3	22	PBS	No eye drops	14 days
Cage 548 M2	14	PBS	No eye drops	15 days
Cage 645 M2	5	PBS	No eye drops	20 days
Cage 682 M2	6	PBS	No eye drops	21 days
Cage 677 M1	6	PBS	No eye drops	35 days
Cage 644 M1	6	PBS	No eye drops	35 days
Cage 654 M1	6	PBS	No eye drops	3 months
Cage 675 M4	3	PBS	No eye drops	6 months
Cage 678 M1	6	PBS	No eye drops	6 months
Cage 392 M2	4	PBS	PBS eye drops	7 days
Cage 422 M3	16	PBS	PBS eye drops	7 days
Cage 402 M2	20	PBS	PBS eye drops	7 days
Cage 414 M1	23	PBS	PBS eye drops	14 days
Cage 592 M2	4	PBS	PBS eye drops	21 days
Cage 427 M1	16	PBS	PBS eye drops	28 days
Cage 598 M3	3	PBS	Mino eye drops	7 days
Cage 425 M1	17	PBS	Mino eye drops	7 days
Cage 414 M2	23	PBS	Mino eye drops	14 days
Cage 427 M2	16	PBS	Mino eye drops	28 days
Cage 599 M2	3	PBS	TKP eye drops	7 days
Cage 598 M4	3	PBS	TKP eye drops	7 days
Cage 425 M2	17	PBS	TKP eye drops	7 days
Cage 414 M3	23	PBS	TKP eye drops	14 days
Cage 427 M3	16	PBS	TKP eye drops	28 days
Cage 639 M1	3	Sham	No eye drops	12 days
Cage 645 M1	5	Sham	No eye drops	20 days
Cage 682 M3	6	Sham	No eye drops	21 days
Cage 677 M2	3	Sham	No eye drops	1 months
Cage 654 M3	5	Sham	No eye drops	3 months
Cage 651 M1	4	Sham	No eye drops	4 months
Cage 632 M1	4	Sham	No eye drops	4 months
Cage 675 M2	3	Sham	No eye drops	5 months
Cage 419 M1	5	Negative control	No	
Cage 429 M1	6	Negative control	No	
Cage 492 M1	3	Negative control	No	

Cage 608 M1	3	Negative control	No	
Cage 641 M3	5	Negative control	No	
Cage 682 M4	5	Negative control	No	
Cage 414 M4	21	Negative control	No	
ZTE eliminated	18	Negative control	No	
ZTE eliminated	19	Negative control	No	
ZTE eliminated	19	Negative control	No	

Acknowledgements

Firstly, I would like to thanks my supervisor Prof. Dr. Peter Heiduschka and director of the University Eye Hospital, Münster, Prof. Dr. Nicole Eter for the opportunities they have provided and the understanding as well as support they have given for me, so that my job can be done.

Prof. Dr. Peter Heiduschka always had great patience to tutor and help me. He is a very good teacher, he is not only knowledgeable, but also, he knows how to teach. He has given me great instructions and encouragements throughout the process of selecting the research topic, performing the research, and writing the thesis. His insightful suggestions on every draft, which provide me with many enlightening ideas, have inspired me to a better level. Without his patient guidance, my thesis could not be finished. He raised me up, let me do more than I can be.

Secondly, I would like to express my sincere gratitude to Dr. Martin Dominik Leclaire, who helped me revise parts of my thesis, and gave me very good advice and guidance in time. And I owe many thanks to Mrs. Gerburg Nettels-Hackert, who introduced me to the working processes in our laboratory, and Mrs. Tanja Plagemann, Ms. Mechthild Wissing with Gerburg Nettels-Hackert, who taught me the skills of handling all the experimental procedures that were demanded for my thesis. Thanks for your help and support.

Thirdly, I would like to extend my gratefulness to my colleagues who are in Germany and China, especially Dr. rer. nat. Uwe Hansen, Ms. Karin Gäher, Dr. Julian Zimmermann, Ms. Dißelkötter Judith, Prof. Yu Zhu, Prof. Xuanping Cao and Ms. Zhen Xing. Also, to my beloved elder parents, husband, and daughter whose understanding support, help and encouragement have made my achievement possible. Thank you so much!

Finally, I am very grateful to everyone who have offered me support, encouragement, and have always been helping me out with difficulties during my study.

Nan Su